

Two-Sided Flexibility in Platforms

Daniel Freund

Massachusetts Institute of Technology, Cambridge, MA
dfreund@mit.edu

Sébastien Martin

Northwestern University, Evanston, IL
sebastien.martin@kellogg.northwestern.edu

Jiayu (Kamessi) Zhao

Massachusetts Institute of Technology, Cambridge, MA
kamessi@mit.edu

Flexibility is a cornerstone of operations management, crucial to hedge stochasticity in product demands, service requirements, and resource allocation. In two-sided platforms, flexibility is also two-sided and can be viewed as the compatibility of agents on one side with agents on the other side. Platform actions often influence the flexibility on either the demand or the supply side. But how should flexibility be jointly allocated across different sides? Whereas the literature has traditionally focused on only one side at a time, our work initiates the study of two-sided flexibility in matching platforms. We propose a parsimonious matching model in random graphs and identify the flexibility allocation that optimizes the expected size of a maximum matching. Our findings reveal that flexibility allocation is a first-order issue: for a given flexibility budget, the resulting matching size can vary greatly depending on how the budget is allocated. Moreover, even in the simple and symmetric settings we study, the quest for the optimal allocation is complicated. In particular, easy and costly mistakes can be made if the flexibility decisions on the demand and supply side are optimized independently (e.g., by two different teams in the company), rather than jointly. To guide the search for optimal flexibility allocation, we uncover two effects – flexibility cannibalization and flexibility asymmetry – that govern when the optimal design places the flexibility budget only on one side or equally on both sides. In doing so we identify the study of two-sided flexibility as a significant aspect of platform efficiency.

Key words: Flexibility, Two-sided Platforms, Bipartite Matching, Incentive Designs

1. Introduction

Flexibility is one of the fundamental topics in operations research and computer systems. As an operational concept, it classically applies to a range of settings including (1) the ability of a plant to process multiple types of products in a manufacturing system (Jordan and Graves 1995), e.g., the long chain design illustrated in Fig. 1 (a), (2) the ability of servers, due to cross-training, to handle multiple types of requests (Wallace and Whitt 2005), or (3) the pooling of resources in a network of newsvendors (Bassamboo et al. 2010). In these applications, flexibility is widely recognized for its value in hedging against demand uncertainty and improving system performance.

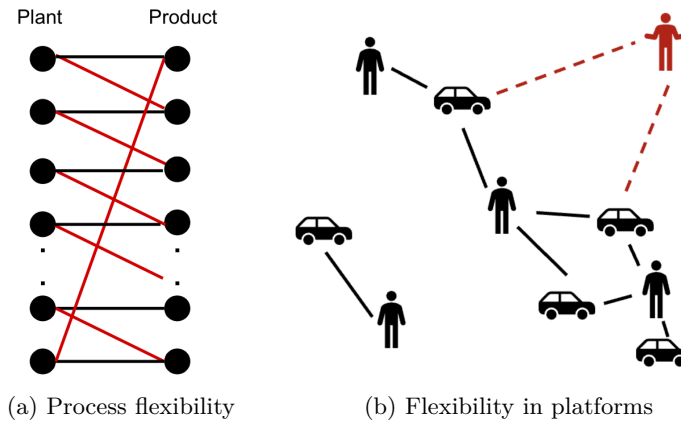


Figure 1 The plots contrast process flexibility in manufacturing systems with flexibility in platforms. The red edges in the long chain design highlight the additional compatibility introduced deterministically into the system. In contrast, platform flexibility is achieved through agents with a higher probability of being compatible with other agents. The figure shows one realization of this compatibility; notice that the flexible red rider is willing to accept further away matches.

Many modern service platforms face similar uncertainty on both the demand and the supply side, which motivates the natural question whether flexibility can also be leveraged in their operations. For instance, the matching problem solved by ride-hailing platforms has a bipartite structure, with riders on the demand side and drivers on the supply side. As illustrated in Fig. 1 (b), the edges between agents represent their compatibility (here, whether it is possible to match a given driver and rider), and the platform finds a matching using these available edges. Though the problems in Fig. 1 (a) and (b) share a similar bipartite structure and additional edges are valuable in both systems, there are fundamental differences in how these edges are created. In a manufacturing system, additional compatibility is configured deterministically by a central planner who invests in equipment for the corresponding plants. In contrast, the impact of flexibility in modern platforms is better modeled in a stochastic way. For instance, the “Wait and Save” option in Fig. 2 (a) illustrates how platforms incentivize riders to be more flexible with their pickup times. A rider choosing this option accepts to wait longer before being matched. This allows the platform to match her with drivers within a wider radius, providing flexibility to generate more efficient matches overall. However, the number of drivers within the radius is stochastic. Therefore, a flexible rider will likely be compatible with more drivers, but not always. For example in Fig. 1 (b) the flexible rider has two edges, but there are non-flexible riders with three edges, as, in this situation, the flexible rider is further away from available drivers. This is why, more generally, the flexibility of an agent (supply or demand) can be interpreted as its likelihood of being compatible with agents on the other side. In a more abstract matching terminology, a flexible node is a node that is more likely to have edges with other nodes, which, in turn, helps platforms find more profitable matching solutions. However, a second fundamental

difference in how flexibility arises on platforms is due to the fact that platforms cannot compel agents to be flexible; rather they offer incentives to encourage flexibility. In contrast to the manufacturing setting, where a central decision maker configures flexible edges deterministically, we thus model flexibility in two stochastic stages. In the first, agents opt-in to be flexible, and in the second, edges realize based on the agents’ choices *and* additional conditional randomness.

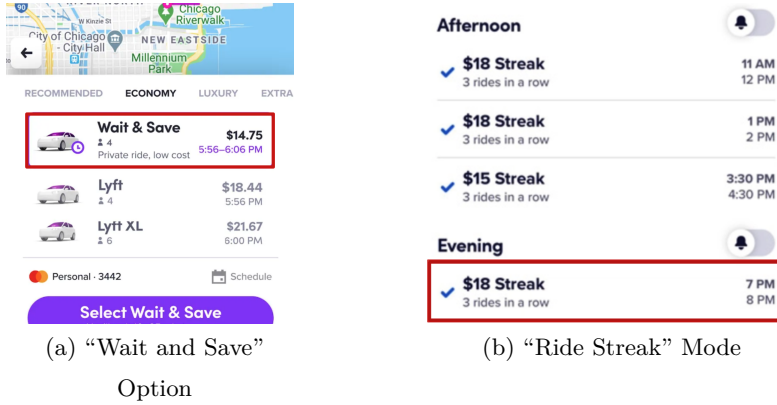


Figure 2 Examples of flexibility incentives on demand and supply sides of Lyft, a ride-hailing platform.

Another fundamental aspect of platform flexibility, and the main focus of this paper, is that it is really two-sided. As detailed in Table 1, different platforms have different levers to promote flexibility among agents on both market sides. Consider, for example, Lyft’s incentives for drivers and riders. In addition to the above-described Wait & Save option, Lyft also provides “Ride Streak” driver bonuses to its drivers, see Fig. 2 (b). This bonus incentivizes drivers to work for longer on the platform and to decline rides from competitors like Uber. Suppose, for instance, that Lyft wanted to match a driver with a rider 10 minutes away; without the bonus, the platform may assume that the driver would not accept the ride, preferring to instead wait for a closer match, and therefore treat the driver-rider pair as non-compatible. However, given the Ride Streak bonus, the driver is more likely to accept the match despite the long pick-up time. Therefore, both drivers and riders become more “flexible” in our graph representation in the sense that they are incident to more edges and thus more “flexible” in Lyft’s matching optimization. In Appendix A we discuss in greater detail how other matching platforms deploy incentives on both market sides and thereby enhance the likelihood of compatible connections between demand and supply.

The examples illustrate that flexibility can simultaneously exist on both the demand and supply sides, which raises the question of how flexible agents on both sides interact with each other. Specifically, what flexibility structure is best for matching? Is it more effective to concentrate flexibility on one side of the platform, or is it better to invest in both sides? Despite the significant investments through which platforms create flexibility on both the demand and the supply side, the interaction

Industry	Platform(s)	Demand side lever	Supply side lever
Ride-hailing	Lyft	Wait and save	Ride streak
Food delivery	Uber Eats	No rush delivery	Surge incentives
Freelancing	Upwork	Project catalog	Upwork academy

Table 1 Examples of two-sided platforms that use flexibility incentives on both the supply and demand sides. These incentives are designed to increase the likelihood that agents on one side are compatible with those on the opposite side of the market.

of flexibility on both sides is not well-understood. Indeed, we know of no work in the literature that examines the interaction of two-sided flexibility on platforms. And, in practice, platforms usually have different teams managing flexibility incentives on each market side, with each team focusing on a single lever and using experimentation to determine the optimal incentive level. Such a one-sided experimentation-driven approach neither reveals nor exploits the interaction of different flexibility incentives, and we will show that it can come at a great cost.

Motivated by this gap in the literature, we study how a given budget of flexibility should be allocated across the two sides of a platform. Our focus on the allocation question differs from traditional studies of flexibility that usually focus on just one flexibility lever, rather than their interactions. Since Table 1 shows that two-sided flexibility can arise in a variety of settings, we focus on highlighting general effects that are likely relevant to any matching platform. We develop a parsimonious matching model to identify a platform’s optimal flexibility investment on both market sides. Our matching problem is represented as a bipartite random graph, where *flexible nodes* (on either side) have a higher chance of forming connections with the other side of the graph compared to *regular nodes*. The platform’s objective is to maximize the expected number of matches in a maximum matching. We study how a fixed flexibility budget should be allocated, and whether and when platforms should invest in flexibility on both market sides.

Our results show that the choice of flexibility allocation has a significant impact on the performance of a two-sided matching platform. Even with a fixed flexibility budget, the matching probability (and consequently the profit of a matching platform) can vary significantly depending on how the budget is allocated between the two sides of the platform (see Fig. 14). Moreover, by comparing two natural flexibility allocation strategies: (1) the one-sided allocation, which places flexibility only on one side, and (2) the balanced allocation, which evenly distributes half of the flexibility budget to both sides, we find that either of these allocations can improve the matching size by more than 8% compared to the other (see Fig. 5). Hence, matching platforms with flexibility levers on both sides may pay a high price if they only optimize their flexibility budget but not its allocation.

Despite the impact of the flexibility allocation, optimizing it poses nontrivial difficulties. Even in a simple and symmetric matching model, the geometry of the maximum matching size (as a function

of the flexibility allocation) reveals saddle points in which a platform might get stuck. In particular, the current practice of many platforms, wherein separate teams optimize separate flexibility levers on different market sides, might converge to such saddle points. Near these saddle points, both teams mistakenly perceive themselves to be at an optimum, as flexibility should neither be increased nor decreased on either market side; however, the platform would benefit from jointly reducing flexibility on one side while increasing it on the other. These structural insights are unique to our study of two-sided flexibility, and our numerical results show that they generalize beyond our particular models. We show that these geometries and the dominance of different flexibility allocations are driven by an interplay of two opposing effects: *flexibility cannibalization* and *flexibility asymmetry*. These effects lend strength to the one-sided and the balanced allocations respectively, and they allow us to outline the parameter regimes where each effect and the corresponding flexibility allocation dominate. In identifying these different behaviors, and their first-order impact on performance, our results underscore the need to understand the interactions of different flexibility levers to enable more efficient market designs.

1.1. Contributions

Our work initiates the study of two-sided flexibility in platforms. It characterizes the interactions between different flexibility levers through a parsimonious matching model and allows us to study different questions regarding the optimal allocation of flexibility.

Optimal flexibility structures. Our study of one-sided and balanced flexibility allocations reveals that either structure can dominate the other. In Sections 3 and 4, we introduce two key effects – *flexibility cannibalization* and *flexibility asymmetry* – that respectively drive the dominance of the one-sided and balanced allocations. Intuitively, flexibility cannibalization is a waste of flexibility in the balanced allocation: as flexible nodes form edges with each other, their degree increases while their incident edges are wasted since each flexible node can only be matched once. In contrast, flexibility asymmetry arises in the one-sided allocation, where regular nodes on the same side as the flexible nodes cannot have any flexible neighbors and are thus much less likely to form any edges at all when compared to regular nodes on the opposite side. The asymmetry can result in a large number of degree-0 nodes in the one-sided allocation, leaving the isolated nodes unmatched. In Section 3 and 4, we characterize the parameter regimes where these effects are most pronounced, and in Section 5 we identify the dominant allocation across all parameters. Our structural insights have profound implications for platform experimentation, which we explore in Section 6. There, we highlight a potential inefficiency when the supply and demand sides conduct independent searches for the optimal flexibility incentives. Beyond the matching model considered in Section 2, Section 7 demonstrates the robustness of our findings in models that exhibit spatial structures and imbalanced market sizes.

Analyses of sparse bipartite random graphs. Our main technical contributions lie in analyzing the asymptotic maximum matching sizes in sparse bipartite random graphs with heterogeneous node types. Characterizing the asymptotic size of maximum matchings in random graphs is a long-studied but notoriously challenging area in extremal combinatorics. To compare the maximum matching sizes of different flexibility designs, we develop three distinct techniques. In Section 3 we design a careful coupling between realizations under the balanced and the one-sided flexibility allocations and show, for certain parameters, that flexibility cannibalization leads to a smaller matching size for the balanced allocation. Then, in Section 4 we apply concentration bounds for parameters where flexible nodes have high average degrees. In such settings, both allocations match almost all flexible nodes, but the balanced allocation is better at matching regular ones. Finally, in Section 5 we analyze the Karp-Sipser (KS) algorithm (Karp and Sipser 1981) to explicitly characterize the asymptotic matching probability in the so-called subcritical regime. Our KS-style analysis innovates upon prior works in that we (i) analyze a graph with heterogeneous node types, and (ii) explicitly compute the asymptotic matching probability with a provable level of precision in order to compare different flexibility allocations in computer-aided proofs.

1.2. Related Work

Flexibility in operations. Flexibility has a long history in operations with early works, dating back to Buzacott and Yao (1986) and Fine and Freund (1990), focusing on the ability of a manufacturing system to produce multiple types of products. Most early works in this literature have focused on determining the optimal amount of flexible manufacturing capacity (Fine and Freund 1990, Van Mieghem 1998, Netessine et al. 2002, Chod and Rudi 2005), thus optimizing over a single dimension on the supply side. In contrast, our decision also involves the demand side. More importantly, we identify not just the optimal flexibility investment, but also structural properties that arise from the interplay of flexibility on both sides and can cause potential pitfalls in practice.

In our focus on structural insights, our study relates more closely to those works in process flexibility that aim to identify the optimal flexibility design rather than the optimal amount of flexibility. The seminal work of (Jordan and Graves 1995) first introduced the “long chain”, which enables a small amount of flexibility ($2n$ carefully placed edges in a manufacturing system with n plants and n types of products) to yield almost all the benefits of a perfectly flexible system (one with all n^2 edges). Since then, a vast literature has studied process flexible designs and the value thereof for manufacturing and service systems (Iravani et al. 2005, Akşin and Karaesmen 2007, Chou et al. 2011, Simchi-Levi and Wei 2012, Chen et al. 2015, Désir et al. 2016). Effective flexibility designs have also been investigated in staffing (Wallace and Whitt 2005), queuing (Tsitsiklis and Xu 2017), and network interdiction (Ang and Feng 2024), among other settings. A key distinction between our work

and this stream of work lies in the structure of our flexibility levers: as most contemporary matching platforms involve stochastically formed edges that connect the supply and demand sides, we cannot model flexibility as a fixed compatibility design. Instead, platforms use various incentive levers to increase the likelihood of compatibility between the supply and demand sides of the market. As such, our approach optimizes over the fraction of flexible nodes on each side, rather than optimizing over specific edges, and requires a fundamentally different toolkit.

Our work also relates to papers that study flexibility on online marketplaces, though they focus on flexibility on a single side. In ride-hailing services, prior works study supply-side levers such as driver repositioning incentives (Ong et al. 2021) or a priority mode (Krishnan et al. 2022), and demand-side levers such as waiting mechanisms (Freund and van Ryzin 2021) or subscriptions Berger et al. (2023). More explicitly focused on demand-side flexibility, some works study opaque selling Elmachtoub et al. (2019) and flexible time windows (Zhou 2021) in online retail. Our work differs from all of these in that we focus on the interplay of two different flexibility levers.

In-organization Incentives. A reasonable interpretation of our structural results is that modern platforms are unlikely to find the optimal flexibility allocation if they optimize over two sides independently (see Section 6). Nonetheless, given the organizational structure of many platforms, with separate verticals working on the supply and the demand side, jointly experimenting and thus optimizing over levers on different market sides is uncommon. This misalignment relates to a stream of literature that identifies conflicting organizational incentives, e.g., the so-called marketing-operations alignment. There, organizations may face inefficiencies due to two departments (marketing and operations) having opposing incentives (Shapiro 1977). Solutions for marketing-operations conflicts focus on aligning incentives, including through internal integration of different functional teams within an organization (Weir et al. 2000), increasing the interface between manufacturing and marketing management (Hausman et al. 2002), and achieving a strategic alignment between external positioning and internal arrangement (Henderson and Venkatraman 1999). In our work, the separate verticals do not have misaligned incentives. Instead, the inefficiency arises from a lack of visibility, i.e., without joint experimentation, both teams lack visibility over the interplay between the two flexibility decisions.

Random graphs. Our technical contribution consists of different asymptotic analyses of the maximum matching size in sparse random graphs. A classical tool for these types of analyses is the Karp-Sipser (KS) algorithm (Karp and Sipser 1981), which is asymptotically optimal for the canonical maximum matching problem in sparse Erdős–Rényi random graphs with n nodes and a uniform edge probability c/n between any two nodes (for constant c as $n \rightarrow \infty$). Moreover, it gives rise to a system of nonlinear equations that characterize the asymptotic matching size. Since then, decades of research have extended this type of analysis to characterize the expected size of a maximum matching in random graphs with different generating processes (Aronson et al. 1998, Bohman and Frieze 2011,

Zdeborová and Mézard 2006, Balister and Gerke 2015). This is a notoriously difficult problem with each of these papers, like ours, only extending the analysis to new special cases. The closest setting to ours is the “configuration model” studied by Balister and Gerke (2015); however, their model does not capture our setting with flexible and regular nodes.¹ Moreover, beyond the canonical setting, the KS-style analyses often encounter fundamental limitations as the average expected degree of a node exceeds e , the Euler’s number (Bollobás and Brightwell 1995, Mastin and Jaillet 2013). Our work primarily differs from this literature in that our ultimate goal is to compare the maximum matching sizes under different flexibility allocations rather than to just characterize these quantities. To do so, we employ two approaches: (1) we identify parameter regimes where the matching sizes under different allocations are so different that we can compare them without characterizing them explicitly (Theorems 1 and 2); (2) we extend the KS-style analysis to some parameter regimes of our types of random graphs and use the resulting characterization in a proof that requires continuity arguments and a computer-aided grid search. Despite computer-aided proofs having a long tradition in combinatorics, including proofs of the four-color theorem (Appel and Haken 1977, Robertson et al. 1996), we know of no other papers with provable comparisons of the limiting behavior of different random graphs that rely on these sets of tools. In that regard, Gamarnik et al. (2006) may be closest to our approach, though they only compute a single explicit solution to a nonlinear equation (to compute the size of a largest independent set), whereas our grid search requires us to solve, within provable tolerance, approximately $\approx 6 \times 10^6$ systems of nonlinear equations.

2. Model

We study two-sided flexibility in platforms through a model of maximum matching in a random bipartite graph G , wherein nodes on both sides are either *flexible* or *regular*. Here, we formally introduce our parsimonious model, which we analyze throughout Sections 3–6. Section 7 and its appendices will study closely related variants of our main model and show how our findings apply more broadly.

Random Graph Generation. We begin by describing the random bipartite graph G through which we model flexibility. Denote the set of nodes on the left-hand side and right-hand side of G by V_l and V_r , respectively, and let $V = V_l \cup V_r$. Each node on one side represents a demand agent (e.g., a rider) and each node on the other represents a supply agent (e.g., a driver). We assume that there are $n \in \mathbb{N}^+$ nodes on each side² and index them such that $V_l = \{v_1^l, \dots, v_n^l\}$ and $V_r = \{v_1^r, \dots, v_n^r\}$; $[n]$ denotes the set $\{1, \dots, n\}$. Whether a node is *flexible* or *regular* is determined by the decision

¹E.g., our model, but not theirs, allows two nodes with positive expected degree to have 0 probability of being adjacent.

²While we focus on balanced bipartite graphs in most of the paper, we also consider imbalanced markets in Section 7.3.

variable $\mathbf{b} = (b_l, b_r) \in [0, 1]^2$, where b_l and b_r respectively specify the probability that a node on the left-hand side and right-hand side opts into being *flexible*. Formally, for all $i \in [n], k \in \{l, r\}$ we independently sample a Bernoulli random variable $F_i^k \sim \text{Bernoulli}(b_k)$ and node $v_i^k \in V_k$ is *flexible* if $F_i^k = 1$; otherwise, it is *regular*.

We model compatibility, i.e., the presence of an edge (v_i^l, v_j^r) , as an independent Bernoulli random variable R_{ij} , such that the edge realizes if and only if $R_{ij} = 1$. In line with the examples in the introduction, we want edges with flexible nodes to be more likely to exist. Therefore, the probability that $R_{ij} = 1$ must be increasing in F_i^l (the left node is flexible) and F_j^r (the right node is flexible). We focus on the *sparse* random graph regime, where the expected degree of each node remains constant as the size of the graph n scales large.³ Specifically, we take non-negative parameters $\alpha^f > \alpha$ as given and define $p_n^f = \alpha^f/n$ and $p_n = \alpha/n$. Then, the probability of an edge forming between two regular nodes is $2p_n$, the probability of an edge between two flexible nodes is $2p_n^f$, and the probability of an edge between a flexible and a regular node is $p_n + p_n^f$. Formally, this can be written as

$$\mathbb{P}[R_{ij} = 1 | F_i^l, F_j^r] = 2p_n + (F_i^l + F_j^r) \cdot (p_n^f - p_n), \forall i, j \in [n].$$

Intuitively, α and α^f control how likely regular and flexible nodes are to be compatible with nodes on the other side, which is why we have $\alpha^f > \alpha$. We illustrate the resulting edge probabilities in Fig. 3. This setting is symmetric, as flexibility on either side contributes equally to form an edge, with such contributions being additive and independent of i and j . This additive edge probability is a careful modeling choice: indeed, note that the expected total number of edges in the graph is given by $n^2(2p_n + (b_l + b_r)(p_n^f - p_n))$. This is a function of $B = b_l + b_r$, which can be interpreted as the total “flexibility level” in the platform. Therefore, the expected number of edges in the graph is invariant to (b_l, b_r) for fixed B – it only depends on the total flexibility, not how we allocate it.⁴ As discussed later, this feature allows us to investigate effects that are driven by the *distribution* of edges within a graph rather than the *number* of edges.

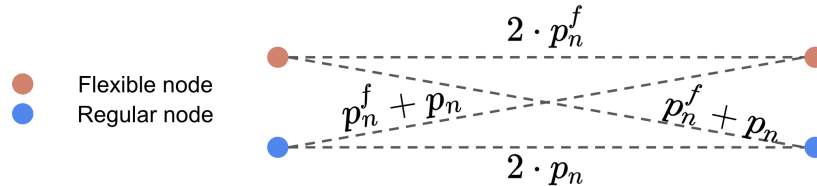


Figure 3 Illustration of the edge probabilities between possible types of nodes.

³Erdős and Rényi (1966) proved for $c > 1$ that a random graph with n nodes and i.i.d. edge probability $c \cdot \log(n)/n$ almost surely possesses a perfect matching as $n \rightarrow \infty$. Thus, subsequent studies (Karp and Sipser 1981, Balister and Gerke 2015) often focus on the case where the edge probability is in $\mathcal{O}(1/n)$ and each node’s expected degree is $\mathcal{O}(1)$.

⁴In Section 7.2, we consider a spatial setting that relaxes this invariance assumption.

Maximum Matching. In the resulting $n \times n$ random bipartite graph G , we use the random variable $\mathcal{M}_n(b_l, b_r)$ to denote the size of a *maximum matching*. A matching is a set of edges in the bipartite graph such that each node can be in at most one edge, and a maximum matching contains the largest possible number of edges across all matchings. We define the *matching probability* $\mu_n(b_l, b_r)$ as the expected fraction of nodes that are part of a maximum matching, i.e., $\mu_n(b_l, b_r) = \mathbb{E}[\mathcal{M}_n(b_l, b_r)/n]$. Maximizing $\mu_n(b_l, b_r)$ is a good parsimonious model for the objective of a matching platform that tries to make as many matches as possible. We are interested in the asymptotic behavior of $\mu_n(b_l, b_r)$ with respect to (b_l, b_r) as $n \rightarrow \infty$, a conventional scale of interest in the study of random graphs. We denote this asymptotic quantity by $\mu(b_l, b_r) := \limsup_{n \rightarrow \infty} \mu_n(b_l, b_r)$, which is equal to $\lim_{n \rightarrow \infty} \mu_n(b_l, b_r)$ when the latter exists. By focusing on the expected size of a maximum matching instead of simplified matching heuristics (e.g., greedy), we guarantee that our results are truly driven by the interactions of two-sided flexibility and not by artifacts of suboptimal matching schemes. At the same time, this introduces significant analytical challenges since the asymptotic size of a maximum matching is notoriously difficult to compute, with an active area of research identifying special cases for particular sparse random graphs of interest (see Section 1.2). Some of our results can be seen as advancing that area as our model creates a new special case that is of particular interest to matching platforms.

We complement our theoretical results on $\mu(b_l, b_r)$ with simulations that compute the empirical matching probability for given (b_l, b_r) . Provided with s samples of random graph that yield maximum matching sizes $\mathcal{M}_n^1(b_l, b_r), \mathcal{M}_n^2(b_l, b_r), \dots, \mathcal{M}_n^s(b_l, b_r)$, we compute the empirical mean as

$$\mu_{n,s}^{\text{EMP}}(b_l, b_r) := \frac{\sum_{s'} \mathcal{M}_n^{s'}(b_l, b_r)}{s \cdot n}.$$

Since the samples are independently and identically distributed (i.i.d.), the Law of Large Numbers (LLN) implies that $\mu_{n,s}^{\text{EMP}}(b_l, b_r) \rightarrow \mu_n(b_l, b_r)$ almost surely as $s \rightarrow \infty$. In our experiments, unless stated otherwise, we use $n = 100, s = 10000$ and omit the dependency of $\mu_{n,s}^{\text{EMP}}(b_l, b_r)$ on n and s for brevity.

Objective. Our work examines whether and when platforms should invest in flexibility across both market sides. As we are particularly interested in the flexibility allocation problem (i.e., what is the best way to allocate a given amount of flexibility), most of the paper assumes a fixed flexibility budget $B = b_l + b_r \geq 0$ and compares two different allocations (b_l, b_r) of that budget: the *one-sided* allocation does not make use of flexibility across both market sides and instead invests the entire budget on one side, whereas the *balanced* allocation allocates the flexibility budget equally on both sides.⁵

⁵We could study all allocations such that $b_l + b_r = B$ instead of limiting ourselves to the balanced and one-sided allocations. However, (i) these are the two most natural choices given the symmetry of the problem, (ii) these allocations have nice symmetry properties that simplify our already arduous analysis, and (iii) our numerical results suggest, as displayed in Figure 4, that the optimal allocation is always either the one-sided or the balanced allocation.

DEFINITION 1. For a given budget $B \in (0, 1]$, the flexibility allocation $\mathbf{b} = (B, 0)$ or $\mathbf{b} = (0, B)$ is called the *one-sided allocation*, whereas $\mathbf{b} = (B/2, B/2)$ is called the *balanced allocation*.

At first sight, fixing the budget B may not seem realistic. However, the problem of deciding both b_l and b_r can be decomposed into the problem of choosing B and the allocation problem. Most of the paper focuses on the allocation problem, as our goal is to study the interplay between the two types of flexibility. Then, Section 6 will study the general problem where the platform can choose b_l and b_r to maximize profit.

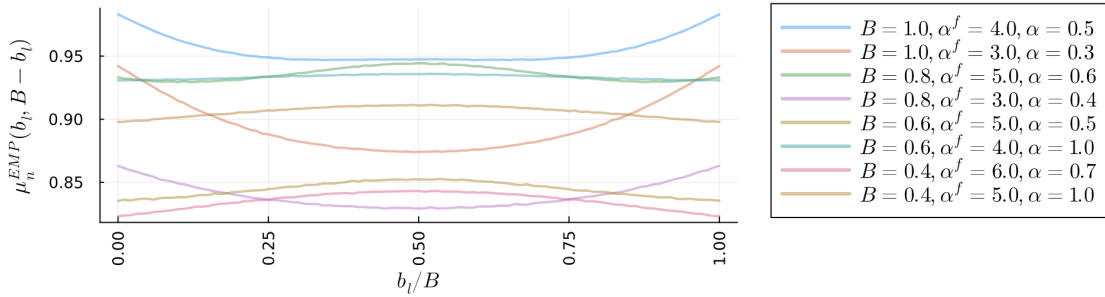


Figure 4 Illustration of $\mu_n^{\text{EMP}}(b_l, B - b_l)$ with respect to b_l/B for varying values of B, α^f and α .

Surprisingly, depending on the parameters, either of the two allocations can lead to a significantly higher matching probability than the other (see Figures 4 and 5). Since the expected number of edges in our model is invariant to different allocations of a fixed budget B , the differences between $\mu(B, 0)$ and $\mu(B/2, B/2)$ must be driven by the *distribution* of edges within a graph rather than the *number* of edges. This occurs because a maximum matching does not contain all edges in the graph and some allocations of flexibility yield many realized edges that do not produce additional matches. Our work uncovers the effects that determine when each flexibility allocation is particularly conducive to matching and thus helps realize the significant efficiency gains from the optimal flexibility allocation.

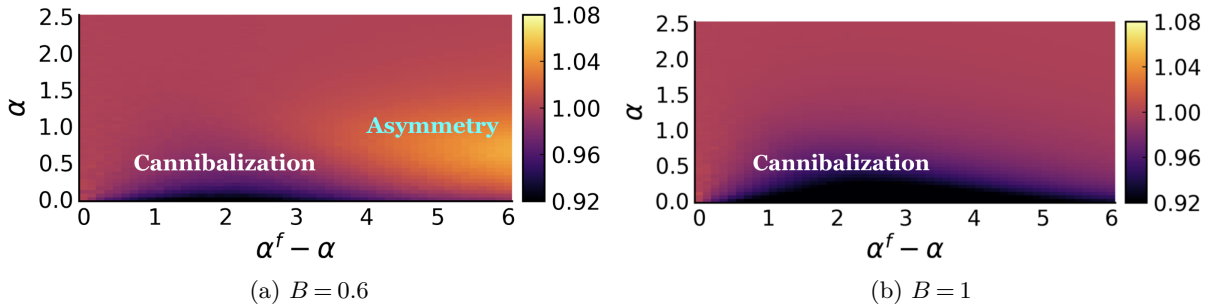


Figure 5 The heatmaps present values of $\frac{\mu_n^{\text{EMP}}(B/2, B/2)}{\mu_n^{\text{EMP}}(B, 0)}$ for varying α and $\alpha^f - \alpha$ and highlight the parameter regimes where the ratio is highest or lowest due to the dominance of the flexibility cannibalization or the asymmetry effect.

Plans for the subsequent sections. In Sections 3 and 4 we describe two key effects – *flexibility cannibalization* (which favors the one-sided allocation) and *flexibility asymmetry* (which favors the balanced one). Together, they guide the search for the optimal flexibility allocation. We provide intuitions for the types of platforms on which the effects emerge and formalize them by characterizing the parameter regimes where they are most consequential. Specifically, in Section 3, we exploit the flexibility cannibalization effect to show that the one-sided dominates the balanced allocation when $B = 1$ and $\alpha = 0$, regardless of the value of α^f . In contrast, we show that when $B < 1$ and α is a small positive value, flexibility asymmetry emerges, and the balanced allocation may yield a significantly larger maximum matching size, especially when α^f is large (see Section 4). Then, in Section 5 we adapt classical approaches in random graph theory to further compare different allocations. We prove that the Karp-Sipser algorithm characterizes the asymptotic matching size for special cases of our bipartite graph model. However, it faces fundamental limitations in providing theoretical results beyond the cases where α^f and α are small.⁶ Nonetheless, our analysis provides us with a surrogate function $\mu^{\text{KS}}(b_l, b_r)$ that offers a more complete numerical picture and allows us to quantify the difference between the one-sided and the balanced allocations across varying B, α^f and α .

Subsequently, in Section 6 we incorporate the cost of flexibility to find the flexibility designs that optimize over both the budget B and its allocation. We identify geometric properties of $\mu(b_l, b_r)$ and highlight their managerial implications for platform experimentation. Last but not least, in Section 7, we show that our findings are robust under different matching platform models. We conclude with open directions for future research in Section 8.

3. Flexibility Cannibalization

In the balanced allocation, flexible nodes on one side may form edges with flexible nodes on the other side, despite such edges likely being wasteful as we would prefer the flexible nodes to be paired with harder-to-match regular nodes: we call this the flexibility cannibalization effect. To understand it, recall that a feasible matching includes at most one of the edges incident to any given node. As such, flexibility designs should strive to avoid having many edges incident to the same node, many of which would be wasted. And, as the expected total number of edges is fixed given B , wasting edges can lead to fewer matches. The left side of Fig. 6 illustrates how flexible nodes tend to have a higher average degree in the balanced allocation than in the one-sided allocation. In the balanced allocation, it shows that edges concentrate in the subgraph of flexible nodes. The right side of the figure shows that this may create edges that are incident to the same flexible nodes, which *cannibalize* each other while leaving many regular nodes unmatched.

⁶Prior works had shown comparable results for other classes of sparse random graphs (see Section 1.2).

This intuition is confirmed with a simple computation: in expectation, the average degree of flexible nodes in allocation $(b_l, B - b_l)$ is $(\alpha^f + \alpha) + (\alpha^f - \alpha) \cdot 2b_l(B - b_l)/B$. The first term, $(\alpha^f + \alpha)$, is independent of b_l , whereas the term $(\alpha^f - \alpha) \cdot 2b_l(B - b_l)/B$ captures the contribution of edges between flexible nodes. This contribution is maximized when $b_l = B/2$, i.e., in the balanced allocation, which, therefore, is particularly likely to have edges incident to flexible nodes cannibalizing each other. Of course, this is just a description of the flexibility cannibalization effect, not proof that the balanced allocation is suboptimal. Before diving into the mathematical formalization to understand when this is the case, we now provide an example of how flexibility cannibalization may arise in practice.

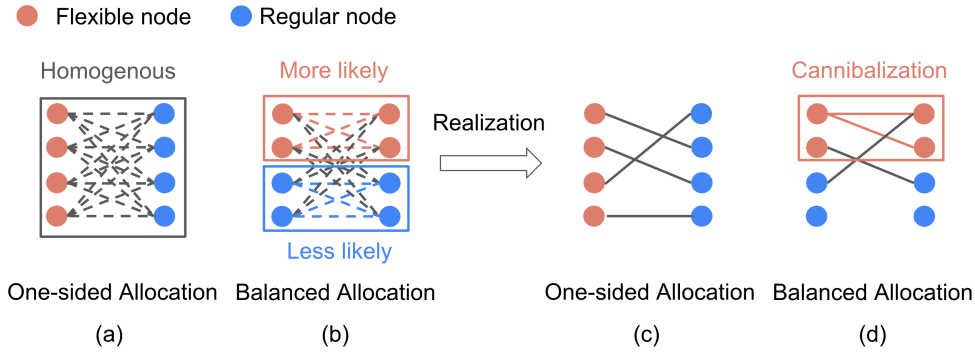


Figure 6 Illustration of flexibility cannibalization. Plots (a)-(b) compare edge probabilities and plots (c)-(d) illustrate possible realizations of one-sided and balanced allocations. In the balanced allocation, edges are more likely to realize in the upper subgraph of flexible nodes than in the lower subgraph. Consequently, despite plots (c) and (d) containing the same number of realized edges, (d) leads to fewer matches due to the cannibalization of edges in the upper subgraph.

Consider the example of the ride-hailing platform from the introduction and Fig. 2. It employs flexibility incentives on both market sides: “Wait and Save” on the demand side and “Ride Streak” on the supply side – this can be interpreted as the balanced allocation in our parsimonious model. Flexibility cannibalization occurs when flexible drivers and flexible riders end up clustered in the same area, which often happens naturally due to the stochastic nature of supply and demand. The platform then has no choice but to match flexible drivers with flexible riders, as there are no regular alternatives around. The platform also has difficulty finding feasible matches in other areas without flexible drivers and riders. In our model, this is analogous to edge realizations such that flexible nodes form edges with each other rather than with regular nodes in the balanced allocation. In that situation, the platform has to pay twice the cost of flexibility for each flexible-flexible match (Wait and Save discount and Ride Streak bonus), and this flexibility does not help with the harder-to-match regular nodes. In contrast, by incentivizing only one side of the market, the platform avoids ever ending up paying twice for flexibility, and all the flexibility is guaranteed to be used to help match regular nodes.

Returning to the theory, Theorem 1 constructs a coupling that exploits the flexibility cannibalization effect to prove the dominance of the one-sided allocation when $B = 1$ and $\alpha = 0$.

THEOREM 1. *If (i) $B = 1$ (“half of the nodes are flexible”), and (ii) $\alpha = 0$ (“no edges between regular nodes”), then $\mu(B, 0) \geq \mu(B/2, B/2)$.*

The conditions $B = 1$ and $\alpha = 0$ identify a parameter regime wherein, due to flexibility cannibalization, the one-sided allocation dominates for any α^f . However, while cannibalization also exists in regimes when $B < 1$ and $\alpha > 0$, Section 4 will show that another effect can counteract cannibalization. Before diving into that second effect, we use the rest of this section to showcase the proof of Theorem 1, wherein we develop a novel coupling technique to highlight the role of flexibility cannibalization.

Proof of Theorem 1. We prove that the one-sided allocation dominates the balanced one when $B = 1$ and $\alpha = 0$. Below, we state two lemmas and prove they imply the theorem, deferring the proofs and constructions for the lemmas to Section 3.1-3.2 and the corresponding appendices.

We first introduce a new bipartite random graph distribution, denoted G_n^b . This distribution is easier to analyze than the balanced allocation random graph (denoted $G_n(1/2, 1/2)$) but has the same asymptotic matching probability. In G_n^b , exactly $n/2$ nodes are flexible on each side (see Fig. 7). Each flexible node generates directed edges to the nodes on the other side (flexible or not), independently and with a probability p_n^f for each edge. This means that an edge between two flexible nodes can be generated in both directions (as shown in the right plot of Fig. 7). When computing a maximum matching in G_n^b we ignore the directionality of the edges and treat such double edges between nodes as just a single edge. We introduce G_n^b as its realizations can be more easily coupled with the random graph of the one-sided allocation. Denoting the size of a realized maximum matching in G_n^b by the random variable \mathcal{M}_n^b and that of $G_n(1/2, 1/2)$ by $\mathcal{M}_n(1/2, 1/2)$, we show nodes in G_n^b and $G_n(1/2, 1/2)$ have the same asymptotic matching probability.

LEMMA 1. *With the above construction, $\limsup_{n \rightarrow \infty} \mathbb{E} [\mathcal{M}_n(1/2, 1/2) - \mathcal{M}_n^b] / n = 0$.*

Now, we compare G_n^b to the random graph with one-sided allocation. We denote the latter by G_n^o and its maximum matching size by $\mathcal{M}_n(1, 0)$. The next lemma compares \mathcal{M}_n^b and $\mathcal{M}_n(1, 0)$ in a non-asymptotic way. This is the key step of this proof, relying on an intricate coupling of interest in its own right.

LEMMA 2. *With the above construction, $\mathbb{E} [\mathcal{M}_n^b] \leq \mathbb{E} [\mathcal{M}_n(1, 0)] \forall n$.*

In the following derivation, Lemma 1 gives us the second equality and Lemma 2 the inequality:

$$\mu(1/2, 1/2) = \limsup_{n \rightarrow \infty} \mathbb{E} \left[\frac{\mathcal{M}_n(1/2, 1/2)}{n} \right] = \limsup_{n \rightarrow \infty} \mathbb{E} \left[\frac{\mathcal{M}_n^b}{n} \right] \leq \limsup_{n \rightarrow \infty} \mathbb{E} \left[\frac{\mathcal{M}_n(1, 0)}{n} \right] = \mu(1, 0),$$

which completes the proof of Theorem 1. \square

3.1. Proof sketch of Lemma 1

As illustrated in Fig. 7, the graph G_n^b is a directed random graph that contains edges generated from left to right (denoted R_{ij}^l) and edges generated from right to left (R_{ij}^r). The edge probabilities are given by:

$$\mathbb{P}\left[R_{ij}^l = 1\right] = p_n^f, \forall i \in [n/2], j \in [n] \text{ and } \mathbb{P}\left[R_{ij}^r = 1\right] = p_n^f, \forall j \in [n/2], i \in [n]. \quad (1)$$

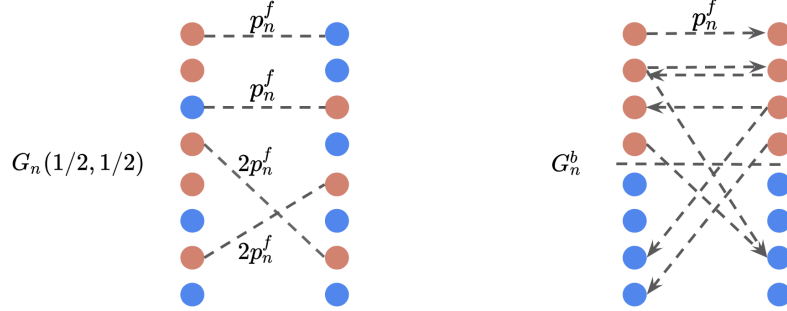


Figure 7 Illustration of $G_n(1/2, 1/2)$ and G_n^b . In G_n^b we assume that the top $n/2$ nodes on each side are “flexible” nodes that generate a directed edge towards any node on the opposite side with probability p_n^f .

G_n^b differs from $G_n(1/2, 1/2)$ in two ways: (i) G_n^b contains $n/2$ flexible nodes on each side of the bipartite graph, whereas every node in $G_n(1/2, 1/2)$ is flexible with probability $1/2$; (ii) in G_n^b an edge between v_i^l and $v_j^r, i, j \in [n/2]$, is generated from each side with probability p_n^f , instead of being generated only once with probability $2p_n^f$. It is intuitive that neither (i) or (ii) significantly change the asymptotic matching size: standard concentration bounds guarantee that (i) affects $o(n)$ nodes, and (ii) affects $\sum_{i,j \in [n/2]} (p_n^f)^2 = \sum_{i,j \in [n/2]} (\alpha^f/n)^2 \in \mathcal{O}(1)$ possible edges in expectation. In Appendix C.1.1, we formalize this intuition.

3.2. Proof sketch of Lemma 2

In our proof, we construct a coupling between *pairs* of realizations of G_n^b and of G_n^o to compare the maximum matching sizes therein. First, we show that this coupling is valid in the sense that the coupled realizations occur with the same probability in their respective graphs. Second, we show that the sum of the maximum matching size in the pair of realizations in G_n^b is smaller-equal to that in G_n^o for *any* realization. We present the key steps of our proof here and defer the complete proof to Appendix C.1.2.

Coupling the Realizations of Graphs. We partition the directed edges in a realization of G_n^b into sets X_1, X_2, X_3 and X_4 , depending on whether they are from left/right to top/bottom (see Fig. 8 (A)).

We couple each realization of edges, i.e., of sets X_1, X_2, X_3 and X_4 , with a second realization (B), also from G_n^b , that occurs with the same probability (Fig. 8 (B)). Essentially, we “flip” the edges

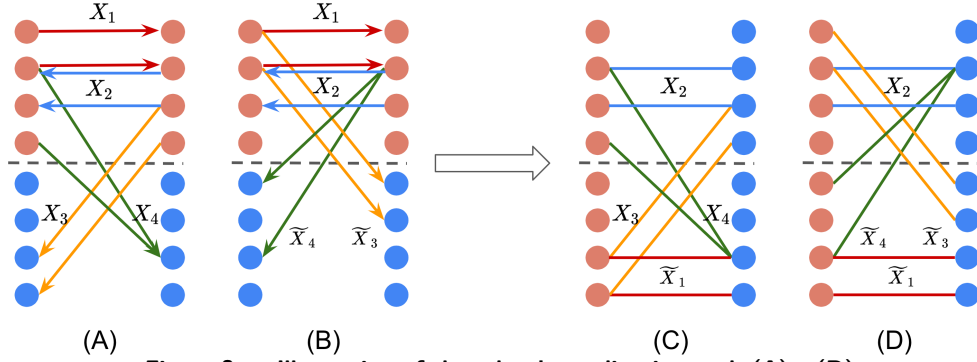


Figure 8 Illustration of the edges' coupling in graph (A) - (D)

in X_3 and X_4 across the vertical axis to obtain the sets \tilde{X}_3 and \tilde{X}_4 . Then, we couple (A) and (B) with two realizations, (C) and (D) (see Fig. 8 (C) and (D)), of G_n^o . There, we “flip” the edges in X_1 from the upper subgraph in (A) and (B) to the lower subgraph in (C) and (D). Intuitively, as flexibility cannibalization can happen in the upper subgraph of G_n^b , where the edges in X_1 and X_2 are concentrated, we want our coupling to “flip” the edges in X_1 to the less dense lower subgraph and thereby hopefully increase the number of matches. However, denoting by M_A, M_B, M_C, M_D the maximum matching sizes in the respective graphs, it is not always true that $M_A \leq M_C$ or $M_B \leq M_D$. Instead, we will show that $M_A + M_B \leq M_C + M_D$ holds for all X_1, X_2, X_3 , and X_4 , and thereby guarantee that $\mathbb{E}[\mathcal{M}_n^b] \leq \mathbb{E}[\mathcal{M}_n(1, 0)]$. We include the formal coupling in Appendix C.1.2.

Proving the Dominance of One-sided Allocation. Our proof concludes by showing that the required property $M_A + M_B \leq M_C + M_D$ indeed holds for arbitrary X_1, X_2, X_3 and X_4 , which shows that the flexibility cannibalization in the upper graphs of (A) and (B) indeed induces a lower number of matches. As illustrated in Fig. 9, in (A) we denote by sets $Y_i \subset X_i$ the edges that are part of a given maximum matching; similarly, in (B), we denote by sets $Y'_1 \subset X_1, Y'_2 \subset X_2, \tilde{Y}_3 \subset \tilde{X}_3$ and $\tilde{Y}_4 \subset \tilde{X}_4$ the edges that are part of a maximum matching. We then injectively map all edges of M_A and M_B (i.e., those in $Y_1, Y_2, Y_3, Y_4, Y'_1, Y'_2, \tilde{Y}_3$ and \tilde{Y}_4) into existing edges of (C) and (D) that also form a matching; this immediately proves $M_A + M_B \leq M_C + M_D$. We construct this mapping in two steps.

Step 1: mapping Y_1, Y_2, Y'_1 and Y'_2 . We start by directly copying the matched edges from Y_1, Y_2, Y'_1 and Y'_2 into (C) and (D), following the coupling rules. This corresponds to the red, blue, pink, and navy edges in Fig. 9.

Step 2: mapping Y_3, Y_4, \tilde{Y}_3 and \tilde{Y}_4 . The rest of the matched edges (the yellow and green edges) can also be mapped into (C) and (D), but this mapping is not static and depends on the matches that are already copied into the graphs. As the nodes in (C) and (D) that are matched through these copied edges can no longer be matched to any other node in the graphs, we denote the remaining nodes in (C) and (D) by \bar{C} and \bar{D} and the set of edges among these nodes by $E(\bar{C})$ and $E(\bar{D})$. Then, it suffices to show that we can injectively map all other matches (that we have not copied already) in

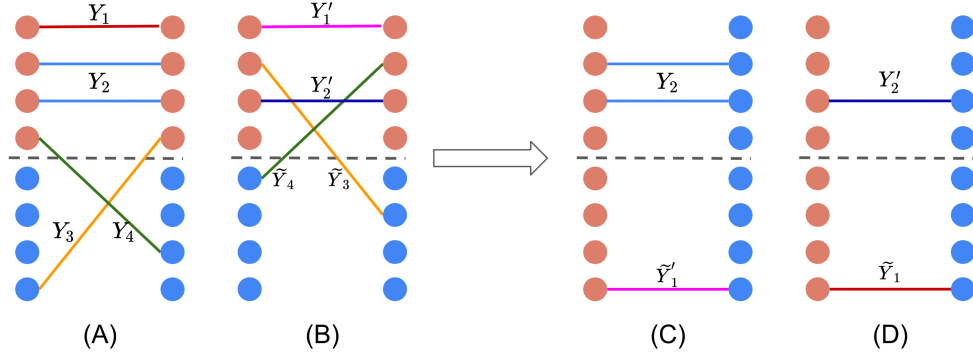


Figure 9 Illustration of the matches in (A) and (B), and the position they are copied into in (C) and (D).

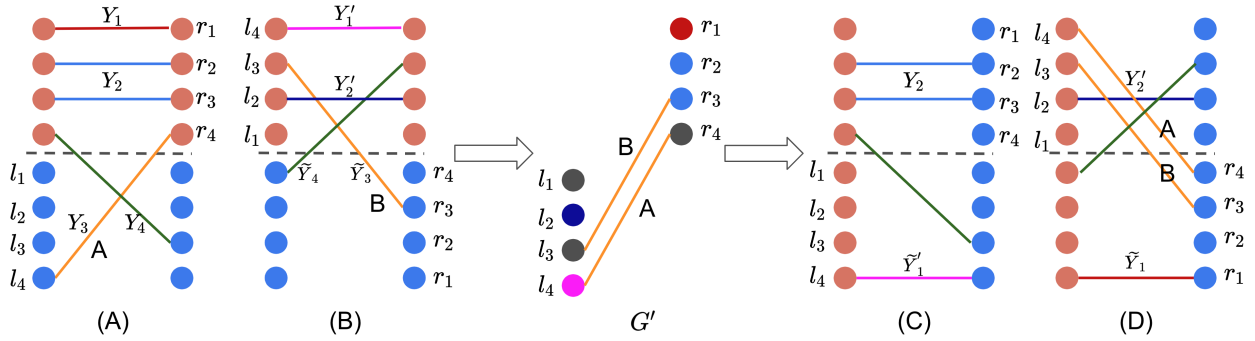


Figure 10 The plot illustrates the mapping of edges in Y_3 and \tilde{Y}_3 (the yellow edges) to (C) and (D) through the constructed graph G' . The labels indicate the correspondence between nodes/edges in G' and those in graphs (A)-(D). A second graph G'' can be constructed to map the edges in Y_4 and \tilde{Y}_4 (the green edges) into the indicated positions in (C) and (D).

(A) and (B) to $M(\bar{C}) \cup M(\bar{D})$, where $M(\bar{C})$ and $M(\bar{D})$ are respectively matchings that we construct in $E(\bar{C})$ and $E(\bar{D})$. We construct such a mapping for edges in Y_3 and \tilde{Y}_3 based on a $\frac{n}{2} \times \frac{n}{2}$ colored bipartite multigraph G' (see Fig. 10). G' includes all edges from Y_3 and \tilde{Y}_3 that occur in graph (A) and (B); we label edges in G' that come from Y_3 as type A edges and edges from \tilde{Y}_3 as type B edges (there can be two edges, one of type A and one of type B, between a pair of nodes in G'). We color the nodes in G' based on whether the corresponding nodes in (A) and (B) are incident to Y_1, Y_2, Y'_1 and Y'_2 . Analogous to G' , we create a second graph G'' that contains all the edges from X_4 that are part of maximum matchings in (A) and (B). We show that edges in G', G'' can be mapped into graphs (C) and/or (D) based on their types and the colors of their incident nodes so that, together with the already copied edges, they produce feasible matchings in (C) and (D). As a result, each edge from M_A and M_B can be found in a matching in either (C) or (D), implying that $M_A + M_B \leq M_C + M_D$. Thus, $\mathbb{E}[\mathcal{M}_n^b] \leq \mathbb{E}[\mathcal{M}_n(1, 0)], \forall n$ when $\alpha = 0$. We formalize these constructions in Appendix C.1.2.

4. Flexibility Asymmetry

Moving away from the parameter regimes in Theorem 1, we now study when the balanced allocation may dominate the one-sided one. This dominance is driven by a second effect, which we refer to as *flexibility asymmetry* and which is particularly strong for large α^f .

Unlike cannibalization, asymmetry is an effect that focuses on regular nodes. When $B < 1$ (i.e., less than half the nodes are flexible), any flexibility allocation has regular nodes on both sides. When the allocation is not perfectly balanced, regular nodes on the side of the graph with more flexible nodes — on the left in Figure 11 (a) and (c) — have fewer neighbors in expectation than regular nodes on the other side. This is most pronounced in a one-sided allocation. When $B < 1$ (so that there are regular nodes on both sides), it can be easily found that the $(1 - B)n$ regular nodes on the side of the graph where flexibility is allocated have an expected degree of 2α (all their potential neighbors are regular nodes). In contrast, the ones on the other side have an expected degree of $2\alpha + B(\alpha^f - \alpha)$, which grows with $\alpha^f - \alpha$. Therefore, the imbalance of the flexibility allocation creates an *asymmetry* in the random graph, where regular nodes on one side may be “easier” to match than regular nodes on the other. For example, for small α , the small expected degree of some regular nodes may cause many of those to be isolated and thus impossible to match. This intuition is confirmed in our next result: when $B < 1$ and $\alpha^f - \alpha$ is large, the balanced allocation provably yields the fewest isolated nodes across all possible allocations, while the one-sided allocation maximizes their number.

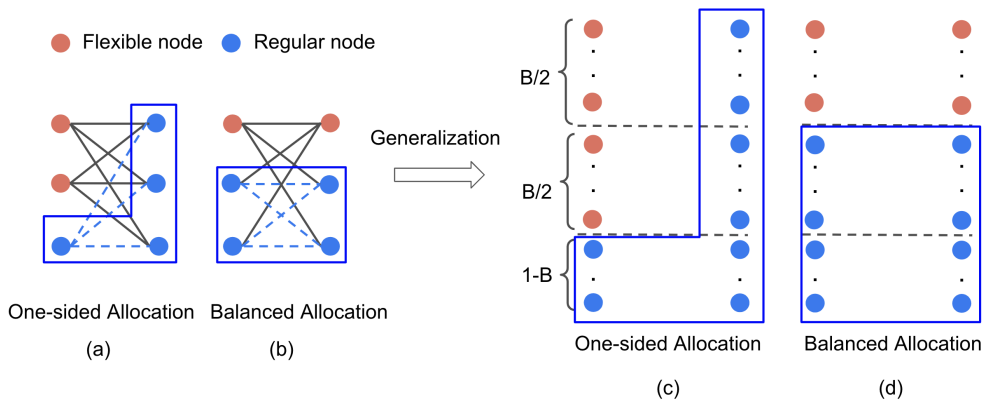


Figure 11 To gain intuition for the flexibility asymmetry effect, plots (a) and (b) assume that each flexible node is connected to all nodes on the other side of the graph, which resembles the case of α^f being large. A perfect matching in (a) requires the realization of one of the three dashed edges, while (b) requires one of four dashed edges to realize. This intuition holds at a larger scale: the expected number of edges in the subgraph of regular nodes is $(1 - B/2)^2 / (1 - B) > 1$ times greater for the balanced allocation in (d) than for the one-sided allocation in (c). Since the size of a maximum matching is close to the number of edges when α is small, the balanced allocation is more conducive to matching the regular nodes among themselves.

PROPOSITION 1. For any $B \in (0, 1)$, $\alpha \geq 0$ and $\alpha^f - \alpha > \frac{2}{1-B}$, the asymptotic fraction of degree-0 nodes (as $n \rightarrow \infty$) is minimized at allocation $(B/2, B/2)$ and maximized at $(B, 0)$

This shows that there may be an issue with the one-sided allocation, as isolated nodes cannot be part of a maximum matching, and that this issue arises when B is smaller than 1 (not many flexible nodes) and α^f is large (flexibility is strong). The fact that α^f must be large is intuitive: it weakens the cannibalization effect, as the high degree of flexible nodes makes the wastefulness of flexible-flexible edges a less pressing concern. However, the intricate combinatorial nature of a maximum matching is much more complex than simply counting the number of isolated nodes. To understand intuitively why asymmetry can reduce the matching probability in the one-sided allocation, consider an example when flexibility is so strong that flexible nodes can be matched with any node, as illustrated in Figure 11 (a) and (b). In that specific case, a simpler two-stage matching algorithm is optimal. First, we find a maximum match in the subgraph of regular nodes (marked in blue in the figure), and then we add the flexible nodes to make as many additional matches as possible. Interestingly, when α is small enough, regardless of the allocation, there are almost always sufficiently many regular nodes unmatched after the first stage for the second stage to add exactly Bn matches by matching all flexible nodes to available regular nodes. Therefore, when α is small enough, the allocation that maximizes the probability of a match is the one that is best in the first stage, i.e., the allocation that can maximize the probability of a match in the regular node subgraph. Interestingly, Figure 11 and its caption illustrate that the one-sided regular node subgraph is *asymmetric* and explain why asymmetric graphs lead to fewer matches as long as $\alpha > 0$. In other words, when flexibility is strong but limited, and when it is not too easy to match regular nodes with regular nodes, the best allocation is the one that enables the maximum number of regular-regular matches. The following theorem formalizes this intuition, but instead of taking α^f to infinity, we use similar ideas to find a range of parameters where the balanced allocation provably dominates.

THEOREM 2. If (i) $\alpha^f \geq 22$, (ii) $\alpha \in [0.01, 0.05]$, and (iii) $B \in [0.4, 0.8]$, then $\mu(B/2, B/2) > \mu(B, 0)$.

We can prove that the balanced allocation dominates in a parameter regime where the asymmetry effect is particularly strong: (i) flexible nodes must be especially easy to match ($\alpha^f \geq 22$); (ii) regular nodes should be hard – but not impossible – to match so that regular-regular matches matter ($\alpha \in [0.01, 0.05]$); (iii) B should not be close to 1 (otherwise, all allocations are equivalent because flexible nodes are sufficient to match everyone) and more than 0 (otherwise, all allocations are equivalent because there is no flexibility). Before discussing the proof of the theorem, we want to highlight that there are important applications in this parameter regime. For instance, the freelancing platform Upwork offers a digital learning program called “Upwork Academy” to train highly skilled freelancers

to handle a wide range of tasks. This type of flexibility is valuable in allowing the high-skilled freelancers to be matched with demanding customers who otherwise cannot be served. On the demand side, similarly, the platform uses a feature called “Project Catalog” to incentivize users to choose from a standardized pool of tasks that most freelancers can fulfill. Essentially, employing flexibility on both market sides allows the platform to match flexible agents on each side with “difficult” agents on the opposite side. With flexible agents on only one side of the platform, it can be difficult to match regular agents on that side of the platform. In particular, when some freelancers are well-trained but all customers are quite demanding, it becomes difficult for freelancers with a limited skill set to find a job. Similarly, when some customers have standard requests but no freelancers receive specialized training, it becomes difficult for the platform to serve the demanding customers.

Proof sketch of Theorem 2. Our proof (Appendix C.2.3) leverages the two-stage matching procedure to analyze $\mu(B/2, B/2)$: we first study the size of a maximum matching among the regular nodes (stage 1), and then quantify the additional matches that can be added using the flexible nodes (stage 2). This allows us to derive a lower bound on the number of matched nodes under balanced flexibility. Similarly, we derive an upper bound on the maximum matching size under one-sided flexibility by bounding the number of isolated nodes in the graph. We then prove the theorem by verifying that the upper bound is dominated by the lower bound in the specified parameter regime.

Lower bound on the number of matched nodes for balanced flexibility. For balanced flexibility, we lower bound the size of a maximum matching among the regular nodes, and then show that almost all flexible nodes can be matched afterward. As illustrated in Fig. 11 (d), in stage 1, the balanced allocation faces an equal number of regular nodes on both sides. We prove (Appendix C.2.2) the following bound on the maximum matching size in a $(1 - B/2)n \times (1 - B/2)n$ graph of regular nodes,⁷ denoted by random variable m_1 :

$$\text{LEMMA 3. } \mathbb{E}[m_1] \geq 2 \cdot (1 - B/2)n \left[1 - (1 - B/2)\alpha - e^{-2\alpha(1 - B/2)} \right] \text{ as } n \rightarrow \infty.$$

Intuitively, for small α the expected maximum matching size should be close to the expected number of edges because very few nodes have a degree more than 1. Our proof explicitly characterizes this, and lower bounds m_1 by subtracting the number of “redundant edges” (those incident to nodes with degree > 1) from the total number of edges. This allows us to derive the lower bound for $\mathbb{E}[m_1]$ in Lemma 3.

Upper bound on the number of matched nodes for one-sided flexibility. To upper-bound the matching size under one-sided flexibility, we simply quantify the expected number of isolated regular nodes on the side on which there is flexibility. As illustrated in Fig. 11 (c), since there are about $(1 - B)n$ regular

⁷While the number of regular nodes on each side of the graph is not deterministically $(1 - B/2)n$, it concentrates around this value as n scales large and we assume this deterministic number for the purpose of this proof sketch.

nodes on this side, about $(1 - B)ne^{-2\alpha}$ of these are isolated. It follows that at most $(1 - B)(1 - e^{-2\alpha})n$ of these regular nodes can be matched.

Combining the bounds. For the purposes of this proof sketch, we assume that all flexible nodes can be matched to regular nodes in stage 2 of the algorithm. Then, the number of matches under the one-sided allocation is at most $Bn + (1 - B)(1 - e^{-2\alpha})n$ whereas the number of matches under the balanced allocation is at least $Bn + \mathbb{E}[m_1]$. By verifying that

$$Bn + (1 - B)(1 - e^{-2\alpha})n < Bn + 2 \cdot (1 - B/2)n \left[1 - (1 - B/2)\alpha - e^{-2\alpha(1 - B/2)} \right] =$$

for $\alpha \in [0.01, 0.05]$ and $B \in [0.4, 0.8]$, we confirm that the balanced allocation creates more matches than the one-sided allocation in the stated regime. In Appendix C.2.3 we show that the gap in the above inequality is sufficiently large to account for the fact that, in the balanced allocation, some flexible nodes may not be matched in stage 2. We highlight that $\alpha > 0$ is necessary for this comparison as otherwise no regular nodes could be matched in stage 1 (under either allocation) and the two sides of the inequality would be equal.

5. Identifying the Right Allocation Across All Parameters

In this section, we analyze the properties of $\mu(b_l, b_r)$ for a broader range of parameters using the Karp-Sipser (KS) algorithm, a less intuitive but more classical tool in the study of sparse random graphs. As formalized in Algorithm 1 in Appendix C.3, the KS algorithm iteratively matches and prunes nodes with degree 1 until no such nodes remain; thereafter, it randomly selects edges to match. This algorithm has two advantages: first, its simple “greedy” structure makes it amenable to theoretical study, and prior works have described its behavior on random graphs. Second, it can be optimal in sparse settings. For example, it is always optimal if the graph is a tree and yields asymptotically optimal matchings for some classes of sparse random graphs (Karp and Sipser 1981, Balister and Gerke 2015). These two facts combined make it a valuable tool to study maximum matching in sparse settings. Though prior works do not encapsulate the random graphs we study (see Section 1.2), we show that the KS algorithm is amenable to our model. However, to formalize the additional complexity arising from the comparisons between different flexibility allocations, we additionally require computer-aided proofs. We include the derivations and proofs corresponding to this section in Appendix C.3.

Our analysis is based on the quantity $\mu^{\text{KS}}(b_l, b_r)$, which is constructed from a set of nonlinear equations (see Equation (11) and Theorem 8 in the appendix). Such equations are common in KS-based analyses to characterize the fraction of nodes that are a “target” or a “loser” (Karp and Sipser 1981). Whereas Karp and Sipser’s original analysis focused on a homogeneous Erdős-Rényi graph and thus relied on just 2 of these equations, ours requires 8 equations to determine the probability

for flexible or regular nodes on either side to be either a target or a loser. When $B = 1$, Theorem 3 below states the equivalence of $\mu(b_l, b_r)$ and $\mu^{\text{KS}}(b_l, b_r)$ for the one-sided and balanced allocations in almost all of the *subcritical regime*, classically defined (Aronson et al. 1998) as the setting where the average expected degree of a node, $\alpha^f + \alpha$ in our case, is smaller than Euler’s number e .

THEOREM 3. *When $10^{-4} < \alpha < \alpha^f, \alpha^f + \alpha < e$, and $\mathbf{b} = (1, 0)$ or $(1/2, 1/2)$, $\mu(b_l, b_r) = \mu^{\text{KS}}(b_l, b_r)$.*

Though Theorem 3 characterizes a region in which $\mu(\cdot, \cdot) = \mu^{\text{KS}}(\cdot, \cdot)$, this does not suffice to make formal comparisons between $\mu(1, 0)$ and $\mu(1/2, 1/2)$; since there are no closed-form solutions to these nonlinear equations, we need to show that we can solve the nonlinear equations characterizing $\mu^{\text{KS}}(b_l, b_r)$ to provable numerical precision for the region specified by the theorem (see (25) in Appendix C.3.3). This then allows us to compare $\mu(1, 0)$ and $\mu(1/2, 1/2)$ for these values of α^f and α . Moreover, we derive a continuity property of μ^{KS} in α^f and α , that lets us construct local lower bounds for $\mu(1, 0) - \mu(1/2, 1/2)$ (see (23) and (24)). We conclude by verifying in a computer-aided proof that these lower bounds exceed 0 across the parameters specified in the following theorem:

THEOREM 4. *$\mu(1, 0) > \mu(1/2, 1/2)$ when (i) $\alpha^f + \alpha < e$ and (ii) $10^{-4} < \alpha < 0.77\alpha^f - 0.16$.⁸*

Theorem 4 allows us to prove the dominance of the one-sided allocation for a wider set of parameters in which $\alpha^f + \alpha$ remains relatively small (recall that Theorem 1 allows for arbitrarily large α^f but requires $\alpha = 0$). Beyond the subcritical regime, KS-style analyses have fundamental limitations for two reasons: first, the asymptotic optimality of KS is not known for bipartite graphs beyond the subcritical regime (see Bollobás and Brightwell (1995), Mastin and Jaillet (2013)); and secondly, our computer-aided comparison of different flexibility allocations requires the nonlinear equations to have a unique set of solutions, which is known (Karp and Sipser 1981, Lemma 1) to require the subcritical regime.

Despite the analytical challenges in extending Theorem 3 and 4 to other parameter regimes, our numerical results (see Fig. 12) suggest that $\mu_n^{\text{EMP}}(b_l, b_r)$ approaches $\mu^{\text{KS}}(b_l, b_r)$ as $n \rightarrow \infty$ for a much wider set of parameters. We, therefore, use $\mu^{\text{KS}}(b_l, b_r)$ as a surrogate function to evaluate different flexibility allocations, not just the balanced and one-sided one, across a wider range of parameters. This is not doable with μ^{EMP} due to the heavy computations needed to evaluate it with high precision. Specifically, we conduct a grid search over $B, \alpha^f, \alpha, b_l, b_r$ with the set of parameters denoted S (details in Appendix C.3.6); we trust this to give a better estimate of the true asymptotic matching probability while also being computationally more efficient. We highlight the following observations:

⁸The boundary in condition (ii) arises from the ability for a computer-aided proof to verify the inequality within a reasonable runtime: for $\delta > 0$, we construct and compute a lower bound the value of $\mu(1, 0) - \mu(1/2, 1/2)$ within each set of $[\alpha^f, \alpha^f + \delta) \times [\alpha, \alpha + \delta)$ within the subcritical regime. Taking $\delta = 0.001$ yields the boundary in Theorem 4 (ii) and runs in about 20 hours.

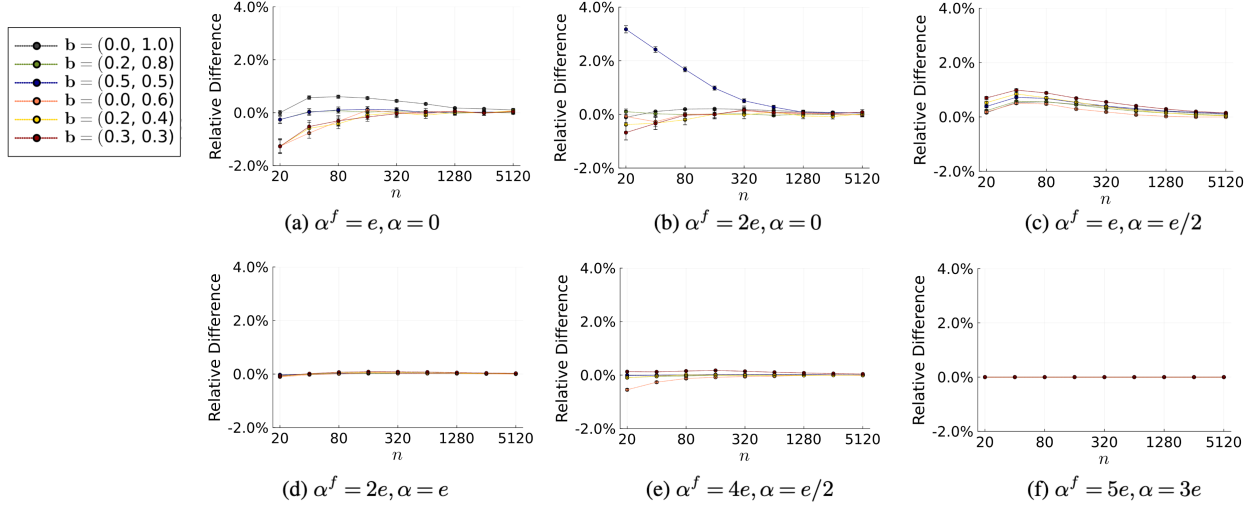


Figure 12 The plots present $(\mu^{\text{KS}}(b_l, b_r) - \mu_n^{\text{EMP}}(b_l, b_r)) / \mu_n^{\text{EMP}}(b_l, b_r)$ across varying (b_l, b_r) as n scales large.

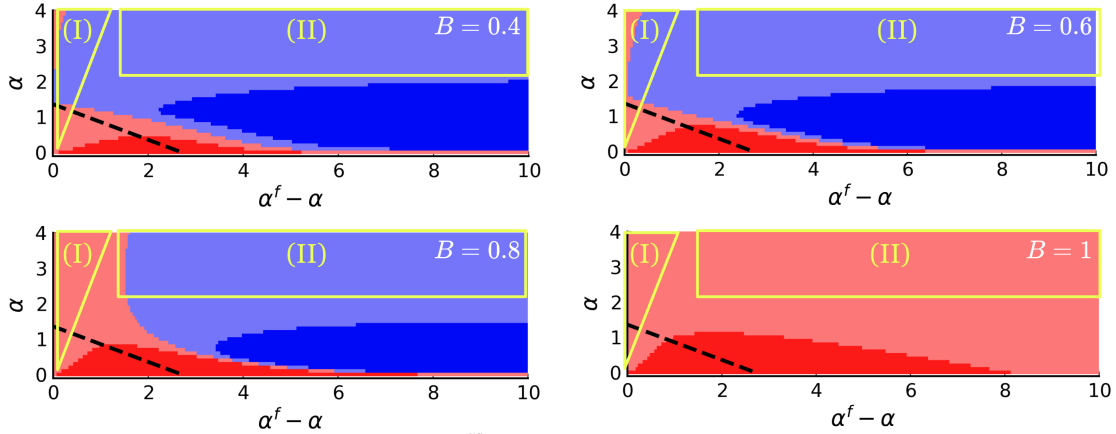


Figure 13 The plots present the values of $\frac{\mu^{\text{KS}}(B/2, B/2)}{\mu^{\text{KS}}(B, 0)}$ across varying α^f , $\alpha - \alpha^f$ and B : the ratio is smaller than 1 in the red region (light red if between 0.99 and 1) and greater than 1 in blue region (light blue if between 1 and 1.01). The dashed line highlights the boundary of the subcritical regime, and regions (I)-(II) indicate where the two allocations have comparable performances.

Either the one-sided or the balanced allocation is optimal. In line with the findings in Fig. 4, our more extensive numerical results show that, across our grid search, $\mu^{\text{KS}}(b_l, b_r)$ is always maximized by one of the one-sided or the balanced allocation. It thus supports our focus on comparing these two. Intuitively, the one-sided allocation (i) minimizes the cannibalization effect by eliminating potential flexible-to-flexible edges, but (ii) maximizes the asymmetry effect by making it harder to match regular nodes with each other. For the balanced allocation, these two are exactly reversed. Our numerical findings suggest an optimal allocation always minimizes one of the two effects.

In the subcritical regime, the one-sided allocation is better. In Theorem 4, we proved this result for most of the subcritical regime and $B = 1$. When $B < 1$, our computer-aided proof breaks because we cannot prove that the nonlinear equations in (11) have a unique set of solutions. However, we still find numerically that the one-sided allocation is better within the subcritical regime for all

tested values of B (see Fig. 13). This also matches our theoretical findings in that α^f cannot be too large in the subcritical regime, which naturally limits the effect of flexibility asymmetry (see Theorem 2). In particular, even though Proposition 1 shows that the balanced allocation may be minimizing and the one-sided allocation may be maximizing the fraction of isolated nodes in this regime, this is outweighed by the effect of flexibility cannibalization.

When $B = 1$ or $\alpha = 0$ the one-sided allocation is better. We find that $B = 1$ and $\alpha = 0$ are the special cases where the one-sided allocation always dominates,⁹ regardless of the value of α^f . Comparing this with our two-stage matching procedure in Section 4, we find that these are exactly the cases where the flexibility asymmetry effect dissipates. This also explains why the coupling technique presented in Section 3 is specific to $B = 1$ and $\alpha = 0$: for large α^f , Fig. 13 shows that the dominance of the one-sided allocation breaks down very close to the regime where $B = 1$ and $\alpha = 0$.

Characterizing when the flexibility allocation matters. Finally, our numerical results in Fig. 13 also allow us to characterize the regions in which the flexibility allocation is of second-order importance. In region (I), flexibility does not notably increase the edge probability as $\alpha^f/\alpha \approx 1$; thus, neither the budget nor the allocation of flexibility has a sizable effect. In region (II), with large α and α^f , almost all nodes are matched irrespective of the flexibility allocation. Thus, in (I) and (II), any allocation of a fixed flexibility budget results in a similar matching size. In contrast, in regions where flexibility cannibalization (moderate values of α and α^f) and flexibility asymmetry (small α , large α^f , and $B < 1$) are most prominent, the surrogate function identifies a larger gap between the one-sided and the balanced allocation. This mirrors our observation in Fig. 5 that either of the two allocations can dominate the other by at least 8% in these regions.

6. Managerial Implications for Platform Experimentation

Flexibility cannibalization and asymmetry can have important managerial implications. To highlight them, we extend our model slightly to study the geometry of a platform profit function that incorporates both the benefit and the cost of flexibility. Formally, we assume that the flexibility decision (b_l, b_r) incurs a linear cost of $c \cdot (b_l + b_r)$ for some constant $c > 0$. That is, we focus on the optimization problem

$$\max_{\mathbf{b} \in [0,1]^2} \mu(b_l, b_r) - c \cdot (b_l + b_r) \quad (2)$$

Such a linear cost model reflects a setting wherein the marginal cost of more agents becoming flexible is approximately constant. This simplicity allows us to underline our main point, but our high-level observations would likely translate to other cost structures. We use the notation $g(b_l, b_r) := \mu(b_l, b_r) - c \cdot (b_l + b_r)$ to refer to this objective function and $g^{\text{KS}}(b_l, b_r)$ to denote $\mu^{\text{KS}}(b_l, b_r) - c \cdot (b_l + b_r)$.

⁹For $\alpha = 0$, though hard to see in the plots, there is always a thin red line just above the x-axis.

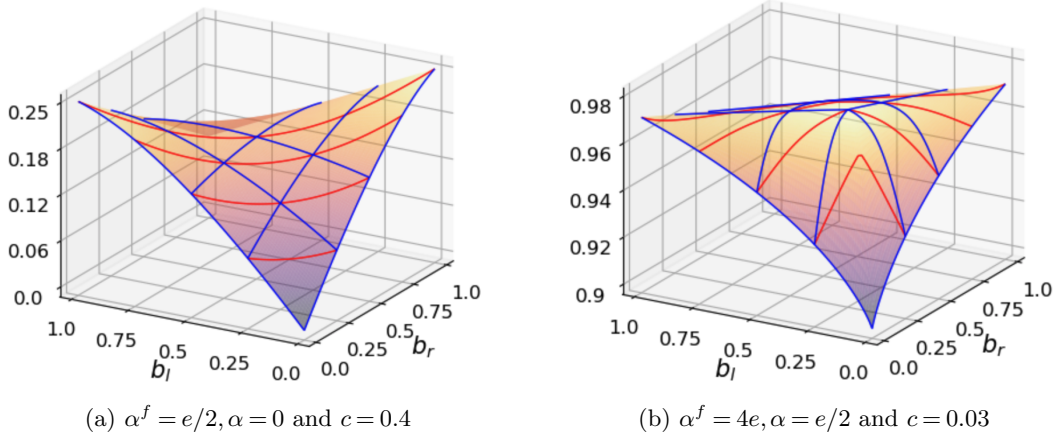


Figure 14 The plots present the value of $g^{\text{KS}}(b_l, b_r)$ for varying α^f, α and c . We highlight the values of the function in the directions $(1, 0)$ and $(0, 1)$ in blue, and in the direction $(-1, 1)$ in red.

In Fig. 14 we plot $g^{\text{KS}}(b_l, b_r)$ for two different sets of parameters of α^f, α and c . The plots reveal distinct convexity and concavity properties in the directions of $(1, 0)$, $(0, 1)$, and $(-1, 1)$. In the directions of $(1, 0)$ and $(0, 1)$, we consistently observe a concave function g^{KS} regardless of the starting point, i.e., the value of flexibility in our matching model exhibits decreasing returns. A similar decrease in the marginal value of flexibility is present in those works that identify that *a little flexibility* is almost as valuable as full flexibility (Bassamboo et al. 2012, Elmachoub et al. 2019). However, we also observe interesting geometric effects in the direction of $(1, -1)$; this direction captures the tradeoff between investing a fixed budget of flexibility on one side or the other. Depending on the values of α^f and α , Fig. 4 and Fig. 14 show that $\mu^{\text{KS}}(b_l, b_r)$, respectively $g^{\text{KS}}(b_l, b_r)$, can be convex, concave or neither in the direction $(-1, 1)$. Both the concavity in directions $(0, 1)$ and $(1, 0)$ and the potential convexity in direction $(1, -1)$ are supported by theoretical findings in Appendix B.

In the remainder of this section, we first discuss two serious practical ramifications of such geometric properties and then argue how an understanding of flexibility cannibalization and asymmetry can help avoid a potential pitfall of current platform experimentation designs. Many platforms today operate with separate teams dedicated to controlling flexibility incentives on the demand and supply sides. Through frequent experimentation, including continuous local improvement of algorithmic parameters, these teams aim to optimize the flexibility investment on each respective side of the market. For illustrative purposes, suppose the supply and demand teams iteratively vary the flexibility investment on their own side (b_l and b_r) by γ whenever doing so improves the objective. The teams would eventually settle at a point where neither has an incentive to further change its flexibility investment. In Fig. 15, we build upon $g^{\text{KS}}(b_l, b_r)$ to illustrate the outcomes of such experiments, which yields the following two observations:

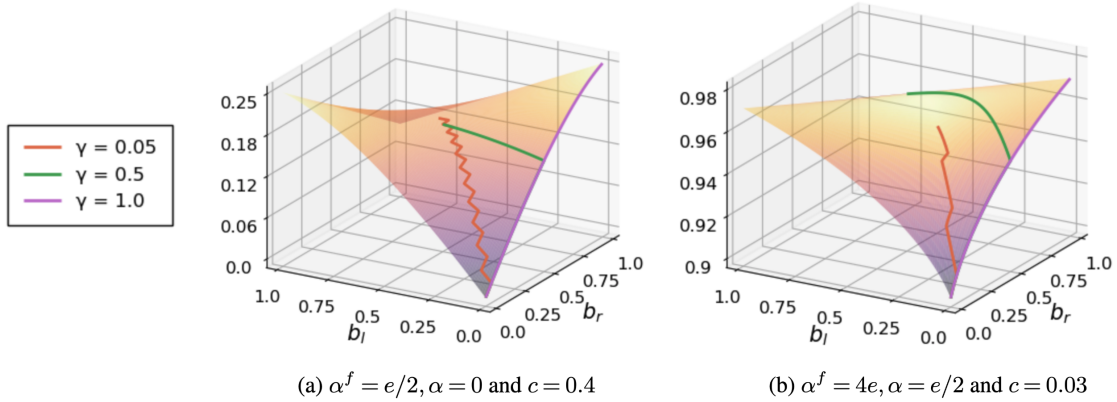


Figure 15 The colored lines illustrate the trajectory of experimentation on the surface of $g^{\text{KS}}(b_l, b_r)$ for different choices of γ . The experiment terminates around a suboptimal balanced allocation in (a) when γ is too small, and around a suboptimal one-sided allocation in (b) when γ is too large.

Suboptimality due to the lack of joint experimentation. Teams may settle at a suboptimal flexibility design due to not experimenting jointly. In other words, they may find themselves at a point where neither team can unilaterally improve the joint objective even though a joint experiment in the direction of either $(1, -1)$ or $(-1, 1)$ would yield a strict improvement. Fig. 15 (a) illustrates that this can arise, when γ is small, near a suboptimal balanced allocation. At this suboptimal allocation, each team faces a concave objective and optimally manages its own levers (i.e., $g^{\text{KS}}(b_l, b_r)$ is locally optimal in the directions $(1, 0)$ and $(0, 1)$), but the overall flexibility decision remains suboptimal for the platform. In Appendix B, we formalize this observation by modeling the flexibility optimization along two axes as a game between two verticals within an organization (see Section 1.2); even though the verticals have the same payoff functions, we show that the suboptimal allocation can emerge as a local Nash Equilibrium (see Appendix B). Though the suboptimal allocation in Fig. 15 (a) can be avoided by setting γ sufficiently large, Fig. 15 (b) illustrates that this does not generally address the suboptimality. Indeed, such large γ may cause an outcome wherein one team operates with more flexibility than is jointly optimal, leading the other team to not invest in flexibility at all. Thus, the platform becomes trapped in a one-sided flexibility allocation, even though adopting flexibility on both market sides would be more profitable.

Suboptimality due to the existence of saddle points. Surprisingly, joint experimentation is not enough to avoid suboptimal flexibility designs. When α and α^f are small, the concavity of $g^{\text{KS}}(b_l, b_r)$ in the direction $(1, 0)$ and convexity in the direction $(1, -1)$ give rise to a saddle point on the surface of $g^{\text{KS}}(b_l, b_r)$, as illustrated in Fig. 15 (a). Near the saddle point, the gradient of $g^{\text{KS}}(b_l, b_r)$ is close to 0 in all directions. As a result, when γ is too small, even with joint experimentation, the platform may fail to capture value in the $(1, -1)$ direction. The profit at the saddle point can be vastly smaller than that at the globally optimal one-sided allocation: in Fig. 15 (a), the locally optimal balanced

allocation achieves just 73% of the profit of the globally optimal one-sided allocation, and for other parameters the gap can be even larger, especially when the platform’s margins are small. For instance, with $\alpha^f = 2e, \alpha = 0$ and $c = 0.99$, the profit of a locally optimal balanced allocation is less than 10% of that of the globally optimal allocation.

As any local experimentation scheme, joint or not, may face obstacles in exploring the complicated geometry of g^{KS} , an understanding of the cannibalization and asymmetry effects can also help platforms design non-local experiments. Consider a digital matching market with high α^f that operates with just one lever of flexibility at $(B, 0)$; introducing a second lever on the opposite side of the market, one would usually invest in a little flexibility by experimenting with (B, ϵ) . In contrast, our study shows that $(B, 0)$ may be a local optimum of g^{KS} (see Fig. 4) whereas $(B/2, B/2)$ would yield a much greater profit. Similarly, a ride-hailing platform with small (α, α^f) may be locally stuck at a balanced allocation despite a one-sided one being much more profitable. To avoid both of these outcomes, our findings suggest that platforms may want to supplement local experimentation with experiments on qualitatively different flexibility designs, i.e., moving from one-sided to balanced or vice versa. Given the high cost of experimentation, it may make sense in practice to first leverage non-local simulation before then attempting experiments in significantly altered parameter regimes; nonetheless, our results emphasize the need to explore non-locally, which stands in contrast to common industry practices. Of course, another distinction in practice is that the impact of flexibility levers is likely to be less symmetric: costs may depend on the side of the market, the value of flexibility $(\alpha^f - \alpha)$ may vary across sides, and the edge formation process need not be independent (see next section). However, these additional features (i) are more likely to further complexify the geometry of g^{KS} than to remove saddle points and local optima, and (ii) do not eradicate the impact of flexibility cannibalization and asymmetry. As a result, the practical takeaway from our findings is that matching platforms ought to explore non-locally, in simulations or experiments, by leveraging a high-level understanding of the matching function’s geometry.

7. Robustness in Alternative Graph Models

In this section we show that the intuitions behind flexibility cannibalization and asymmetry effects extend to three alternative models of matching in random graphs. The goal of these models is to capture dependencies among the edges that realize, which is common in many platforms that solve matching problems in the physical world (e.g., when edges are proximity-based). We first consider a “local model” wherein nodes are only eligible to form edges with neighbors. Next, we consider a spatial model wherein the realization of edges is governed by the distances between supply and demand nodes. Finally, we use the spatial model to investigate imbalanced markets that allow an uneven number of supply and demand nodes. For all of these models we find that, even as different

models create new effects, (i) flexibility cannibalization and asymmetry remain the crucial drivers of the optimal flexibility allocation and (ii) both effects remain dominant in the same parameter regime we previously identified.

7.1. Local Model

We now define and analyze the local model, which is the simplest model to capture dependencies among the edges that realize. As illustrated in Fig. 16, we assume that for any $i \in [n]$, $v_i^l \in V_l$ is only eligible to connect to $v_i^r, v_{(i+1) \bmod n}^r, \dots, v_{(i+k) \bmod n}^r$ in V_r , where k is a constant that specifies the number of eligible neighbors of a node. In particular, in line with our previous model in Section 2, we assume that the probabilities associated with flexible and regular nodes now scale with k (rather than n), giving $p^f = \alpha^f/k$ and $p = \alpha/k$ for constant α^f and α . We require that $0 \leq p < p^f \leq 1/2$ for the edge probabilities to remain in $[0, 1]$ and obtain the following additive model of conditional edge generation:

$$\mathbb{P}[R_{ij} = 1 \mid F_i^l, F_j^r] = \begin{cases} 2p + (F_i^l + F_j^r) \cdot (p^f - p) & \text{if } ((j - i) \bmod n) \leq k - 1 \\ 0 & \text{otherwise} \end{cases}$$

With a slight abuse of notation, we use $\mathcal{M}_n(b_l, b_r)$ to denote the size of a maximum matching in the local model, as we did in previous sections, and $\mu(b_l, b_r)$ to denote $\lim_{n \rightarrow \infty} \mathbb{E} \left[\frac{\mathcal{M}_n(b_l, b_r)}{n} \right]$.¹⁰

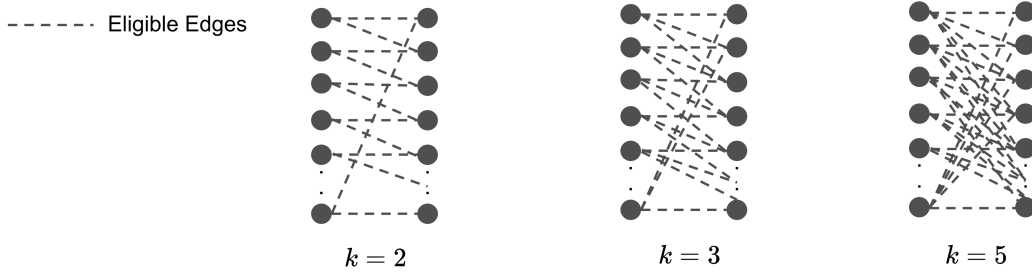


Figure 16 Illustration of local models with different values of k .

For small k , we find that flexibility asymmetry cannot be a significant effect in the local model. In particular, as in Section 4, the one-sided allocation yields expected degrees among regular nodes that are equal to $B(\alpha^f - \alpha) + 2\alpha$ and 2α on the two sides respectively. The gap between these is small when $\alpha^f - \alpha$ is small; however, under small k in the local model, α^f must also be small to ensure $\alpha^f/k = p^f \leq 1/2$. Thus, intuitively, we expect flexibility cannibalization to dominate in that regime. Indeed, when $k = 2$, the next result shows the dominance of the one-sided allocation across the entire feasible parameter space:

THEOREM 5. *When $k = 2$, $\mu(B, 0) > \mu(B/2, B/2)$ for any $B \in (0, 1]$ and p, p^f with $0 \leq p < p^f \leq 1/2$.*

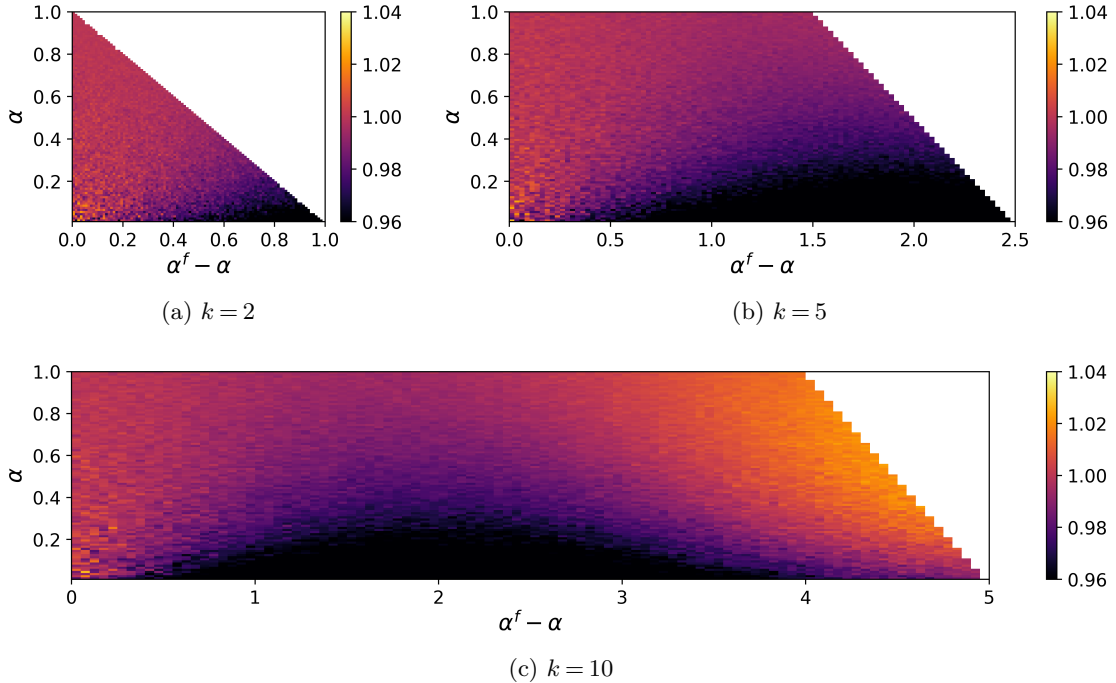


Figure 17 The heatmaps present values of $\frac{\mu^{\text{EMP}}(B/2, B/2)}{\mu^{\text{EMP}}(B, 0)}$ in the local model when $B = 0.6$ for varying k , α and $\alpha^f - \alpha$. The parameter regimes that violate $0 \leq p < p^f \leq 1/2$ are left blank.

To prove Theorem 5, we derive a closed-form solution for $\mu(b_l, b_r)$ through the combinatorial analysis of each possible local structure (see Appendix D.1). However, such an analysis becomes intractable for larger k . Our numerical results¹¹ in Fig. 17 indicate that as we increase k , the resulting plots begin to closely resemble Fig. 5 with a gradual emergence of the flexibility asymmetry effect. In the parameter regime where cannibalization previously dominated, which captures the entire parameter regime for small k , we observe that the one-sided allocation continues to dominate. In contrast, when k becomes large enough for $\alpha^f - \alpha$ to create significant asymmetry, we again observe the balanced allocation performing better.

7.2. Spatial Matching

In this subsection and the next, we focus on a model with spatial dependencies to better capture the matching problems faced by ride-hailing and food delivery platforms. In such platforms, the compatibility between pairs of agents is primarily governed by the distances between them. Thus, we start by considering a two-dimensional cell $[0, 1]^2$ with uniformly distributed drivers and riders. The n drivers are at locations denoted by vectors $\mathbf{d}_1, \mathbf{d}_2, \dots, \mathbf{d}_n$, and the n riders at $\mathbf{r}_1, \mathbf{r}_2, \dots, \mathbf{r}_n$. For a given flexibility allocation $\mathbf{b} = (b_l, b_r)$, driver i is flexible if random variable $F_i^l \sim \text{Bernoulli}(b_l)$ takes the

¹⁰We show the existence of this limit in the proof of Theorem 5.

¹¹As before, we denote the empirical average matching probability by $\mu_{n,s}^{\text{EMP}}(b_l, b_r)$. Across Section 7 we fix $n = 100, s = 1000$ and drop the dependency of $\mu_{n,s}^{\text{EMP}}(b_l, b_r)$ on these two parameters.

value of 1, otherwise the driver is regular. Similarly, each rider j is associated with $F_j^r \sim \text{Bernoulli}(b_r)$, and the rider is flexible if and only if $F_j^r = 1$. We take constants α^f and α such that $0 \leq \alpha < \alpha^f$ and define $p_n^f = \alpha^f/\sqrt{n}, p_n = \alpha/\sqrt{n}$, respectively. We assume that an edge exists between a driver i and a rider j if their distance is within a threshold decided by their respective flexibility types:

$$\mathbb{P}\left[R_{ij} = 1 \mid F_i^l, F_j^r\right] = \begin{cases} 1 & \text{if } \|\mathbf{d}_i - \mathbf{r}_j\|_2 \leq 2p_n + (F_i^l + F_j^r) \cdot (p_n^f - p_n) \\ 0 & \text{otherwise} \end{cases}$$

In other words, \mathbf{r}_j has an edge with \mathbf{d}_i if their distance is within $2p_n + (F_i^l + F_j^r) \cdot (p_n^f - p_n)$. The asymptotic set-up $p_n^f, p_n \in \Theta(1/\sqrt{n})$ ensures that the expected number of edges in the spatial graph is the same $\Theta(n)$ that we considered in our previous asymptotic regime.

The spatial model relaxes two assumptions common to the previous models we have examined: (1) the conditional independence assumption on edge realization R_{ij} with respect to indices i and j , and (2) the equivalence of different flexibility allocations in expected edge counts. In particular, in the one-sided allocation the expected number of riders that connects to a random driver is¹²

$$\left(B(p_n^f + p_n)^2 + (1 - B)(2p_n)^2\right) \cdot \pi \cdot n.$$

This is smaller than the expected number of riders that connects to a random driver under the balanced allocation, which equals

$$\left((B/2)^2 (2p_n^f)^2 + 2 \cdot B/2(1 - B/2) (p_n^f + p_n)^2 + (1 - B/2)^2 (2p_n)^2\right) \cdot \pi \cdot n.$$

As such, we expect the balanced allocation to have an advantage over the one-sided allocation in the spatial setting. Indeed, in Fig. 18 we find that in a parameter regime with small α^f and α , the balanced allocation outperforms the one-sided allocation. This follows because the maximum matching size is close to the number of edges in this very sparse regime, and the latter is higher in expectation in the balanced allocation. In other parts of the heatmap, we find consistency with the results in our main model: the one-sided allocation can outperform the balanced allocation by over 8% when $B = 1$ or when α^f is moderate; moreover, it can be worse by more than 8% when α^f is very large, α is a small positive number, and $B < 1$.

We highlight that α^f and α capture the density of the spatial market: multiplying α^f and α by a factor of $\eta > 1$ in a cell with side length 1 is equivalent to maintaining the number of uniformly distributed agents in the two-dimensional cell $[0, 1/\eta]^2$ but with the same compatibility as before, i.e., with α^f and α kept constant. As a result, we can interpret the setting with very small α^f and α as a spatial market in which (i) the density is very low, but (ii) drivers and riders nonetheless

¹²We assume for simplicity that the driver is at least $2p_n$ away from the boundary of the $[0, 1]^2$ cell, an event that occurs with probability 1 as $n \rightarrow \infty$.

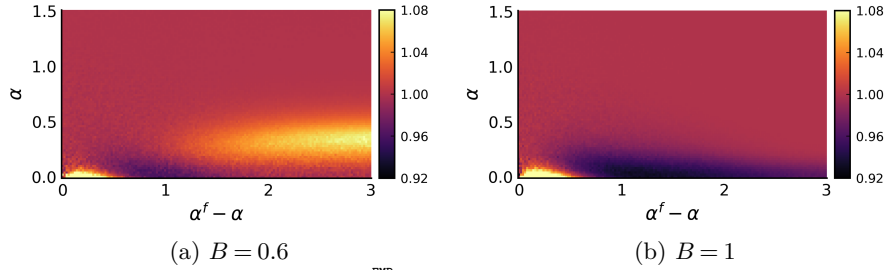


Figure 18 The heatmaps present values of $\frac{\mu^{\text{ENP}}(B/2, B/2)}{\mu^{\text{ENP}}(B, 0)}$ in the spatial matching model across varying α and $\alpha^f - \alpha$.

“expect” to be matched with agents that are very close. In contrast, as the market density increases, agents form more edges, which leads, at first, to flexibility cannibalization. With a further increase in density, we observe that when $B < 1$ flexibility asymmetry becomes a dominant effect and the balanced allocation yields a much larger matching size than the one-sided allocation. Therefore, a natural interpretation of our results is that the optimal flexibility allocation depends on the market density, the flexible/regular agents’ acceptable dispatch radius, and the flexibility penetration B .

7.3. Imbalanced Market

In this subsection we numerically investigate whether the structural insights we identified in fully symmetric settings are robust to imbalances in matching markets. Specifically, we extend the spatial model in the previous subsection by allowing $\lambda \cdot n$ rather than n riders, where $\lambda \in (0, 1]$ (we ignore for symmetry the setting where the market has more demand than supply). We assume that, for a given flexibility allocation (b_l, b_r) , each driver is flexible with probability $b_l \cdot \lambda$ and each rider is flexible with probability b_r . This set-up ensures that the cost of incentivizing an equal number of riders and drivers remains the same.¹³ We remark that the one-sided flexibility allocation $(B, 0)$ is no longer equivalent to $(0, B)$, as the latter generates more edges in expectation. This difference leads to $(0, B)$ being a better allocation than $(B, 0)$, and moreover it also weakens the flexibility asymmetry effect: in Fig. 19 (a) and (b) we show that the region in which the one-sided allocation is dominated by the balanced one almost vanishes. In contrast, the regions with the strongest advantage for the one-sided allocation are consistent with all of our previous findings.

¹³In Appendix E we consider an alternative model that assumes drivers and riders are flexible with probability b_l and b_r , respectively.

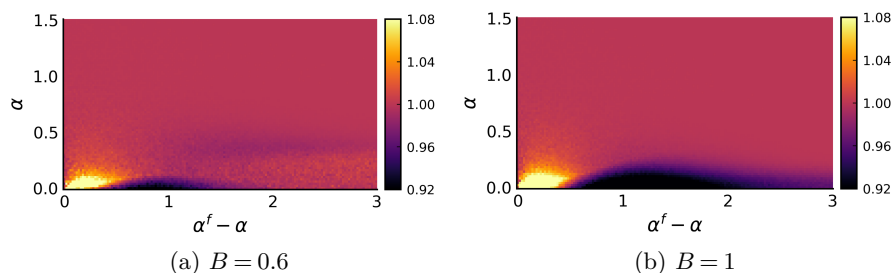


Figure 19 The heatmaps present values of $\frac{\mu^{\text{EMP}}(B/2, B/2)}{\mu^{\text{EMP}}(B, 0)}$ in the imbalanced model across varying α and $\alpha^f - \alpha$ when $\lambda = 0.8$.

8. Conclusion

In summary, our work initiates the study of two-sided flexibility. Our model is not meant to represent any specific platform accurately but to gather structural insights likely to generalize to realistic settings. In particular, we identify flexibility cannibalization and asymmetry, which are respective drawbacks of the balanced and one-sided allocations, showcasing that two-sided flexibility can interact in complex ways. We characterize the typical parameter regimes where each effect dominates and numerically evaluate their strength. Our main practical recommendation for platforms is that their various products affecting flexibility on both sides interact and should therefore not be considered independently. The teams in charge of these products should communicate and conduct experiments and simulations that jointly vary different levers to avoid suboptimal outcomes that can easily arise otherwise.

On the theoretical side, comparing the expected maximum matching sizes in graphs with different flexibility allocations is a challenge, and we leverage a coupling construction, employ concentration bounds, and generalize KS algorithm-based analyses with computer-aided proofs. Nonetheless, our work leaves many questions open. Firstly, our model intentionally focuses on a particular type of edge probability distribution, which keeps the expected number of edges invariant for a given budget B . However, different constructions (e.g., based on random geometric graphs) may be of practical interest. Secondly, though our effects seem to be robust under some such different constructions (see Section 7), all of our results are based on a central decision maker maximizing an unweighted matching, whereas many platforms in practice involve choice among agents on both sides; we know of no results in this direction and believe it to likely yield interesting findings. Finally, our work focuses on a matching model, but two-sided flexibility may also appear in queueing and manufacturing settings. All of these directions may be fruitful and, together, potentially reveal a general theory of two-sided flexibility.

References

- O Zeynep Akşin and Fikri Karaesmen. Characterizing the performance of process flexibility structures. *Operations Research Letters*, 35(4):477–484, 2007.

-
- Eugene TY Ang and Yifan Feng. Disconnectedness brings robustness? on network design for matching with vertex interdiction. *On Network Design For Matching With Vertex Interdiction (October 31, 2024)*, 2024.
- Kenneth Appel and Wolfgang Haken. The solution of the four-color-map problem. *Scientific American*, 237(4):108–121, 1977.
- Jonathan Aronson, Alan Frieze, and Boris G Pittel. Maximum matchings in sparse random graphs: Karp–sipser revisited. *Random Structures & Algorithms*, 12(2):111–177, 1998.
- Paul N Balister and Stefanie Gerke. Controllability and matchings in random bipartite graphs. *Surveys in combinatorics*, 424:119, 2015.
- Achal Bassamboo, Ramandeep S Randhawa, and Jan A Van Mieghem. Optimal flexibility configurations in newsvendor networks: Going beyond chaining and pairing. *Management Science*, 56(8):1285–1303, 2010.
- Achal Bassamboo, Ramandeep S Randhawa, and Jan A Van Mieghem. A little flexibility is all you need: on the asymptotic value of flexible capacity in parallel queuing systems. *Operations Research*, 60(6):1423–1435, 2012.
- Ben Berger, Hongyao Ma, David Parkes, and Shreyas Sekar. Optimal subscription pricing design for ridesharing platforms. 2023.
- Tom Bohman and Alan Frieze. Karp–sipser on random graphs with a fixed degree sequence. *Combinatorics, Probability and Computing*, 20(5):721–741, 2011.
- Béla Bollobás and Graham Brightwell. The width of random graph orders. *Mathematical Scientist*, 20:69–90, 1995.
- John A Buzacott and David D Yao. Flexible manufacturing systems: a review of analytical models. *Management science*, 32(7):890–905, 1986.
- Xi Chen, Jiawei Zhang, and Yuan Zhou. Optimal sparse designs for process flexibility via probabilistic expanders. *Operations Research*, 63(5):1159–1176, 2015.
- Jiri Chod and Nils Rudi. Resource flexibility with responsive pricing. *Operations Research*, 53(3):532–548, 2005.
- Mabel C Chou, Geoffrey A Chua, Chung-Piaw Teo, and Huan Zheng. Process flexibility revisited: The graph expander and its applications. *Operations research*, 59(5):1090–1105, 2011.
- Antoine Désir, Vineet Goyal, Yehua Wei, and Jiawei Zhang. Sparse process flexibility designs: Is the long chain really optimal? *Operations Research*, 64(2):416–431, 2016.
- Adam N Elmachtoub, David Yao, and Yeqing Zhou. The value of flexibility from opaque selling. *Available at SSRN 3483872*, 2019.
- Pál Erdős and Alfréd Rényi. On the existence of a factor of degree one of a connected random graph. *Acta Math. Acad. Sci. Hungar*, 17:359–368, 1966.

- Charles H Fine and Robert M Freund. Optimal investment in product-flexible manufacturing capacity. *Management science*, 36(4):449–466, 1990.
- Daniel Freund and Garrett van Ryzin. Pricing fast and slow: Limitations of dynamic pricing mechanisms in ride-hailing. *Available at SSRN 3931844*, 2021.
- David Gamarnik, Tomasz Nowicki, and Grzegorz Swirszcz. Maximum weight independent sets and matchings in sparse random graphs. exact results using the local weak convergence method. *Random Structures & Algorithms*, 28(1):76–106, 2006.
- Warren H Hausman, David B Montgomery, and Aleda V Roth. Why should marketing and manufacturing work together?: Some exploratory empirical results. *Journal of operations management*, 20(3):241–257, 2002.
- John C Henderson and Harihara Venkatraman. Strategic alignment: Leveraging information technology for transforming organizations. *IBM systems journal*, 38(2.3):472–484, 1999.
- Seyed M Iravani, Mark P Van Oyen, and Katharine T Sims. Structural flexibility: A new perspective on the design of manufacturing and service operations. *Management Science*, 51(2):151–166, 2005.
- William C Jordan and Stephen C Graves. Principles on the benefits of manufacturing process flexibility. *Management science*, 41(4):577–594, 1995.
- Richard M Karp and Michael Sipser. Maximum matching in sparse random graphs. In *22nd Annual Symposium on Foundations of Computer Science (sfcs 1981)*, pages 364–375. IEEE, 1981.
- Varun Krishnan, Ramon Iglesias, Sebastien Martin, Su Wang, Varun Pattabhiraman, and Garrett Van Ryzin. Solving the ride-sharing productivity paradox: Priority dispatch and optimal priority sets. *INFORMS Journal on Applied Analytics*, 52(5):433–445, 2022.
- Andrew Mastin and Patrick Jaillet. Greedy online bipartite matching on random graphs. *arXiv preprint arXiv:1307.2536*, 2013.
- Serguei Netessine, Gregory Dobson, and Robert A Shumsky. Flexible service capacity: Optimal investment and the impact of demand correlation. *Operations Research*, 50(2):375–388, 2002.
- NLsolve. NLsolve.jl: A Julia package for solving nonlinear equations. <https://github.com/JuliaNLSolvers/NLsolve.jl>, 2017. Version v4.5.1, MIT License.
- Hao Yi Ong, Daniel Freund, and Davide Crapis. Driver positioning and incentive budgeting with an escrow mechanism for ride-sharing platforms. *INFORMS Journal on Applied Analytics*, 51(5):373–390, 2021.
- Neil Robertson, Daniel Sanders, Paul Seymour, and Robin Thomas. A new proof of the four-colour theorem. *Electronic research announcements of the American Mathematical Society*, 2(1):17–25, 1996.
- Benson P Shapiro. Can marketing and manufacturing co-exist. *Harvard Business Review*, 55(5):104, 1977.
- David Simchi-Levi and Yehua Wei. Understanding the performance of the long chain and sparse designs in process flexibility. *Operations research*, 60(5):1125–1141, 2012.

- John N Tsitsiklis and Kuang Xu. Flexible queueing architectures. *Operations Research*, 65(5):1398–1413, 2017.
- Jan A Van Mieghem. Investment strategies for flexible resources. *Management Science*, 44(8):1071–1078, 1998.
- Rodney B Wallace and Ward Whitt. A staffing algorithm for call centers with skill-based routing. *Manufacturing & Service Operations Management*, 7(4):276–294, 2005.
- KA Weir, AK Kochhar, SA LeBeau, and DG Edgeley. An empirical study of the alignment between manufacturing and marketing strategies. *Long Range Planning*, 33(6):831–848, 2000.
- Douglas Brent West et al. *Introduction to graph theory*, volume 2. Prentice hall Upper Saddle River, 2001.
- Lenka Zdeborová and Marc Mézard. The number of matchings in random graphs. *Journal of Statistical Mechanics: Theory and Experiment*, 2006(05):P05003, 2006.
- Yeqing Zhou. *Supply Chain and Service Operations with Demand-Side Flexibility*. Columbia University, 2021.

Appendix A: Additional Examples of Two-sided Flexibility in Platforms

In this appendix, we provide additional examples of two-sided flexibility in platforms. As illustrated in Fig. 20 (a), the “No Rush Delivery” option on Uber Eats works similarly to the “Wait and Save” feature on Lyft. This flexibility incentive allows eaters to receive a discount if they are willing to accommodate a delay in their food delivery. By opting into this feature, eaters allow Uber Eats more flexibility in matching them with delivery drivers, as the platform is given a broader pool of eligible drivers with which to match orders. On the supply side, Uber Eats also offers surge incentives, such as small bonuses (Fig. 20 (b)), to encourage drivers to remain committed to the platform and fulfill deliveries during busy periods. Similar to Lyft’s “Ride Streak” bonuses, surge incentives make drivers compatible with a wider of assigned deliveries as they incentivize the acceptance of jobs that would otherwise be declined.



Figure 20 Examples of flexibility incentives on demand and supply sides of Uber Eats, a food-delivery platform.

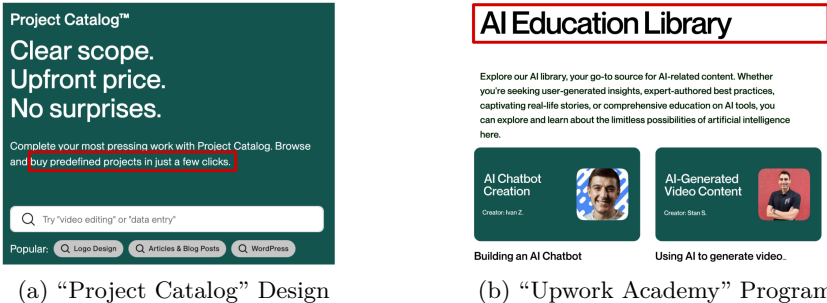


Figure 21 Examples of flexibility incentives on demand and supply sides of Upwork, an online freelancing platform.

Examples of two-sided flexibility can also be found in online freelancing platforms. The platform Upwork has designed a “Project Catalog” that allows freelancers to post predefined project offerings (Fig. 21 (a)). This contrasts with the platform’s traditional business model where customers post specialized requests and freelancers bid on them. With Project Catalog, less picky customers (i.e., those that do not have specialized requests in mind) can opt for standardized services, such as video editing or data entry, that can be fulfilled by a broad range of freelancers. By limiting the scope of customization, the platform makes it easier for these customers to match with freelancers. On the supply side, Upwork promotes flexibility through its Upwork Academy, which offers training courses in specialized skills, such as AI chatbot creation and video content generation (Fig. 21 (b)), to enable freelancers to expand their skill sets. These courses then allow the

freelancers to take on more types of jobs and increases their compatibility with customer requests. Through these examples we find that platforms commonly enhance the overall matching efficiency by steering agents on both market sides to be more flexible.

Appendix B: Implications of the Structural Properties

In this appendix, we demonstrate that in various models considered in the main body of our paper, the platform’s objective can be concave in the directions $(1,0)$ and $(0,1)$ yet convex in the direction $(-1,1)$. We then interpret these results within the framework of a game between two players who set the flexibility on each side. This framework reflects two separate verticals or teams within an organization, each independently controlling one lever of flexibility. Our characterizations in this appendix illustrate that a balanced allocation may emerge as a suboptimal (local) Nash Equilibrium (NE) in such a context.

We start by establishing the geometric properties of the surrogate function $\mu^{\text{KS}}(1/2, 1/2)$ for our main model in Section 2:

THEOREM 6. *When $10^{-4} < \alpha < 0.64\alpha^f - 0.03$ and $0.62\alpha^f + \alpha < 1.68$, $\mu^{\text{KS}}(1/2, 1/2)$ is (i) strictly concave in the directions $(0,1)$ and $(1,0)$, and (ii) strictly convex in the direction $(1, -1)$.*

The above result is proved in Appendix C.3.4 using KS-style analyses, and as illustrated in Fig. 26, the conditions cover most of the subcritical regime. Beyond the subcritical regime, the geometries become more nuanced, and Fig. 4 shows that $\mu^{\text{EMP}}(1/2, 1/2)$ is not necessarily convex in the direction $(1, -1)$.

Furthermore, we prove that for the local model (with $k = 2$) considered in Section 7.1, a simpler setting where the one-sided allocation always dominates, similar geometric properties hold across the entire parametric space of α^f and α (see proof in Appendix D.2):

THEOREM 7. *When $k = 2$ in the local model, $\mu(b_l, b_r)$ is strictly concave in the direction $(0,1)$ when $b_l \in \{0, \frac{1}{2}\}$ and in the direction $(1,0)$ when $b_r \in \{0, \frac{1}{2}\}$. Moreover, $\mu(b_l, b_r)$ is strictly convex in the direction $(1, -1)$ when $b_l + b_r = 1$.*

We next formalize the interpretations of these geometric properties in the context of a game.

B.1. Nash Equilibrium and Saddle Point

We start by providing, in Definition 2 - 3, the textbook definition of NE and local NE for a general payoff function $g(b_l, b_r)$; we also define saddle points in Definition 4. We then verify these conditions for the platform’s objective function defined in our paper. Notably, the suboptimal outcomes occur in our settings in spite of both teams sharing the same objective, i.e., there is no misalignment of incentives.

DEFINITION 2 (GAME Γ). A game Γ is defined by:

1. The set of players $\{1, 2\}$;
2. For each player $i \in \{1, 2\}$, $\mathcal{B}_i = [0, 1]$ is the set of strategies available to player i ;
3. $g : b_l \times b_r \rightarrow \mathbb{R}$ is the payoff function, with $g(b_l, b_r)$ representing the payoff to each player for the strategy profile $\mathbf{b} = (b_l, b_r) \in \mathcal{B}_1 \times \mathcal{B}_2 \subseteq \mathbb{R}^2$.

DEFINITION 3 (NASH EQUILIBRIUM). In a game Γ where the function $g(b_l, b_r)$ has its domain $\mathcal{B} = \mathcal{B}_1 \times \mathcal{B}_2 \subseteq \mathbb{R}^2$,

(i) A point \mathbf{b}' is a *Nash Equilibrium (NE)* if

$$g(b'_l, b'_r) \geq g(b_l, b'_r), \forall b_l \in \mathcal{B}_1 \text{ and } g(b'_l, b'_r) \geq g(b'_l, b_r), \forall b_r \in \mathcal{B}_2.$$

(ii) A point \mathbf{b}' is a *local Nash Equilibrium* if there exists some $\delta > 0$ such that

$$\begin{aligned} g(b'_l, b'_r) &\geq g(b_l, b'_r), \forall b_l \in \mathcal{B}_1 \cap (b_l - \delta, b_l + \delta), \text{ and} \\ g(b'_l, b'_r) &\geq g(b'_l, b_r), \forall b_r \in \mathcal{B}_2 \cap (b_r - \delta, b_r + \delta). \end{aligned}$$

(iii) A point \mathbf{b}' is a *suboptimal (local) Nash Equilibrium* if \mathbf{b}' is an (local) NE but there exists another point \mathbf{b}^* for which $g(b^*_l, b^*_r) > g(b'_l, b'_r)$.

DEFINITION 4 (SADDLE POINT). For a function $g(b_l, b_r) : \mathcal{B} = \mathcal{B}_1 \times \mathcal{B}_2 \rightarrow \mathbb{R}$, assume that its first and second directional derivatives exist in all directions at $\mathbf{b}' \in \mathcal{B}$. Then, \mathbf{b}' is said to be a saddle point of g if the following conditions are satisfied:

(i) The gradient $\nabla g(\mathbf{b}') = \mathbf{0}$;

(ii) The second directional derivatives $\nabla_{\mathbf{v}}^2 g(\mathbf{b}') < 0$ and $\nabla_{\mathbf{u}}^2 g(\mathbf{b}') > 0$ in some directions \mathbf{v} and $\mathbf{u} \in \mathbb{R}^2$.

To identify suboptimal (local) NE in the models we leverage the results that $g(b_l, b_r)$ is concave in the directions $(0, 1)$ and $(1, 0)$, and convex in the directions $(-1, 1)$ and $(1, -1)$. Because the directional derivative at an NE is zero along all directions, having both concavity and convexity effectively means that the NE is also a saddle point. We formalize these conditions in Lemma 4 and Lemma 5.

DEFINITION 5 (INTERIOR OF A SET). Let (\mathcal{B}, τ) be a topological space. Then

(i) A point $\mathbf{b} \in \mathcal{B}$ is an *interior point* of the set \mathcal{B} if there exists an open set U with $\mathbf{b} \in U \subseteq \mathcal{B}$.

(ii) The *interior* of \mathcal{B} , denoted by $\text{int}(\mathcal{B})$, consists of all its interior points.

LEMMA 4 (Suboptimal NE and Saddle Point). *In a game Γ where the function $g(b_l, b_r)$ has its domain $\mathcal{B} \subseteq \mathbb{R}^2$, assume that its first and second directional derivatives exist in all directions for any $\mathbf{b} \in \text{int}(\mathcal{B})$. Suppose some NE $\mathbf{b}' \in \text{int}(\mathcal{B})$ satisfies the following conditions:*

(i) $g(b_l, b_r)$ is strictly concave in the direction $(0, 1)$ at any $\mathbf{b} \in \text{int}(\mathcal{B})$ such that $b_l = b'_l$;

(ii) $g(b_l, b_r)$ is strictly concave in the direction $(1, 0)$ at any $\mathbf{b} \in \text{int}(\mathcal{B})$ such that $b_r = b'_r$;

(iii) $g(b_l, b_r)$ is strictly convex in the direction $(1, -1)$ for any $\mathbf{b} \in \text{int}(\mathcal{B})$ such that $b_l + b_r = b'_l + b'_r$.

Then \mathbf{b}' is a suboptimal NE and a saddle point.

LEMMA 5 (Suboptimal Local NE and Saddle Point). *In a game Γ where the function $g(b_l, b_r)$ has its domain $\mathcal{B} \subseteq \mathbb{R}^2$, assume that its first and second directional derivatives exist in all directions at $\mathbf{b}' \in \text{int}(\mathcal{B})$.*

Suppose

(i) $g(b_l, b_r)$ is strictly concave in the directions $(0, 1)$ and $(1, 0)$ at \mathbf{b}' ;

(ii) $g(b_l, b_r)$ is strictly convex in the direction $(1, -1)$ at \mathbf{b}' ;

(iii) *The gradient of $g(b_l, b_r)$ is the zero vector at \mathbf{b}' .*

Then \mathbf{b}' is a suboptimal local NE and a saddle point.

We now demonstrate that the balanced allocation is indeed a suboptimal NE and a saddle point for graph models examined in this paper.

PROPOSITION 2. *With $k = 2$ in the local model, there exists $c > 0$ such that $\mathbf{b}' = (1/2, 1/2)$ is a suboptimal NE and a saddle point for $g(b_l, b_r) = \mu(b_l, b_r) - c \cdot (b_l, b_r)$.*

PROPOSITION 3. *Assume that $10^{-4} < \alpha < 0.64\alpha^f - 0.03$ and $0.62\alpha^f + \alpha < 1.68$. Then, there exists $c > 0$ such that $\mathbf{b}' = (1/2, 1/2)$ is a suboptimal local NE and a saddle point for $\bar{g}(b_l, b_r) := \mu^{KS}(b_l, b_r) - c \cdot (b_l, b_r)$.*

B.2. Proofs of the Results in Appendix B.1

Proof of Lemma 4 Let \mathbf{b}' be a Nash Equilibrium (NE) in $\text{int}(\mathcal{B})$ for the function $g(b_l, b_r)$ with domain $\mathcal{B} \subseteq \mathcal{R}^2$. We start by showing that $g(b_l, b_r)$ has a gradient of $\mathbf{0}$ at \mathbf{b}' . If $\nabla_{(0,1)}g(\mathbf{b}') > 0$, then there exists $\epsilon > 0$ such that $g(b'_l, b'_r + \epsilon) > g(b'_l, b'_r)$, contradicting the definition of NE. Similarly, if $\nabla_{(0,1)}g(\mathbf{b}') < 0$, then there exists $\epsilon > 0$ such that $g(b'_l, b'_r - \epsilon) > g(b'_l, b'_r)$, again contradicting the definition of NE. Thus, $\nabla_{(0,1)}g(\mathbf{b}') = 0$. Applying a similar argument to the direction of $(1, 0)$ we find that $\nabla_{(1,0)}g(\mathbf{b}') = 0$. Since $g(b_l, b_r)$ has a directional derivative of 0 in two orthogonal directions at \mathbf{b}' , it has a gradient of $\mathbf{0}$ at \mathbf{b}' . Since we also know that $\nabla_{(0,1)}^2g(\mathbf{b}') < 0$ and $\nabla_{(1,-1)}^2g(\mathbf{b}') > 0$, \mathbf{b}' is a saddle point.

We then show that \mathbf{b}' is a suboptimal NE. Since $g(b_l, b_r)$ is strictly convex in the direction of $(1, -1)$ at any \mathbf{b} such that $b_l + b_r = b'_l + b'_r$ and $g(b_l, b_r)$ has a gradient of $\mathbf{0}$ at \mathbf{b}' , \mathbf{b}' is a global minimum in the direction of $(1, -1)$. That is, there exists $\epsilon > 0$ such that $g(b'_l + \epsilon, b'_r - \epsilon) > g(b'_l, b'_r)$. Thus, $g(b_l, b_r)$ is a suboptimal NE. \square

Proof of Lemma 5 Since $g(b_l, b_r)$ is strictly concave in the direction of $(0, 1)$ and $(1, 0)$ but also strictly convex in the direction of $(1, -1)$ at \mathbf{b}' , \mathbf{b}' is neither a local maximum nor a local minimum. Combined with the condition that $g(b_l, b_r)$ has a gradient of $\mathbf{0}$ at \mathbf{b}' , we conclude that \mathbf{b}' is a saddle point.

Now, since $\nabla_{(0,1)}g(\mathbf{b}') = 0$ and $\nabla_{(0,1)}^2g(b_l, b_r) < 0$, we know that \mathbf{b}' is a local maximum in the direction of $(0, 1)$ and we can find $\epsilon_1 > 0$ such that

$$g(b'_l, b'_r) \geq g(b'_l, b_r), \forall b_r \in b_r \cap (b_r - \epsilon_1, b_r + \epsilon_1).$$

Similarly, from $\nabla_{(1,0)}g(\mathbf{b}') = 0$ and $\nabla_{(1,0)}^2g(b_l, b_r) < 0$ we find $\epsilon_2 > 0$ such that

$$g(b'_l, b'_r) \geq g(b_l, b'_r), \forall b_l \in b_l \cap (b_l - \epsilon_2, b_l + \epsilon_2).$$

Taking $\delta = \min(\epsilon_1, \epsilon_2)$, we find that \mathbf{b}' is a local NE.

We then show that \mathbf{b}' is a suboptimal local NE. Since $\nabla_{(1,-1)}g(\mathbf{b}') = 0$ and $\nabla_{(1,-1)}^2g(b_l, b_r) > 0$, \mathbf{b}' is a local minimum in the direction of $(1, -1)$. That is, there exists $\epsilon > 0$ such that $g(b'_l + \epsilon, b'_r - \epsilon) > g(b'_l, b'_r)$. Thus, $g(b_l, b_r)$ is a suboptimal local NE. \square

Proof of Proposition 2 As established in Theorem 7, we have verified the local convexity of $\mu(b_l, b_r)$ in the direction $(1, -1)$ and local concavity in the directions $(0, 1)$ and $(1, 0)$ along diagonals that intersect at $\mathbf{b}' = (1/2, 1/2)$. Consequently, the function $g(b_l, b_r)$ exhibits the same local convexity and concavity properties. According to Lemma 4, to demonstrate the existence of a constant $c > 0$ such that $\mathbf{b}' = (1/2, 1/2)$ is a suboptimal Nash Equilibrium (NE) for $\bar{g}(b_l, b_r)$, it is sufficient to show that $(1/2, 1/2)$ is indeed an NE.

We construct $c = \nabla_{(1,0)}\mu(b_l, b_r) = \left. \frac{\partial\mu(b_l, 1/2)}{\partial b_l} \right|_{b_l=1/2}$. Then, we have

$$\nabla_{(1,0)}g(b_l, b_r) = \nabla_{(1,0)}\mu(b_l, b_r) - c = 0.$$

Since $g(b_l, b_r)$ is strictly concave in the direction of $(1, 0)$ when $b_r = 1/2$, $\mathbf{b}' = (1/2, 1/2)$ is a global maximum in the direction $(1, 0)$. That is,

$$g(1/2, 1/2) \geq g(b_l, 1/2), \forall b_l \in (0, 1).$$

By symmetry, the same result holds in the direction $(0, 1)$. Thus, according to Definition 3 (i), we conclude that the point $\mathbf{b}' = (1/2, 1/2)$ is indeed an NE for the selected constant c . This completes the proof. \square

Proof of Proposition 3 Given that Theorem 6 has established the local convexity of $\mu^{\text{KS}}(b_l, b_r)$ in the direction $(1, -1)$ and its local concavity in the directions $(0, 1)$ and $(1, 0)$ within the specified region of α^f and α , the same local convexity and concavity properties hold for $\bar{g}(b_l, b_r)$. By Lemma 5, to show that there exists $c > 0$ such that $\mathbf{b}' = (1/2, 1/2)$ is a suboptimal local NE for $\bar{g}(b_l, b_r)$, it suffices to show that there exists $c > 0$ such that the gradient of $\bar{g}(b_l, b_r)$ is the zero vector at $\mathbf{b} = (1/2, 1/2)$.

Since $\nabla_{(1,-1)}^2\bar{g}(b_l, b_r) > 0$ at $(1/2, 1/2)$ and by symmetry we have $\bar{g}(b_l, b_r) = \bar{g}(b_r, b_l), \forall (b_l, b_r) \in (0, 1)^2$, $\nabla_{(1,-1)}\bar{g}(b_l, b_r)$ is well-defined at $(1/2, 1/2)$. Now, if the directional derivative is strictly positive, we know that there exists $\epsilon > 0$ such that $\bar{g}(1/2 + \epsilon, 1/2 - \epsilon) > \bar{g}(1/2 - \epsilon, 1/2 + \epsilon)$, which contradicts the symmetry condition. By the same argument, the directional derivative cannot be strictly negative, so we find that $\nabla_{(1,-1)}\bar{g}(b_l, b_r) = 0$ at $(1/2, 1/2)$.

We then construct $c = \left. \frac{\partial\mu^{\text{KS}}(b_l, 1/2)}{\partial b_l} \right|_{b_l=1/2}$. Since $\nabla_{(1,0)}^2\mu^{\text{KS}}(b_l, b_r) < 0$ at $(1/2, 1/2)$, $\nabla_{(1,0)}\mu^{\text{KS}}(b_l, b_r)$ is well-defined and equal to $\left. \frac{\partial\mu^{\text{KS}}(b_l, 1/2)}{\partial b_l} \right|_{b_l=1/2}$. Now, since $c = \left. \frac{\partial\mu^{\text{KS}}(b_l, 1/2)}{\partial b_l} \right|_{b_l=1/2}$, we have

$$\nabla_{(1,0)}\bar{g}(b_l, b_r) = \nabla_{(1,0)}\mu^{\text{KS}}(b_l, b_r) - c = 0.$$

Since the derivative of $\bar{g}(b_l, b_r)$ at $\mathbf{b}' = (1/2, 1/2)$ is zero in two independent directions, it implies that the gradient of $\bar{g}(b_l, b_r)$ is a zero vector at $\mathbf{b}' = (1/2, 1/2)$, thereby completing the proof. \square

Appendix C: Proofs of the Main Results

C.1. Proofs of the Results in Section 3

In this section, we prove Lemma 1 and Lemma 2, which are the key auxiliary results for Theorem 1.

C.1.1. Proof of Lemma 1

Proof. Recall that we have constructed a random graph G_n^b in (1) that decomposes the $2p_n^f$ edges as two groups of directed edges, in each of which an edge exists with probability p_n^f . Notice that when constructing a maximum matching in G_n^b , we do not differentiate between edges of different directions. However, we maintain the requirement that no two edges (of either direction) can share a node in the matching. In the rest of the proof we show that neither difference (i) nor (ii) identified in Section 3.1 changes the asymptotic matching size.

We assume without loss of generality that n is an even number (else, we can ignore nodes v_n^l and v_n^r without changing the asymptotic matching probability). We start by applying standard concentration bounds to

show that assuming $n/2$ flexible nodes on each side leads to $o(n)$ error in the asymptotic matching size. Specifically, we define the event that in $G_n(1/2, 1/2)$

$$E_1 := \left\{ \left| \sum_i F_i^l - n/2 \right| \leq n^{5/8} \text{ and } \left| \sum_j F_j^r - n/2 \right| \leq n^{5/8} \right\}.$$

Specifically, letting E_1^c be the complement of event E_1 , we have

$$\begin{aligned} \mathbb{E} \left[\mathcal{M}_n(1/2, 1/2) - \mathcal{M}_n^b \right] &= \mathbb{E} \left[\mathcal{M}_n(1/2, 1/2) \middle| E_1^c \right] \mathbb{P} [E_1^c] + \mathbb{E} \left[\mathcal{M}_n(1/2, 1/2) \middle| E_1 \right] \mathbb{P} [E_1] - \mathbb{E} \left[\mathcal{M}_n^b \right] \\ &\leq n \cdot e^{-\Omega(n^{1/4})} + \mathbb{E} \left[\mathcal{M}_n(1/2, 1/2) \middle| E_1 \right] - \mathbb{E} \left[\mathcal{M}_n^b \right] \\ &\leq \mathbb{E} \left[\mathcal{M}_n(1/2, 1/2) \middle| E_1 \right] - \mathbb{E} \left[\mathcal{M}_n^b \right] + \mathcal{O}(1) \\ &\leq \mathbb{E} \left[\mathcal{M}_n(1/2, 1/2) \middle| \sum_i F_i^l = \sum_j F_j^r = n/2 \right] + o(n) - \mathbb{E} \left[\mathcal{M}_n^b \right] + \mathcal{O}(1) \\ &= \mathbb{E} \left[\mathcal{M}_n(1/2, 1/2) - \mathcal{M}_n^b \middle| \sum_i F_i^l = \sum_j F_j^r = n/2 \right] + o(n). \end{aligned}$$

Notice that the first inequality above is a concentration result that follows from the Chernoff bound, and the third inequality above follows from the fact that having $n^{5/8}$ additional flexible nodes on each side of $G_n(1/2, 1/2)$ creates at most $o(n)$ additional matches.

We next show that drawing two edges, each with probability p_n^f , is close to drawing a single edge with probability $2p_n^f$ in the asymptotic regime we study. With $\sum_i F_i^l = \sum_j F_j^r = n/2$, we reorder the nodes such that the first $n/2$ nodes on each side of $G_n(1/2, 1/2)$ are flexible. We then couple the edges in the two graphs (G_n^b and a balanced graph with $\sum_i F_i^l = \sum_j F_j^r = n/2$) by drawing a random variable $\omega_{ij} \sim U(0, 1)$ for every $i, j \in [n]$ and using ω_{ij} to generate the edge between i and j . Specifically, we set $R_{ij} = 1$ if and only if $\omega_{ij} \leq \mathbb{P} [R_{ij} = 1]$ in the respective graph.¹⁴ In the balanced graph, in which the first $n/2$ nodes are flexible on each side, we obtain $\mathbb{P} [R_{ij} = 1] = 2p_n^f, \forall i, j \in [n/2]$ and in G_n^b we get

$$\mathbb{P} [R_{ij} = 1] = \mathbb{P} [R_{ij}^l + R_{ij}^r \geq 1] = 2p_n^f - (p_n^f)^2, \forall i, j \in [n/2].$$

The probabilities for all other edges are the same in both graphs. This characterization of the probability of $R_{ij} = 1$ in each graph implies for a given realization of ω that

$$\mathbb{E} \left[\mathcal{M}_n(1/2, 1/2) - \mathcal{M}_n^b \middle| \omega, \sum_i F_i^l = \sum_j F_j^r = n/2 \right] \leq \sum_{i, j \in [n/2]} \mathbb{1}_{\omega_{ij} \in [2p_n^f - (p_n^f)^2, 2p_n^f]}$$

because the number of additional matches in $\mathcal{M}_n(1/2, 1/2)$ is upper bounded by the number of additional edges in the graph. Taking expectation over ω , we find that

$$\mathbb{E} \left[\mathcal{M}_n(1/2, 1/2) - \mathcal{M}_n^b \middle| \sum_i F_i^l = \sum_j F_j^r = n/2 \right] \leq \sum_{i, j \in [n/2]} \mathbb{P} \left[\omega_{ij} \in [2p_n^f - (p_n^f)^2, 2p_n^f] \right] = \sum_{i, j \in [n/2]} (p_n^f)^2 = \mathcal{O}(1).$$

¹⁴In G_n^b , $R_{ij} = 1$ if and only if $R_{ij}^l + R_{ij}^r \geq 1$.

This implies that

$$\mathbb{E} \left[\mathcal{M}_n(1/2, 1/2) - \mathcal{M}_n^b \right] \leq \mathbb{E} \left[\mathcal{M}_n(1/2, 1/2) - \mathcal{M}_n^b \middle| \sum_i F_i^l = \sum_j F_j^r = n/2 \right] + o(n) = o(n).$$

Thus, when $\alpha = 0$ we have $\limsup_{n \rightarrow \infty} \mathbb{E} [\mathcal{M}_n(1/2, 1/2) - \mathcal{M}_n^b] / n = 0$. \square

C.1.2. Proof of Lemma 2

Proof. Recall from Section 3.2 that we start by constructing a valid coupling of realizations of G_n^b and G_n^o , and then compare the matching sizes among the coupled graphs. In G_n^b , we denote an edge from v_i^l to v_j^r by (v_i^l, v_j^r) and an edge from v_j^r to v_i^l by (v_j^r, v_i^l) . Then, we partition the realized edges in G_n^b into four groups:

$$\begin{aligned} X_1 &:= \left\{ (v_i^l, v_j^r) \mid i, j \in [n/2], R_{ij}^l = 1 \right\}, & X_2 &:= \left\{ (v_j^r, v_i^l) \mid i, j \in [n/2], R_{ij}^r = 1 \right\}, \\ X_3 &:= \left\{ (v_j^r, v_i^l) \mid j \in [n/2], i \in \{n/2 + 1, \dots, n\}, R_{ij}^r = 1 \right\}, & X_4 &:= \left\{ (v_i^l, v_j^r) \mid i \in [n/2], j \in \{n/2 + 1, \dots, n\}, R_{ij}^l = 1 \right\}. \end{aligned}$$

In Fig. 8 (A) we illustrate the edges in X_1, X_2, X_3, X_4 as red, blue, yellow, and green, respectively.

Fix a realization of X_1, X_2, X_3 and X_4 . We start by flipping X_1, X_3 and X_4 vertically around the middle of the bipartite graph and swapping the directions accordingly, defining

$$\begin{aligned} \tilde{X}_1 &:= \left\{ (v_{n+1-i}^l, v_{n+1-j}^r) \text{ for each } (v_i^l, v_j^r) \in X_1 \right\}, & \tilde{X}_3 &:= \left\{ (v_{n+1-i}^l, v_{n+1-j}^r) \text{ for each } (v_j^r, v_i^l) \in X_3 \right\}, \\ \text{and } \tilde{X}_4 &:= \left\{ (v_{n+1-j}^r, v_{n+1-i}^l) \text{ for each } (v_i^l, v_j^r) \in X_4 \right\}. \end{aligned}$$

Then, we construct the following graphs: graph (A) contains edges in X_1, X_2, X_3 and X_4 ; graph (B) contains edges in X_1, X_2, \tilde{X}_3 and \tilde{X}_4 ; graph (C) contains edges in $\tilde{X}_1, X_2, X_3, X_4$, (and drop their directions); and graph (D) contains edges in $\tilde{X}_1, X_2, \tilde{X}_3, \tilde{X}_4$, (and drop their directions). Fig. 8 provides an illustration of the different graphs. As before, the edges in X_1, X_2, X_3, X_4 are colored in red, blue, yellow, and green, respectively, and the coloring is maintained for their (flipped) copies in graphs (B)-(D). Essentially, we flip X_3 and X_4 to construct graph (B), and then we flip X_1 in (A) and (B) to construct (C) and (D). Our goal is to couple the realizations of G_n^b as (A) or (B) with the realizations of G_n^o as (C) or (D), so that it suffices to compare the combined size of the matchings in graph (A) and (B) with that of (C) and (D). This means that our proof builds on a coupling between two pairs of graphs rather than just one pair; we explain below how this allows us to find for each edge in a matching of either (A) or (B) a corresponding edge that can be part of a matching in (C) or (D).

We denote the sizes of a maximum matching in the four graphs, (A)-(D), by M_A, M_B, M_C , and M_D . Notice that this is a slight abuse of notation because we omitted the dependency of these quantities on X_1, X_2, X_3 and X_4 for notational convenience. We now argue that graph (A) and (B) are possible realizations of G_n^b , while graph (C) and (D) are possible realizations of G_n^o , all of which occur with the same probability in the respective random graphs. With $p_n = \alpha/n = 0$, in G_n^o (as $\alpha = 0$), we have $\mathbb{P}[R_{ij} = 1] = p_n^f, \forall i, j \in [n]$. Combined with (1), we thus know that, given X_1, X_2, X_3 and X_4 ,

$$\begin{aligned} \mathbb{P} \left[G_n^b \text{ realizes as (A)} \right] &= \mathbb{P} \left[G_n^b \text{ realizes as (B)} \right] = \mathbb{P} \left[G_n^o \text{ realizes as (C)} \right] = \mathbb{P} \left[G_n^o \text{ realizes as (D)} \right] \\ &= \left(p_n^f \right)^{|X_1| + |X_2| + |X_3| + |X_4|} \left(1 - p_n^f \right)^{n^2 - (|X_1| + |X_2| + |X_3| + |X_4|)}. \end{aligned}$$

We now prove the coupling based on X_1, X_2, X_3 and X_4 is valid. When $X_3 = \tilde{X}_3$ and $X_4 = \tilde{X}_4$,¹⁵ i.e., (A) and (B) are identical, we trivially have $M_A = M_B$, and the maximum matching size in (A) can be written as $(M_A + M_B)/2$. On the other hand, when $X_3 \neq \tilde{X}_3$ or $X_4 \neq \tilde{X}_4$, since G_n^b realize as (A) and (B) with the same probability the weighted average maximum matching size in (A) and (B) is also $(M_A + M_B)/2$. Thus, for any n ,

$$\mathbb{E}[\mathcal{M}_n^b] = \sum_{\substack{\text{all realizations of} \\ X_1, X_2, X_3, X_4}} \left(p_n^f\right)^{|X_1|+|X_2|+|X_3|+|X_4|} \left(1-p_n^f\right)^{n^2-(|X_1|+|X_2|+|X_3|+|X_4|)} \cdot \frac{M_A + M_B}{2}.$$

Similarly, we find that

$$\mathbb{E}[\mathcal{M}_n(1,0)] = \sum_{\substack{\text{all realizations of} \\ X_1, X_2, X_3, X_4}} \left(p_n^f\right)^{|X_1|+|X_2|+|X_3|+|X_4|} \left(1-p_n^f\right)^{n^2-(|X_1|+|X_2|+|X_3|+|X_4|)} \cdot \frac{M_C + M_D}{2}.$$

Thus, as long as we can show that,

$$\forall X_1, X_2, X_3 \text{ and } X_4 : M_A + M_B \leq M_C + M_D, \quad (3)$$

we can conclude that $\mathbb{E}[\mathcal{M}_n^b] \leq \mathbb{E}[\mathcal{M}_n(1,0)] \forall n$ when $\alpha = 0$.

In the rest of the proof, we verify (3). We pick an arbitrary matching in (A) and denote the edges in X_1, X_2, X_3 and X_4 that are involved in the maximum matching by Y_1, Y_2, Y_3 and Y_4 . Similarly, we pick any matching in (B) and denote the edges in X_1, X_2, \tilde{X}_3 and \tilde{X}_4 that are involved in the maximum matching by Y'_1, Y'_2, \tilde{Y}_3 and \tilde{Y}_4 .¹⁶ Our proof proceeds by constructing feasible matchings in (C) and (D) that have a combined size that is greater-equal to the combined size of the matchings in (A) and (B). We drop the direction of the edges as (v_i^l, v_j^r) and (v_j^r, v_i^l) cannot appear in the same matching, and with a slight abuse of notation, we denote an undirected edge between v_i^l and v_j^r by (v_i^l, v_j^r) . Fig. 9 (A) and (B) illustrate Y_1, Y'_1, Y_2, Y'_2 as red, pink, blue, and navy; moreover, the plots illustrate Y_3 and \tilde{Y}_3 as yellow, and Y_4 and \tilde{Y}_4 as green.

To construct matchings in (C) and (D), we flip Y_1, Y'_1 vertically and define

$$\tilde{Y}_1 := \left\{ (v_{n+1-i}^l, v_{n+1-j}^r) \text{ for each } (v_i^l, v_j^r) \in Y_1 \right\} \quad \text{and} \quad \tilde{Y}'_1 := \left\{ (v_{n+1-i}^l, v_{n+1-j}^r) \text{ for each } (v_i^l, v_j^r) \in Y'_1 \right\}.$$

Since graph (C) contains all edges in \tilde{X}_1 and X_2 , \tilde{Y}'_1 and Y_2 are part of a feasible matching in (C). Similarly, since graph (D) also contains all edges in \tilde{X}_1 and X_2 , Y'_2 and \tilde{Y}_1 are part of a feasible matching in (D). As illustrated in Fig. 9 (C) and (D), we copy \tilde{Y}'_1 and Y_2 into the construction of a matching in (C), and copy Y'_2 and \tilde{Y}_1 into a matching in (D) (as before, the figure maintains consistent coloring for the flipped edges in different subgraphs).

Then, it suffices to show that all edges in Y_3, \tilde{Y}_3, Y_4 and \tilde{Y}_4 can also be mapped into (C) and (D). We denote by \bar{C} and \bar{D} the remaining nodes in (C) and (D) that are not incident to the already copied matches, and by $E(\bar{C})$ and $E(\bar{D})$ the available edges among \bar{C} and \bar{D} . Below we construct a mapping that injectively

¹⁵This may occur when all edges in X_3 and X_4 are symmetric around the middle of the bipartite graph, i.e., they “flip” to themselves.

¹⁶Notice that the distinction between Y_1, Y_2 and Y'_1, Y'_2 arises from the fact that the edges in X_1 and X_2 that are involved in a maximum matching for (A) may be different from those for (B).

maps all edges in Y_3, \tilde{Y}_3, Y_4 and \tilde{Y}_4 to two matchings $M(\bar{C})$ in (C) and $M(\bar{D})$ in (D), where $M(\bar{C}) \subseteq E(\bar{C})$ and $M(\bar{D}) \subseteq E(\bar{D})$. This then immediately implies that $M_A + M_B \leq M_C + M_D$.

Since the edges in X_3 (\tilde{X}_3) are not incident to those in X_4 (\tilde{X}_4), the resulting matches Y_3, \tilde{Y}_3 and Y_4, \tilde{Y}_4 can be analyzed separately. We next show that the matches in Y_3 and \tilde{Y}_3 can be injectively mapped to $(M(\bar{C}) \cap X_3) \cup (M(\bar{D}) \cap \tilde{X}_3)$ in graph (C) and (D) by constructing a multigraph G' . The injective mapping from Y_4 and \tilde{Y}_4 to $(M(\bar{C}) \cap X_4) \cup (M(\bar{D}) \cap \tilde{X}_4)$ follows from symmetry through a similarly constructed graph G'' , and thus our focus is on G' for the rest of this proof. Specifically, we construct G' as a bipartite graph with $n/2$ nodes on each side, indexing nodes on the left as v_1^l through $v_{n/2}^l$ and on the right as v_1^r through $v_{n/2}^r$. The edge set of G' consists of¹⁷

$$\left\{ (v_{i-n/2}^l, v_j^r) \text{ for each } (v_i^l, v_j^r) \in Y_3 \right\} \cup \left\{ (v_{n/2+1-i}^l, v_{n+1-j}^r) \text{ for each } (v_i^l, v_j^r) \in \tilde{Y}_3 \right\}.$$

We refer to the former set as type A edges (as they come from Y_3 in graph (A)) and the later set as type B edges. Finally, we color the nodes in G' :¹⁸

- We color v_j^r in G' by red (blue) if in graph (A) v_j^r is matched by an edge in Y_1 (Y_2);
- We color v_i^l in G' by pink (navy) if in graph (B) $v_{n/2+1-i}^l$ is matched by an edge in Y_1' (Y_2').

Fig. 10 provides an illustration of G' that is constructed based on Fig. 9 (A) and (B). Notice that a node on the left of G' cannot be colored twice because it is matched by at most one edge in $Y_1 \cup Y_2$, and similarly those on the right cannot be colored twice because they are matched by at most one edge in $Y_1' \cup Y_2'$.

We begin by analyzing the degree of nodes in G' . Recall that every edge in G' comes from either Y_3 or \tilde{Y}_3 . Thus, each node in G' has degree at most 2, as otherwise at least two incident edges would come from either Y_3 or \tilde{Y}_3 , contradicting that Y_3 and \tilde{Y}_3 are subsets of matchings in (A) and (B), respectively. Indeed, colored nodes in G' have a degree of at most 1 because, if the colored node is already matched by an edge in graph (A), then it cannot connect to any type A edges; if it is matched by an edge in graph (B), then it cannot connect to any type B edges. Thus, in G' each colored node can connect to at most one edge from either type A or type B.

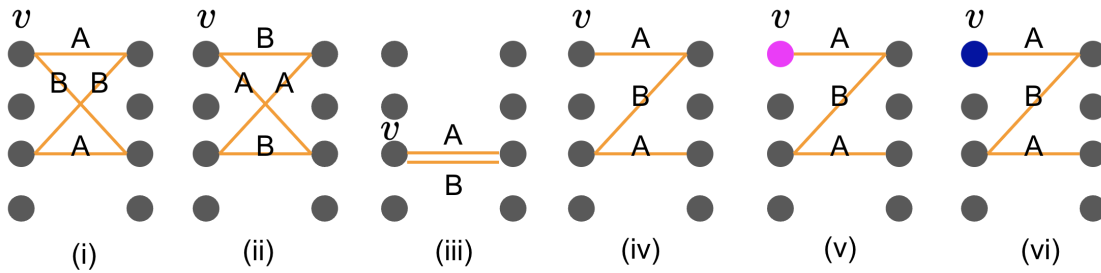


Figure 22 Illustrations of possible connected components in G' .

Since nodes in G' have a degree of at most 2, any connected component in G' is either a path or a cycle (page 109 of West et al. (2001)). Fig. 22 illustrates examples of connected components in G' .¹⁹ We next

¹⁷As G' is a multigraph, this union may contain two copies of the same edge.

¹⁸Notice that the coloring is based on the edges, rather than the colors of the flexible/regular nodes that we used for illustrations in (A)-(D).

¹⁹The result in West et al. (2001) applies only to simple graphs; as nodes in G' have degree at most 2, whenever there are multiple edges between 2 nodes, this means that these 2 nodes have no other edges incident to them (see Figure 22 (iii)). Therefore, such a pair of nodes also forms a cycle.

construct the matchings $M(\bar{C})$ and $M(\bar{D})$ based on the structure of paths and cycles in G' through two mappings that respectively map the edges in G' to $M(\bar{C})$ and $M(\bar{D})$. The mappings ensure that all edges in G' of either type A or B are mapped to either $M(\bar{C}) \cap X_3$ or $M(\bar{D}) \cap \tilde{X}_3$. This then immediately completes the proof. Specifically, we use the following bijective mappings from edges in G' to $M(\bar{C}) \cap X_3$ and $M(\bar{D}) \cap \tilde{X}_3$, which we denote by f_C and f_D , respectively:

$$f_C : (v_i^l, v_j^r) \rightarrow (v_{i+n/2}^l, v_j^r), f_D : (v_i^l, v_j^r) \rightarrow (v_{n/2+1-i}^l, v_{n+1-j}^r), \forall i, j \in [n/2]. \quad (4)$$

In the rest of the proof, we show that every edge in G' is mapped by either f_C or f_D to its respective image in either $M(\bar{C}) \cap X_3$ or $M(\bar{D}) \cap \tilde{X}_3$, i.e., the edge is mapped to part of a feasible matching solution.

We begin by considering the case of cycles in G' . Since all nodes in a cycle have a degree of 2, no node in the cycle can be colored. Moreover, in a bipartite graph, all cycles are of even length. Since no two type A edges or two type B edges may share the same node, the edges in the cycle must be alternating in type A and B. As illustrated in Fig. 22 (i) and (ii), as one traverses through the cycle starting from node v on the top left and moves to the top right, the edges must either be of (1) type A, B, A, B, ..., or (2) type B, A, B, A, ... To create feasible matchings in (C) and (D), we need to ensure that the edges that are incident to the same node in G' are not both mapped by f_C (resp. f_D), since they would otherwise share a node in graph (C) (resp. (D)). Thus, for structure (1), we choose for each type A edge e the edge $f_C(e)$ to become part of the matching in (C) and for each type B edge e the edge $f_D(e)$ to become part of the matching in graph (D).²⁰ These choices always lead to a feasible matching because the allocated edges are not incident to any colored nodes, and thus not incident to any matches already copied from $Y_1, Y_2, Y_1',$ and Y_2' . The construction based on structure (2) is symmetric. We remark that the structure in Fig. 22 (iii), with two edges between a pair of nodes, is a special case of a cycle in G' .

Now, we consider the case of paths. Since all but the endpoints of a path have a degree of 2, only the two endpoints of a path may be colored. Thus, it suffices to consider the following three subcases: (1) the two endpoints of the path are both uncolored, (2) one of the endpoints is colored, and (3) both of the endpoints of the path are colored.

- In subcase (1), as illustrated in Fig. 22 (iv), the path must alternate between edges of type A and B. Thus, we can iteratively include all edges in the path in $M(\bar{C})$ or $M(\bar{D})$, as we did in the case of cycles.
- In subcase (2), if an end-point v is colored pink, as illustrated in Fig. 22 (v), then the edge that connects to the endpoint must be of type A. Any subsequent edge to v must then alternate between type B, A, B, To avoid the first edge sharing a node with \tilde{Y}_1' in graph (C), we include all type A edges by using f_D to map them into $E(\bar{D})$, and all type B edges by using f_C to map them into $E(\bar{C})$. In contrast, if an end-point v is navy, as illustrated in Fig. 22 (vi), then the edge that connects to the endpoint must be of type A. Thus, the subsequent edges follow type B, A, B, To avoid the first edge sharing a node with Y_2' in graph (D), we then include for each type A edge its image in $E(\bar{C})$ under f_C and for each type B edge its image under f_D in $E(\bar{D})$. All subsequent edges in the path are incident to

²⁰An alternative option is to map all type A edges using f_D and type B edges using f_C .

uncolored nodes and thus their images under f_C and f_D are not incident to any edges already copied from Y_1, Y_2, Y'_1 , and Y'_2 . The cases with one of the endpoints being red or blue are symmetric. Fig. 10 shows how type A and type B edges are mapped to graph (C) and (D) based on colors in G' .

- Finally, we observe that it is not possible for both endpoints of a path to be colored. If the path is of odd length, the two endpoints must be on different sides of the bipartite graph. Thus, one of the endpoints is colored pink/navy and the other is colored red/blue. Since the edges, starting from the endpoint colored pink/navy, must alternate between type A and B, with an odd number of edges the last edge must be of type A. This contradicts the feasibility of the matching in graph (A) because the colored node is already occupied by Y_1 or Y_2 in graph (A). On the other hand, if the path is of even length, both of the endpoints must be on the same side of the bipartite graph. Assume without loss of generality that both endpoints are colored pink/navy (the other case is exactly symmetric). Then, starting from one of the endpoints, the path must alternate between edges of type A and B and end with an edge of type B. This contradicts the feasibility of the matching in graph (B) because the colored node is already occupied by Y'_1 or Y'_2 in graph (B). Thus, subcase (3) is not possible.

Therefore, in all possible subcases the matches in Y_3 and \tilde{Y}_3 can be injectively mapped to $(M(\bar{C}) \cap X_3) \cup (M(\bar{D}) \cap \tilde{X}_3)$ in graph (C) and (D). This shows that $M_A + M_B \leq M_C + M_D$ for any X_1, X_2, X_3 and X_4 , and thus $\mathbb{E}[\mathcal{M}_n^b] \leq \mathbb{E}[\mathcal{M}_n(1, 0)] \forall n$ when $\alpha = 0$. \square

C.2. Proofs of the Results in Section 4

C.2.1. Proof of Proposition 1

Proof. We denote the asymptotic fraction of degree-0 nodes by $h(b_l, b_r) := \lim_{n \rightarrow \infty} \mathbb{E} \left[\left| \{v | \deg(v) = 0\} \right| \right] / n$. Given an allocation (b_l, b_r) , we have

$$\begin{aligned} \lim_{n \rightarrow \infty} \mathbb{P} [\deg(v) = 0 | v \text{ is a flexible node in } V_l] &= \lim_{n \rightarrow \infty} \left(1 - 2\alpha^f/n\right)^{b_r n} \left(1 - (\alpha^f + \alpha)/n\right)^{(1-b_r)n} = e^{-(1+b_r)\alpha^f - (1-b_r)\alpha}, \\ \lim_{n \rightarrow \infty} \mathbb{P} [\deg(v) = 0 | v \text{ is a regular node in } V_l] &= \lim_{n \rightarrow \infty} \left(1 - (\alpha^f + \alpha)/n\right)^{b_r n} \left(1 - 2\alpha/n\right)^{(1-b_r)n} = e^{-b_r\alpha^f - (2-b_r)\alpha}. \end{aligned}$$

The argument for $v \in V_r$ follows by symmetry and we obtain

$$\begin{aligned} h(b_l, b_r) &= \lim_{n \rightarrow \infty} \mathbb{E} \left[\left| \{v | \deg(v) = 0\} \right| \right] / n \\ &= b_l e^{-(1+b_r)\alpha^f - (1-b_r)\alpha} + (1 - b_l) e^{-b_r\alpha^f - (2-b_r)\alpha} + b_r e^{-(1+b_l)\alpha^f - (1-b_l)\alpha} + (1 - b_r) e^{-b_l\alpha^f - (2-b_l)\alpha}. \end{aligned}$$

Then, for a given $B \in (0, 1)$, with allocation $(b_l, B - b_l)$ we have

$$\begin{aligned} h(b_l, B - b_l) &= b_l e^{-(1+B-b_l)\alpha^f - (1-B+b_l)\alpha} + (1 - b_l) e^{-(B-b_l)\alpha^f - (2-B+b_l)\alpha} \\ &\quad + (B - b_l) e^{-(1+b_l)\alpha^f - (1-b_l)\alpha} + (1 - B + b_l) e^{-b_l\alpha^f - (2-b_l)\alpha} =: f(b_l). \end{aligned}$$

We compute that

$$\begin{aligned} f'(B/2) &= \left[1 - (1 - B + b_l)(\alpha^f - \alpha)\right] e^{-b_l\alpha^f - (2-b_l)\alpha} - \left[1 - (1 - b_l)(\alpha^f - \alpha)\right] e^{-(B-b_l)\alpha^f - (2-B+b_l)\alpha} \\ &\quad + \left[1 + b_l(\alpha^f - \alpha)\right] e^{-(1+B-b_l)\alpha^f - (1-B+b_l)\alpha} - \left[1 + (B - b_l)(\alpha^f - \alpha)\right] e^{-(1+b_l)\alpha^f - (1-b_l)\alpha}. \end{aligned}$$

and thus $f'(B/2) = 0$. Moreover,

$$f''(B/2) = (\alpha^f - \alpha) \left[(1 - B + b_l)(\alpha^f - \alpha) - 2 \right] e^{-b_l \alpha^f - (2 - b_l) \alpha} + (\alpha^f - \alpha) \left[(1 - b_l)(\alpha^f - \alpha) - 2 \right] e^{-(B - b_l) \alpha^f - (2 - B + b_l) \alpha} \\ + (\alpha^f - \alpha) \left[b_l(\alpha^f - \alpha) + 2 \right] e^{-(1 + B - b_l) \alpha^f - (1 - B + b_l) \alpha} + (\alpha^f - \alpha) \left[(B - b_l)(\alpha^f - \alpha) + 2 \right] e^{-(1 + b_l) \alpha^f - (1 - b_l) \alpha}.$$

Since the exponential terms above are trivially positive, $f''(b_l) > 0$ if the terms

$$(1 - B + b_l)(\alpha^f - \alpha) - 2, (1 - b_l)(\alpha^f - \alpha) - 2, b_l(\alpha^f - \alpha) + 2 \text{ and } (B - b_l)(\alpha^f - \alpha) + 2$$

are positive. We find that for any $B \in (0, 1)$ and $\alpha \geq 0$, with $\alpha^f > \frac{2}{1 - B} + \alpha$, the four terms are indeed positive for any $b_l \in [0, B]$.

Under such conditions of B, α^f and α , we have $f'(B/2) = 0$ and $f''(b_l) > 0$ for any $b_l \in [0, B]$. Thus, $f'(b_l) \leq 0$ for $b_l \in [0, B/2]$ and $f'(b_l) \geq 0$ for $b_l \in [B/2, B]$. We conclude that $h(B/2, B/2) = \min_{b_l \in [0, B]} h(b_l, B - b_l)$ and $h(B, 0) = \max_{b_l \in [0, B]} h(b_l, B - b_l)$. \square

C.2.2. Proof of Lemma 3

Proof. Denote the number of nodes in V_l and V_r that have a degree of d by random variables q_d^l and q_d^r , respectively. We start by showing that, in any realization of the $(1 - B/2)n \times (1 - B/2)n$ bipartite graph,

$$m_1 \geq \sum_d q_d^l \cdot d - \sum_{d=2}^{(1-B/2)n} q_d^l \cdot (d-1) - \sum_{d=2}^{(1-B/2)n} q_d^r \cdot (d-1). \quad (5)$$

Notice that $\sum_d q_d^l \cdot d = \sum_d q_d^r \cdot d$ is the number of edges in the graph, and the second and third term in (5) respectively capture the extra edges, i.e., those incident to nodes with degree > 1 , on the left and right-hand side of the graph. This lower bound holds because, after deleting $d - 1$ edges from all nodes with degree $d > 1$ in V_l and V_r , all remaining edges in the graph would have degree 1 on both ends. In other words, the remaining edges are not incident to each other and thus trivially form a (not necessarily maximum) matching.

Notice that the probability for a node v on the left or right-hand side of the graph to have degree d is the same in this symmetric bipartite graph. Taking expectations over the lower bound in (5), we find that

$$\mathbb{E}[m_1] \geq (1 - B/2)n \sum_{d=1}^{(1-B/2)n} \mathbb{P}[\deg(v) = d] \cdot d - 2(1 - B/2)n \sum_{d=2}^{(1-B/2)n} \mathbb{P}[\deg(v) = d] \cdot (d-1) \\ = (1 - B/2)n \mathbb{E}[\deg(v)] - 2(1 - B/2)n \sum_{d=2}^{(1-B/2)n} \mathbb{P}[\deg(v) = d] \cdot (d-1) \quad (6) \\ = (1 - B/2)^2 n 2\alpha - 2(1 - B/2)n \sum_{d=2}^{(1-B/2)n} \mathbb{P}[\deg(v) = d] \cdot (d-1).$$

We simplify the second term by substituting $t = (1 - B/2)n$ and observing that

$$\lim_{n \rightarrow \infty} \sum_{d=2}^{(1-B/2)n} \mathbb{P}[\deg(v) = d] \cdot (d-1) = \lim_{n \rightarrow \infty} \sum_{d=2}^{(1-B/2)n} \binom{(1-B/2)n}{d} (2\alpha/n)^d \cdot (1 - 2\alpha/n)^{(1-B/2)n-d} \cdot (d-1) \\ = \lim_{t \rightarrow \infty} \sum_{d=2}^t \binom{t}{d} (2\alpha(1 - B/2)/t)^d \cdot (1 - 2\alpha(1 - B/2)/t)^{t-d} \cdot (d-1)$$

$$\begin{aligned}
&= \lim_{t \rightarrow \infty} \sum_{d=1}^t \binom{t}{d} (2\alpha(1-B/2)/t)^d \cdot (1-2\alpha(1-B/2)/t)^{t-d} \cdot (d-1) \\
&= 2\alpha(1-B/2) - \lim_{t \rightarrow \infty} \sum_{d=1}^t \binom{t}{d} (2\alpha(1-B/2)/t)^d \cdot (1-2\alpha(1-B/2)/t)^{t-d} \\
&= 2\alpha(1-B/2) + e^{-2\alpha(1-B/2)} - 1.
\end{aligned}$$

Plugging this into (6), we find that

$$\begin{aligned}
\mathbb{E}[m_1] &\geq (1-B/2)^2 n 2\alpha - 2(1-B/2)n \left(2\alpha(1-B/2) + e^{-2\alpha(1-B/2)} - 1 \right) \\
&= 2 \cdot (1-B/2) n \left[1 - (1-B/2)\alpha - e^{-2\alpha(1-B/2)} \right] \text{ as } n \rightarrow \infty.
\end{aligned}$$

□

C.2.3. Proof of Theorem 2

Proof. We first provide an upper bound on $\mu(B, 0)$ and then derive a lower bound on $\mu(B/2, B/2)$. When $\mathbf{b} = (B, 0)$, a node $v \in V_l$ is regular with probability $1-B$ and all nodes in V_r are regular nodes. Thus, a regular node v forms an edge with a node $u \in V_r$ with probability $2\alpha/n$. Then,

$$\begin{aligned}
\mu(B, 0) &\leq 1 - \lim_{n \rightarrow \infty} \mathbb{P}[v \in V_l \text{ is regular and has degree } 0] \\
&= 1 - \lim_{n \rightarrow \infty} (1-B) (1-2\alpha/n)^n = 1 - (1-B) \cdot e^{-2\alpha}.
\end{aligned} \tag{7}$$

Then, to lower bound $\mu(B/2, B/2)$, we adopt a greedy matching scheme: in the first stage we only match the regular nodes in V_l with the regular nodes in V_r , and in the second stage we greedily match the rest of the flexible nodes. Denote the number of matches formed in stage 1 and 2 by n_1 and n_2 , respectively. Since each node $v \in V_l$ is regular with probability $1-B/2$, we can use a Chernoff bound to find that the event

$$E_1 := \left\{ \left| \sum_i F_i^l - B/2 \cdot n \right| \leq n^{5/8} \text{ and } \left| \sum_j F_j^r - B/2 \cdot n \right| \leq n^{5/8} \right\}$$

occurs with a probability of at least $1 - e^{-\Omega(n^{1/4})}$. By Lemma 3, a graph of $(1-B/2)n$ regular nodes on each side has a maximum matching among its nodes of size at least $2 \cdot (1-B/2)n \left[1 - (1-B/2)\alpha - e^{-2\alpha(1-B/2)} \right] - o(n)$. Correspondingly, a subgraph of $(1-B/2)n - n^{5/8}$ regular nodes on each side has the same asymptotic maximum matching size (up to $o(n)$ nodes that are removed). Conditioning on E_1 Lemma 3 thus implies that as $n \rightarrow \infty$

$$\begin{aligned}
\mathbb{E}[n_1] &= \mathbb{E}[n_1|E_1] \mathbb{P}[E_1] + \mathbb{E}[n_1|E_1^c] \mathbb{P}[E_1^c] \geq (\mathbb{E}[m_1] - o(n)) \cdot \left(1 - e^{-\Omega(n^{1/4})} \right) - n^{5/8} \cdot e^{-\Omega(n^{1/4})} \\
&\geq 2 \cdot (1-B/2) n \left[1 - (1-B/2)\alpha - e^{-2\alpha(1-B/2)} \right] - o(n).
\end{aligned}$$

Through a similar conditioning we find that, for any $\alpha \leq 0.05$ and $B \geq 0.4$,

$$\begin{aligned}
&\lim_{n \rightarrow \infty} \mathbb{P}[\text{regular node } v \in V_l \text{ not connected to any regular node in } V_r] \\
&\geq \lim_{n \rightarrow \infty} (1-2\alpha/n)^{(1-B/2)n+n^{5/8}} \cdot \left(1 - e^{-\Omega(n^{1/4})} \right) + 0 \cdot e^{-\Omega(n^{1/4})} \\
&\geq \lim_{n \rightarrow \infty} (1-0.1/n)^{(1-B/2) \cdot n + n^{5/8}} = e^{-0.1(1-B/2)}.
\end{aligned}$$

Thus, as $n \rightarrow \infty$ we can also upper bound

$$\begin{aligned} \mathbb{E}[n_1] &= \mathbb{E}[n_1|E_1] \mathbb{P}[E_1] + \mathbb{E}[n_1|E_1^c] \mathbb{P}[E_1^c] \\ &\leq \left(1 - e^{-0.1(1-B/2)}\right) \left((1-B/2)n + n^{5/8}\right) \cdot \left(1 - e^{-\Omega(n^{1/4})}\right) + n \cdot e^{-\Omega(n^{1/4})} \\ &< \left(1 - e^{-0.1(1-B/2)}\right) \cdot (1-B/2) \cdot n + o(n). \end{aligned}$$

Now we examine the flexible nodes and argue that, even if we greedily match the flexible nodes to any unmatched regular nodes on the opposite side, almost all of the flexible nodes will be matched in the second stage. Given n' unmatched regular nodes in V_r , the number of edges between a flexible node $v \in V_l$ and these n' nodes is governed by Binom $\left(n', \frac{\alpha^f + \alpha}{n}\right)$. For any $n' \in \Theta(n)$, by the Poisson Limit Theorem we find that Binom $\left(n', \frac{\alpha^f + \alpha}{n}\right)$ converges in distribution to Poisson $\left(\frac{n'}{n}(\alpha^f + \alpha)\right)$ as $n \rightarrow \infty$. Thus, as $n \rightarrow \infty$

$$\mathbb{P}[v \text{ not connected to any unmatched regular node in } V_r | n'] = e^{-\frac{n'}{n}(\alpha^f + \alpha)}.$$

We now apply this bound to the flexible nodes in V_l . Observe that the event

$$E_2 := E_1 \cap \left\{ n_1 \leq \left(1 - e^{-0.1(1-B/2)}\right) (1-B/2)n + 2n^{5/8} \right\}$$

occurs with a probability of at least $1 - e^{-\Omega(n^{1/4})}$ by Chernoff bound.²¹ Under E_2 , we greedily match each flexible node to any unmatched regular node in V_r . In particular, for the i th flexible node under consideration, even if all previous $i-1$ flexible nodes are already matched to regular nodes in V_r , there will still be at least

$$(1-B/2) \cdot n - \left(1 - e^{-0.1(1-B/2)}\right) (1-B/2)n - i - 3 \cdot n^{5/8}$$

unmatched regular nodes in V_r . This allows us to bound:

$$\begin{aligned} &\mathbb{P}[i\text{th flexible node not connected to any unmatched regular node in } V_r | E_2] \\ &\leq e^{-\frac{(1-B/2) \cdot n - (1 - e^{-0.1(1-B/2)}) (1-B/2)n - i - 3 \cdot n^{5/8}}{n} (\alpha^f + \alpha)} \leq e^{-((1-B/2) - (1 - e^{-0.1(1-B/2)}) (1-B/2) - i/n) \alpha^f} \text{ as } n \rightarrow \infty. \end{aligned}$$

Thus, as $n \rightarrow \infty$, through the greedy algorithm that iteratively matches each flexible to any unmatched regular node, the i th flexible node ends up matched with probability at least

$$1 - e^{-((1-B/2) - (1 - e^{-0.1(1-B/2)}) (1-B/2) - i/n) \alpha^f} = 1 - e^{-(-i/n + e^{-0.1(1-B/2)}(1-B/2)) \alpha^f}.$$

This is a lower bound on the matching probability for any $i \in \{1, 2, \dots, B/2 \cdot n - n^{5/8}\}$. In particular, with $B \in [0.4, 0.8]$ the expression $-i/n + e^{-0.1(1-B/2)}(1-B/2)$ is strictly positive, and thus the above probability is monotonically increasing in α^f . The argument for matching flexible nodes in V_r with regular nodes in V_l is symmetric, and we find that when $\alpha \in [0.01, 0.05]$,

$$\lim_{n \rightarrow \infty} \mathbb{E} \left[\frac{n_2}{n} | E_2 \right] \geq 2 \cdot \lim_{n \rightarrow \infty} \left[\sum_{i=1}^{B/2 \cdot n - n^{5/8}} \left(1 - e^{-(-i/n + e^{-0.1(1-B/2)}(1-B/2)) \alpha^f}\right) / n \right]$$

²¹With high probability there are at most $(1-B/2)n + n^{5/8}$ regular nodes on both sides; each such node is isolated with probability $e^{-0.1(1-B/2)}$, so we expect to match at most $\left((1-B/2)n + n^{5/8}\right) (1 - e^{-0.1(1-B/2)})$ of them in the first stage.

$$\begin{aligned}
&= 2 \cdot B/2 - 2 \cdot \lim_{n \rightarrow \infty} \left[\sum_{i=1}^{B/2-n} e^{-(-i/n + e^{-0.1(1-B/2)}(1-B/2))\alpha^f} \right] / n \\
&= B - 2 \cdot \lim_{n \rightarrow \infty} \frac{e^{\alpha^f(1/n - (1-B/2)e^{-0.1(1-B/2)})} (e^{\alpha^f B/2} - 1)}{n (e^{\alpha^f/n} - 1)} \\
&= B - 2 \cdot \frac{\lim_{n \rightarrow \infty} e^{\alpha^f(1/n - (1-B/2)e^{-0.1(1-B/2)})} (e^{\alpha^f B/2} - 1)}{\lim_{n \rightarrow \infty} n (e^{\alpha^f/n} - 1)} \\
&= B - 2 \cdot \frac{e^{-\alpha^f(1-B/2)e^{-0.1(1-B/2)}} (e^{\alpha^f B/2} - 1)}{\lim_{n \rightarrow \infty} n (e^{\alpha^f/n} - 1)} \\
&= B - \frac{2}{\alpha^f} \left[(e^{\alpha^f \cdot B/2} - 1) e^{-\alpha^f(1-B/2)e^{-0.1(1-B/2)}} \right], \tag{8}
\end{aligned}$$

where the second equality comes from the sum of a geometric sequence, the third from the quotient rule, and the fifth from an application of the L'Hôpital's rule on $\lim_{n \rightarrow \infty} (e^{\alpha^f/n} - 1) / (1/n)$. Moreover, from the monotonicity result for $1 - e^{-(-i/n + e^{-0.1(1-B/2)}(1-B/2))\alpha^f}$ with respect to α^f we know that (8) is also monotonically increasing in α^f .

Thus, when $\alpha \in [0.01, 0.05]$,

$$\begin{aligned}
\mu(B/2, B/2) &\geq \lim_{n \rightarrow \infty} \mathbb{E} \left[\frac{n_1 + n_2}{n} \right] \\
&\geq \lim_{n \rightarrow \infty} \mathbb{E} \left[\frac{n_1}{n} \right] + \lim_{n \rightarrow \infty} \left(\mathbb{E} \left[\frac{n_2}{n} | E_2 \right] \cdot \mathbb{P}[E_2] \right) + 0 \cdot \lim_{n \rightarrow \infty} (1 - \mathbb{P}[E_2]) \\
&\geq 2 \cdot (1 - B/2) \left[1 - (1 - B/2)\alpha - e^{-2\alpha(1-B/2)} \right] \\
&\quad + B - \frac{2}{\alpha^f} \left[(e^{\alpha^f \cdot B/2} - 1) e^{-\alpha^f(1-B/2)e^{-0.1(1-B/2)}} \right]. \tag{9}
\end{aligned}$$

Due to the non-linearity of the bounds in (7) and (9), it is difficult compare $\mu(B, 0)$ and $\mu(B/2, B/2)$ analytically for a wide range of B, α^f and α values. Instead, we fix $\alpha^f = 22$,²² and construct local upper and lower bounds for $\mu(B, 0)$ and $\mu(B/2, B/2)$ within a small interval of B and α values to show that $\mu(B, 0) < \mu(B/2, B/2)$ within this small interval. Then, we adopt a computer-aided proof to verify the inequality over all such intervals. Specifically, given $\delta > 0$, for any $(B', \alpha') \in [B - \delta, B] \times [\alpha - \delta, \alpha] \subseteq [0.4, 0.8] \times [0.01, 0.05]$, we can upper bound

$$\mu(B', 0) \leq 1 - (1 - B') \cdot e^{-2\alpha'} \leq 1 - (1 - B) \cdot e^{-2\alpha}$$

and lower bound

$$\begin{aligned}
\mu(B'/2, B'/2) &\geq 2 \cdot (1 - B'/2) \left[1 - (1 - B'/2)\alpha' - e^{-2\alpha'(1-B'/2)} \right] \\
&\quad + B' - \frac{2}{\alpha^f} \left[(e^{\alpha^f \cdot B'/2} - 1) e^{-\alpha^f(1-B'/2)e^{-0.1(1-B'/2)}} \right] \\
&\geq 2 \cdot (1 - B/2) \left[1 - (1 - (B - \delta)/2)\alpha - e^{-2(\alpha - \delta)(1-B/2)} \right] \\
&\quad + (B - \delta) - \frac{2}{\alpha^f} \left[(e^{\alpha^f \cdot B/2} - 1) e^{-\alpha^f(1-B/2)e^{-0.1(1-(B-\delta)/2)}} \right].
\end{aligned}$$

²²The result for $\alpha^f > 22$ follows from the monotonicity of (8) with respect to α^f .

Thus, it suffices to show

$$1 - (1 - B) \cdot e^{-2\alpha} \leq 2 \cdot (1 - B/2) \left[1 - (1 - (B - \delta)/2)\alpha - e^{-2(\alpha - \delta)(1 - B/2)} \right] \\ + (B - \delta) - \frac{2}{\alpha^f} \left[\left(e^{\alpha^f \cdot B/2} - 1 \right) e^{-\alpha^f (1 - B/2) e^{-0.1(1 - (B - \delta)/2)}} \right] \quad (10)$$

to verify that $\mu(B', 0) < \mu(B'/2, B'/2)$ for any $(B', \alpha') \in [B - \delta, B] \times [\alpha - \delta, \alpha]$.

To obtain Theorem 2, we partition the parameter regime $B \in [0.4, 0.8]$ and $\alpha \in [0.01, 0.05]$ into a grid in which all cells are of the form $[B - \delta, B] \times [\alpha - \delta, \alpha]$, and then verify inequality (10) in each such cell. In `Theorem4.ipynb`,²³ we take $\delta = 0.0001$ and verify (10) for all for $B \in \{0.4000, 0.4001, \dots, 0.7999, 0.8000\}$ and $\alpha \in \{0.0100, 0.0101, \dots, 0.0499, 0.0500\}$. Thus, $\mu(B/2, B/2) > \mu(B, 0)$ for any $B \in [0.4, 0.8], \alpha \in [0.01, 0.05]$ and $\alpha^f \geq 22$. \square

C.3. Proofs of the Results in Section 5

This section proceeds as follows: we begin with the definition of the KS algorithm in Algorithm 1. The KS algorithm iteratively prunes nodes in the graph and proceeds in two phases: the first phase ends when no nodes of degree 1 remain in the graph, and the second phase ends when all edges are removed from the graph. We construct a quantity $\mu^{\text{KS}}(b_l, b_r)$ based on analyses of the KS algorithm. Under Condition 1, Theorem 8 shows that this quantity is equal to $\mu(b_l, b_r)$. Thereafter, we verify Condition 1 for a subset of instances, which leads to Theorem 3 that states the equivalence of $\mu(b_l, b_r)$ and $\mu^{\text{KS}}(b_l, b_r)$ for a range of parameters. The quantity $\mu^{\text{KS}}(b_l, b_r)$ relies on solutions to a system of equations, which we can approximate with arbitrary precision. This allows us to compute $\mu^{\text{KS}}(b_l, b_r)$, and consequently $\mu(b_l, b_r)$, at a provable level of precision.

The KS-based analyses facilitate two of the results presented in our work. Firstly, it allows us to analytically compare the one-sided and the balanced allocations in the parameter regimes from Theorem 4. Secondly, it lets us investigate $\mu^{\text{KS}}(b_l, b_r)$ as a proxy measure of interest and establish its structural properties at $\mathbf{b} = (1/2, 1/2)$ in Theorem 6.

C.3.1. KS Derivations. Throughout the section we fix an arbitrary (b_l, b_r) and use G as the shorthand notation for $G_n^{g|b}(b_l, b_r)$. In G , the *degree* of a node v is the number of edges that are incident to v , and we denote this number by $\text{deg}(v)$. We now define the KS algorithm in Algorithm 1.

Based on Algorithm 1, the edges in G' form a matching; our goal will be to characterize the size of this matching. When all edges incident to a node v are deleted from G and yet v has degree 0 in G' , we know that v will not be part of the resulting matching and call it an *isolated* node. The key to finding the size of a matching based on the KS algorithm is to count the number of nodes that either become matched or isolated as edges are deleted from the graph. We denote the iterations before the first occurrence where no nodes have a degree of 1 in G as *Phase 1* of the KS algorithm. The subsequent iterations are referred to as *Phase 2* of the KS algorithm. A key property of the KS algorithm is that it is optimal in its handling of degree-1 vertices: given an edge e that is incident to a degree-1 vertex, there is always a maximum matching that contains e (Bohman and Frieze 2011, Balister and Gerke 2015). This result implies that the KS algorithm is optimal until the end of phase 1. Let M_1^l, M_1^r, M_2^l and M_2^r respectively denote the set of nodes in V_l and

²³The computer-aided proof can be found at <https://bit.ly/3uQwGEI>.

Algorithm 1 Karp-Sipser's (KS) Algorithm

- 1: **Input:** Graph G
 - 2: Initialize graph G' as an empty graph on the same set of nodes as G
 - 3: **while** G has edges **do**
 - 4: **if** there exists a node of degree 1 in G **then**
 - 5: Choose an edge e that is incident to a node of degree 1 uniformly at random
 - 6: **else**
 - 7: Choose an edge e from all remaining edges uniformly at random
 - 8: Add edge e to graph G'
 - 9: Delete edge e and all edges incident to e from graph G
 - 10: **Output:** The number of edges in G'
-

V_r that enter the matching (i.e., incident to edges in G') during phase 1 and 2. By symmetry, we know that $m_1 := |M_1^l| = |M_1^r|$ and $m_2 := |M_2^l| = |M_2^r|$. Similarly, let $\Psi_1^l, \Psi_1^r, \Psi_2^l$ and Ψ_2^r respectively represent the set of nodes that become isolated in V_l and V_r during phase 1 and 2, where Ψ_1^l and Ψ_1^r also include the nodes that are already isolated initially in graph G . We define $\psi_1 := \max\{|\Psi_1^l|, |\Psi_1^r|\}$ and

$$\psi_2 := n - m_1 - m_2 - \psi_1 = \min \left\{ n - |M_1^l| - |M_2^l| - |\Psi_1^l|, n - |M_1^r| - |M_2^r| - |\Psi_1^r| \right\} = \min\{|\Psi_2^l|, |\Psi_2^r|\}.$$

Intuitively, ψ_2 represents the number of nodes that become isolated in Phase 2 of the KS algorithm (excluding those already accounted for in Phase 1). It has been demonstrated that, for different types of sparse random graph settings, that the expected number of nodes becoming isolated in Phase 2 of the KS algorithm is $o(n)$, i.e., $\mathbb{E}[\psi_2] \in o(n)$. We state this as Condition 1, which we later verify for a subset of instances in our model.

Condition 1 *When the KS algorithm is applied to a random graph G of our model, $\mathbb{E}[\psi_2] \in o(n)$.*

As the KS algorithm is optimal in Phase 1, Condition 1 guarantees that it is asymptotically optimal. Specifically, in Phase 2, the expected fraction of nodes that become isolated, and thus unmatched, is vanishingly small, i.e., it involves $o(n)$ nodes. Thus, to identify the number of unmatched nodes in both phases, it suffices to evaluate ψ_1 , for which we evaluate the probability of a node becoming isolated in Phase 1 of the KS algorithm. For $\mathbf{b} = (b_l, b_r)$, we will show that this probability is determined by the following set of equations:

$$\begin{aligned}
w_L^f(\mathbf{b}) &= e^{-2b_r\alpha^f(1-\hat{w}_H^f(\mathbf{b}))-(1-b_r)(\alpha^f+\alpha)(1-\hat{w}_H^{nf}(\mathbf{b}))}, \\
w_L^{nf}(\mathbf{b}) &= e^{-b_r(\alpha^f+\alpha)(1-\hat{w}_H^f(\mathbf{b}))-2(1-b_r)\alpha(1-\hat{w}_H^{nf}(\mathbf{b}))}, \\
w_H^f(\mathbf{b}) &= 1 - e^{-2b_r\alpha^f\hat{w}_L^f(\mathbf{b})-(1-b_r)(\alpha^f+\alpha)\hat{w}_L^{nf}(\mathbf{b})}, \\
w_H^{nf}(\mathbf{b}) &= 1 - e^{-b_r(\alpha^f+\alpha)\hat{w}_L^f(\mathbf{b})-2(1-b_r)\alpha\hat{w}_L^{nf}(\mathbf{b})}, \\
\hat{w}_L^f(\mathbf{b}) &= e^{-2b_l\alpha^f(1-w_H^f(\mathbf{b}))-(1-b_l)(\alpha^f+\alpha)(1-w_H^{nf}(\mathbf{b}))}, \\
\hat{w}_L^{nf}(\mathbf{b}) &= e^{-b_l(\alpha^f+\alpha)(1-w_H^f(\mathbf{b}))-2(1-b_l)\alpha(1-w_H^{nf}(\mathbf{b}))}, \\
\hat{w}_H^f(\mathbf{b}) &= 1 - e^{-2b_l\alpha^f w_L^f(\mathbf{b})-(1-b_l)(\alpha^f+\alpha)w_L^{nf}(\mathbf{b})}, \\
\hat{w}_H^{nf}(\mathbf{b}) &= 1 - e^{-b_l(\alpha^f+\alpha)w_L^f(\mathbf{b})-2(1-b_l)\alpha w_L^{nf}(\mathbf{b})}.
\end{aligned} \tag{11}$$

We denote the smallest set of solutions²⁴

$$\mathbf{w} = \left(w_L^f(\mathbf{b}), w_L^{nf}(\mathbf{b}), w_H^f(\mathbf{b}), w_H^{nf}(\mathbf{b}), \hat{w}_L^f(\mathbf{b}), \hat{w}_L^{nf}(\mathbf{b}), \hat{w}_H^f(\mathbf{b}), \hat{w}_H^{nf}(\mathbf{b}) \right)$$

to (11) by $\mathbf{y} = \left(y_L^f(\mathbf{b}), y_L^{nf}(\mathbf{b}), y_H^f(\mathbf{b}), y_H^{nf}(\mathbf{b}), \hat{y}_L^f(\mathbf{b}), \hat{y}_L^{nf}(\mathbf{b}), \hat{y}_H^f(\mathbf{b}), \hat{y}_H^{nf}(\mathbf{b}) \right)$.

THEOREM 8. *Let*

$$\begin{aligned}
\xi(b_l, b_r) &= 2 - b_l y_L^f(\mathbf{b}) - b_r \left(1 - \hat{y}_H^f(\mathbf{b}) \right) \\
&\quad - b_r \left(1 - \hat{y}_H^f(\mathbf{b}) \right) \left(2b_l \alpha^f y_L^f(\mathbf{b}) + (1-b_l)(\alpha^f + \alpha) y_L^{nf}(\mathbf{b}) \right) \\
&\quad - (1-b_l) y_L^{nf}(\mathbf{b}) - (1-b_r) \left(1 - \hat{y}_H^{nf}(\mathbf{b}) \right) \\
&\quad - (1-b_r) \left(1 - \hat{y}_H^{nf}(\mathbf{b}) \right) \left(b_l(\alpha^f + \alpha) y_L^f(\mathbf{b}) + 2(1-b_l)\alpha y_L^{nf}(\mathbf{b}) \right),
\end{aligned} \tag{12}$$

$$\begin{aligned}
\hat{\xi}(b_l, b_r) &= 2 - b_r \hat{y}_L^f(\mathbf{b}) - b_l \left(1 - y_H^f(\mathbf{b}) \right) \\
&\quad - b_l \left(1 - y_H^f(\mathbf{b}) \right) \left(2b_r \alpha^f \hat{y}_L^f(\mathbf{b}) + (1-b_r)(\alpha^f + \alpha) \hat{y}_L^{nf}(\mathbf{b}) \right) \\
&\quad - (1-b_r) \hat{y}_L^{nf}(\mathbf{b}) - (1-b_l) \left(1 - y_H^{nf}(\mathbf{b}) \right) \\
&\quad - (1-b_l) \left(1 - y_H^{nf}(\mathbf{b}) \right) \left(b_r(\alpha^f + \alpha) \hat{y}_L^f(\mathbf{b}) + 2(1-b_r)\alpha \hat{y}_L^{nf}(\mathbf{b}) \right).
\end{aligned} \tag{13}$$

Define $\mu^{KS}(b_l, b_r) = \min \left(\xi(b_l, b_r), \hat{\xi}(b_l, b_r) \right)$. Then, under Condition 1, $\mu(b_l, b_r) = \mu^{KS}(b_l, b_r)$.

We now translate Condition 1 into a looser (i.e., sufficient but not necessary) condition that is much easier to verify.

LEMMA 6. *Condition 1 holds when the solution to (11) is unique.*

Lemma 6 is instrumental for the proof of Theorem 3. The rest of this appendix is structured as follows:

- In Appendix C.3.2 we prove Theorem 8, Lemma 6, and Theorem 3. This requires us to first state the definitions and auxiliary results commonly associated with KS-style analyses, and we then prove each of these three results.

²⁴In line with terminology in Karp and Sipser (1981), the smallest set of solutions refers to the least fixed point of the system of equations in (11). Note that this is well defined since all variables in \mathbf{w} are increasing functions of each other.

- In Appendix C.3.3 we provide our computer-aided proof of Theorem 4. Our proof partitions the region of interest into small cells and numerically derives lower bounds on $\mu(1, 0)$ and upper bounds on $\mu(1/2, 1/2)$ across each such cell. For each cell, we identify a particular point (α, α^f) at which we numerically solve (11) for both $\mathbf{b} = (1, 0)$ and $\mathbf{b} = (1/2, 1/2)$ within a given tolerance ϵ (see Claim 3). Crucially, that tolerance guarantees that the solution to (11) is within ϵ of the true solution; we analytically translate this bound into a bound on the gap between the numerically computed value and μ^{KS} . We also show that the smallest solution to (11) is continuous in α and α^f , which implies that the bound holds, with an additional error term, within a δ -neighborhood of (α, α^f) , which represents the cell that (α, α^f) is part of (Claim 4). We iterate over cells to verify for the entire region that our lower bounds on $\mu(1, 0)$ are greater than our upper bounds on $\mu(1/2, 1/2)$.
- In Appendix C.3.4 we provide the computer-aided proof of Theorem 6. We take directional second-order derivatives (SOD) of $\mu^{\text{KS}}(b_l, b_r)$ and evaluate them at $\mathbf{b} = (1/2, 1/2)$ to prove concavity and convexity results in the respective directions. In particular, the SODs depend only on α, α^f , and solutions to (11). Then, similar to the approach in Appendix C.3.2, we lower and upper bound the solution to (11) within every small cell and iterate over cells to verify the signs of the directional SODs.
- In Appendix C.3.5 we provide the proof of the auxiliary results in Appendix C.3.2.
- In Appendix C.3.6 we explain the setup of the computational results in Section 5 based on $\mu^{\text{KS}}(b_l, b_r)$, as well as the range of parameters that we experiment with.

C.3.2. Phase 1 of the KS Algorithm In this section, we analyze phase 1 of the KS algorithm for $G_n^{glb}(b_l, b_r)$, hereafter referred to as G for notational simplicity. The set of edges in G is denoted by E , and the set of nodes is denoted by $V := V_l \cup V_r$. Our analysis extends the results for sparse random graphs presented in Karp and Sipser (1981) to random bipartite graphs. Similar to Balister and Gerke (2015), we analyze bipartite graphs in which the degree distributions for nodes are heterogeneous; however, the “configuration model” considered in their paper does not capture our setting with flexible and regular nodes, and we require different probabilistic computations to handle the heterogeneous edge probabilities between nodes of different flexibility types (i.e., 2α between two regular nodes, $\alpha^f + \alpha$ between a flexible and a regular node, and $2\alpha^f$ between two flexible nodes). We next present all auxiliary results needed for Theorem 8, Lemma 6 and Theorem 3, the three main technical results based on KS-style analyses.

We begin by introducing the concept of a *derivation*, which is essential for computing the asymptotic size of a maximum matching. We shall show that nodes that appear in a derivation become either matched or isolated in Phase 1 of the KS algorithm. Moreover, depending on their positions in the derivation, nodes can be classified as either a *target* or a *loser*, which determines the number of nodes that become matched or isolated in Phase 1.

DEFINITION 6. A *derivation* is a sequence $a_1, b_1, a_2, b_2, \dots$, of distinct nodes such that, for $i = 1, 2, \dots$:

- (1) $\{a_i, b_i\} \in E$;
- (2) $\{a_i, b\} \in E$ implies $b \in \{b_1, b_2, \dots, b_i\}$.

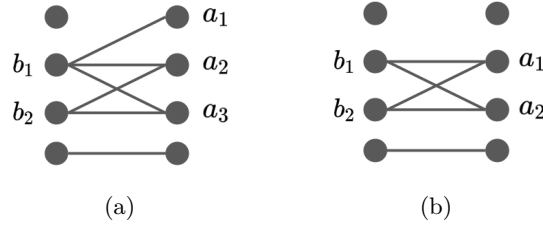


Figure 23 In Fig. 23 (a), the sequence a_1, b_1, a_2, b_2, a_3 is a derivation. Notice that all nodes in this derivation are either matched or isolated in phase 1 of the KS algorithm: the edge (a_1, b_1) is added to graph G' as a_1 is the only node of degree 1 within the connected component; we then delete all edges incident to a_1 and b_1 , leaving (a_2, b_2) and (b_2, a_3) as the only remaining edges in the graph; next, by adding (a_2, b_2) into G' (the case of (b_2, a_3) is symmetric as the sequence a_1, b_1, a_3, b_2, a_2 is also a derivation), a_1, b_1, a_2 and b_2 become matched while a_3 becomes isolated. In contrast, there is no derivation in Fig. 23 (b) that involves the connected component $\{a_1, b_1, a_2, b_2\}$ and none of these nodes become matched or isolated during phase 1 of the KS algorithm.

For example, the sequence a_1, b_1, a_2, b_2, a_3 in Fig. 23 (a) is a derivation: node a_1 fulfills condition (1) because $\{a_1, b_1\} \in E$, and fulfills condition (2) because it is connected to no other node. Next, we verify that a_2 fulfills condition (1) because $\{a_2, b_2\} \in E$, and fulfills condition (2) because it is only connected to b_1 and b_2 . The sequence ends with node a_3 , which is again only connected to b_1 and b_2 . On the other hand, in Fig. 23 (b) there is no derivation involving the nodes $\{a_1, a_2, b_1, b_2\}$: for a_1 and a_2 there exists no ordering of b_1 and b_2 such that $\{a_i, b\} \in E$ uniquely identifies b .

In the upcoming proofs we will demonstrate that by following the KS algorithm one can optimally match nodes that appear in a derivation by starting with nodes of degree 1 and then iteratively resolving the remaining nodes.

Within a derivation, we categorize nodes into *target* and *loser* based on the following definition:

DEFINITION 7. We define the following relation $\otimes \subseteq V \times V$: $v \otimes u$ if there exists a derivation $a_1, b_1, a_2, b_2, \dots$ and an index i such that $v = a_i$ and $u = b_i$. We call u a *target* if for some $v, v \otimes u$, and we call u a *loser* if (1) for some $v, u \otimes v$ or (2) u is the last element of an odd length derivation.

Based on Definition 7, all members of derivations are targets or losers or both. For instance, in the derivation a_1, b_1, a_2, b_2, a_3 in Fig. 23 (a), a_1, a_2 and a_3 are losers while b_1 and b_2 are targets. The next result characterizes the nodes that are *processed*, i.e., that become either matched or isolated in phase 1 of the KS algorithm. The result is an immediate application of Theorem 8 in Karp and Sipser (1981) to bipartite graphs. We defer the proofs of Proposition 4 and all auxiliary results in this section to Appendix C.3.5.

PROPOSITION 4 (Theorem 8 in Karp and Sipser (1981)). Consider any execution of the KS algorithm on G . Denote by M_1 the set of edges (v, u) that are added to G' in Phase 1. Then:

- (i) a node v is processed in phase 1 iff v occurs in some derivation;
- (ii) if u is a target then M_1 contains exactly one edge (v, u) such that $v \otimes u$;
- (iii) if edge $(v, u) \in M_1$ then $v \otimes u$ or $u \otimes v$;
- (iv) if $v \otimes u$ and $u \otimes v$ then edge $(v, u) \in M_1$;

$$(v) \psi_1 = \max \left(\left| \{v \in V_l \mid v \text{ is a loser}\} \right| - \left| \{v \in V_r \mid v \text{ is a target}\} \right|, \left| \{v \in V_r \mid v \text{ is a loser}\} \right| - \left| \{v \in V_l \mid v \text{ is a target}\} \right| \right).$$

Thus, the key to finding $\mathbb{E}[\psi_1]$ and the asymptotic matching probability lies in determining the probability of a node v being a target and/or a loser. We provide asymptotic answers to these questions by (1) conducting a probabilistic analysis of derivations in random trees and (2) demonstrating that a random tree is a good approximation to the structure obtained by selecting a node v in G and conducting a breadth-first search from v .

We now construct a random tree $\bar{G}_n(b_l, b_r)$ to approximate the structure obtained from a breadth-first search from a node v in G . As illustrated in Fig. 24, we construct the layers of the tree sequentially, mimicking a breadth-first search from the root node. The flexibility types of all nodes in a given layer are sampled according to the same distribution, and the distribution for each layer alternates between $\text{Bernoulli}(b_l)$ or $\text{Bernoulli}(b_r)$. This mimics the alternation between nodes in V_l and V_r in the bipartite graph G . Specifically, the construction of $\bar{G}_n(b_l, b_r)$ follows a branching process: assume for simplicity that the flexibility type of the root node v is drawn from the $\text{Bernoulli}(b_l)$ distribution, so that v is a flexible node (i.e., $F_v = 1$) with probability b_l and a regular node with probability $1 - b_l$. Then, v has n potential children, each being a flexible node (i.e., $F_u = 1$) with probability b_r and a regular node with probability $1 - b_r$. A potential child becomes a realized child of v with probability $2p_n + (F_v + F_u) \cdot (p_n^f - p_n)$. Each realized child u then has n potential children, with flexible and regular probabilities of b_l and $1 - b_l$, respectively. This branching process continues until no further child exists for a tree layer, a process that can be either finite or infinite. We omit the dependency on n and \mathbf{b} in $\bar{G}_n(b_l, b_r)$ whenever it is clear from the context.

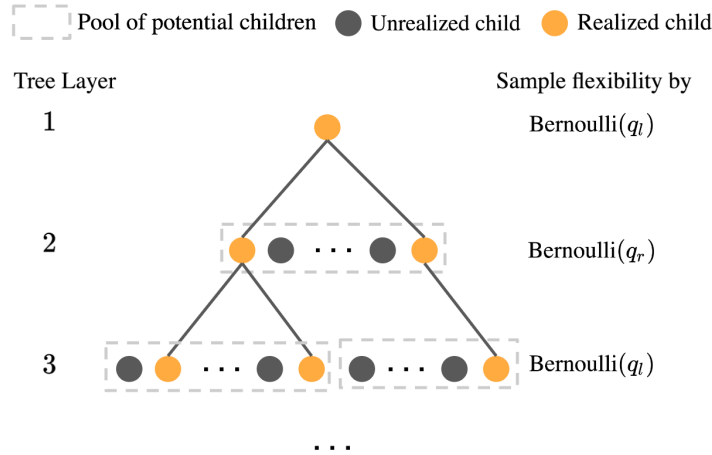


Figure 24 Illustration of the branching process for \bar{G}

To analyze the structure of \bar{G} and connect it to G , we define two subsets of nodes, L and H , through the procedure outlined in Algorithm 2. The set L_d contains all nodes added into set L in the first d repetitions of line 3 of Algorithm 2; similarly, we denote by H_d the nodes added into set H in the first d repetitions of line 3 of Algorithm 2. Since L contain all leaves of \bar{G} and all other nodes in \bar{G} have at least one child, every node in \bar{G} is added into either H or L . The classification of nodes into sets L and H is crucial for our study because it determines whether a node v is a target, a loser, or both, as stated in Lemma 7.

Algorithm 2 Classification of Nodes in \bar{G}

- 1: **Input:** A random tree \bar{G} rooted at v .
 - 2: **Initialize:** $L = \{\text{Nodes in } \bar{G} \text{ with no children in } \bar{G}\}$, $H = \emptyset$
 - 3: **repeat**
 - 4: Add to H those nodes that have at least one child in L .
 - 5: Add to L those nodes that have only children in H .
 - 6: **until** No new nodes are added to either set
-

LEMMA 7 (**Lemma 3 in Karp and Sipser (1981)**). *Let \bar{G} be a random tree rooted at v .*

- (i) v is a target iff v is in H ;
- (ii) v is a loser iff either v is in L or v has exactly 1 child which is not in H .

Given that the nodes across different tree layers exhibit heterogeneity, we define two sets of nodes: the set S_l contains all nodes sampled from layers with Bernoulli(b_l) and the set S_r contains all nodes from layers with Bernoulli(b_r). For a flexible node in S_l , we denote the probabilities of it being in L and H as $y_L^f(\mathbf{b})$ and $y_H^f(\mathbf{b})$, respectively. Similarly, for a regular node in S_l , we denote the probabilities as $y_L^{nf}(\mathbf{b})$ and $y_H^{nf}(\mathbf{b})$. We use an additional hat symbol to denote the counterparts of these probabilities in S_r , a notation consistently applied throughout this paper to differentiate quantities associated with S_r from those associated with S_l . In Lemma 8, we state that the vector

$$\mathbf{y} = \left(y_L^f(\mathbf{b}), y_L^{nf}(\mathbf{b}), y_H^f(\mathbf{b}), y_H^{nf}(\mathbf{b}), \hat{y}_L^f(\mathbf{b}), \hat{y}_L^{nf}(\mathbf{b}), \hat{y}_H^f(\mathbf{b}), \hat{y}_H^{nf}(\mathbf{b}) \right)$$

can be computed as the smallest set of solutions to the equations in (11).

LEMMA 8. *As $n \rightarrow \infty$ the probabilities encoded in \mathbf{y} converge to the smallest solution to (11).*

Now, combining Lemma 7 with Lemma 8, we obtain the probability for nodes in \bar{G} to be a target or a loser.

LEMMA 9. *Let \bar{G} be a random tree rooted at v . Then, as $n \rightarrow \infty$,*

- (i) *if v is a flexible node in S_l , v is a target with probability $y_H^f(\mathbf{b})$ and a loser with probability*

$$y_L^f(\mathbf{b}) + y_L^{nf}(\mathbf{b}) \left((1 + b_r)\alpha^f + (1 - b_r)\alpha - b_r 2\alpha^f \hat{y}_H^f(\mathbf{b}) - (1 - b_r) (\alpha^f + \alpha) \hat{y}_H^{nf}(\mathbf{b}) \right).$$

- (ii) *if v is a regular node in S_l , v is a target with probability $y_H^{nf}(\mathbf{b})$ and a loser with probability*

$$y_L^{nf}(\mathbf{b}) + y_L^f(\mathbf{b}) \left(b_r \alpha^f + (2 - b_r)\alpha - b_r (\alpha^f + \alpha) \hat{y}_H^f(\mathbf{b}) - (1 - b_r) 2\alpha \hat{y}_H^{nf}(\mathbf{b}) \right).$$

- (iii) *if v is a flexible node in S_r , v is a target with probability $\hat{y}_L^f(\mathbf{b})$ and a loser with probability*

$$\hat{y}_L^f(\mathbf{b}) + \hat{y}_H^f(\mathbf{b}) \left((1 + b_l)\alpha^f + (1 - b_l)\alpha - b_l 2\alpha^f y_H^f(\mathbf{b}) - (1 - b_l) (\alpha^f + \alpha) y_H^{nf}(\mathbf{b}) \right).$$

- (iv) *if v is a regular node in S_r , v is a target with probability $\hat{y}_L^{nf}(\mathbf{b})$ and a loser with probability*

$$\hat{y}_H^{nf}(\mathbf{b}) + \hat{y}_L^f(\mathbf{b}) \left(b_l \alpha^f + (2 - b_l)\alpha - b_l (\alpha^f + \alpha) y_H^f(\mathbf{b}) - (1 - b_l) 2\alpha y_H^{nf}(\mathbf{b}) \right).$$

Equipped with Lemma 9, we are ready to compute the probability that v appears in a derivation as $n \rightarrow \infty$.

PROPOSITION 5 (Extension of Theorem 9 (4) in Karp and Sipser (1981)). *Let v be a random node in G . Then, as $n \rightarrow \infty$:*

$$\begin{aligned}
& \lim_{n \rightarrow \infty} \mathbb{P} [v \text{ in a derivation} \mid v \text{ is a flexible node in } V_l] \\
&= y_H^f(\mathbf{b}) + y_L^f(\mathbf{b}) + y_L^f(\mathbf{b}) \left[(1 + b_r)\alpha^f + (1 - b_r)\alpha \right] \cdot \\
& \quad \left[1 - \frac{b_r 2\alpha^f}{(1 + b_r)\alpha^f + (1 - b_r)\alpha} \left(\hat{y}_L^f(\mathbf{b}) + \hat{y}_H^f(\mathbf{b}) \right) - \frac{(1 - b_r)(\alpha^f + \alpha)}{(1 + b_r)\alpha^f + (1 - b_r)\alpha} \left(\hat{y}_L^{nf}(\mathbf{b}) + \hat{y}_H^{nf}(\mathbf{b}) \right) \right], \\
& \lim_{n \rightarrow \infty} \mathbb{P} [v \text{ in a derivation} \mid v \text{ is a regular node in } V_l] \\
&= y_H^{nf}(\mathbf{b}) + y_L^{nf}(\mathbf{b}) + y_L^{nf}(\mathbf{b}) \left[b_r\alpha^f + (2 - b_r)\alpha \right] \cdot \\
& \quad \left[1 - \frac{b_r(\alpha^f + \alpha)}{b_r\alpha^f + (2 - b_r)\alpha} \left(\hat{y}_L^f(\mathbf{b}) + \hat{y}_H^f(\mathbf{b}) \right) - \frac{(1 - b_r)2\alpha}{b_r\alpha^f + (2 - b_r)\alpha} \left(\hat{y}_L^{nf}(\mathbf{b}) + \hat{y}_H^{nf}(\mathbf{b}) \right) \right], \\
& \lim_{n \rightarrow \infty} \mathbb{P} [v \text{ in a derivation} \mid v \text{ is a flexible node in } V_r] \\
&= \hat{y}_H^f(\mathbf{b}) + \hat{y}_L^f(\mathbf{b}) + \hat{y}_L^f(\mathbf{b}) \left[(1 + b_l)\alpha^f + (1 - b_l)\alpha \right] \cdot \\
& \quad \left[1 - \frac{b_l 2\alpha^f}{(1 + b_l)\alpha^f + (1 - b_l)\alpha} \left(y_L^f(\mathbf{b}) + y_H^f(\mathbf{b}) \right) - \frac{(1 - b_l)(\alpha^f + \alpha)}{(1 + b_l)\alpha^f + (1 - b_l)\alpha} \left(y_L^{nf}(\mathbf{b}) + y_H^{nf}(\mathbf{b}) \right) \right], \\
& \lim_{n \rightarrow \infty} \mathbb{P} [v \text{ in a derivation} \mid v \text{ is a regular node in } V_r] \\
&= \hat{y}_H^{nf}(\mathbf{b}) + \hat{y}_L^{nf}(\mathbf{b}) + \hat{y}_L^{nf}(\mathbf{b}) \left[b_l\alpha^f + (2 - b_l)\alpha \right] \cdot \\
& \quad \left[1 - \frac{b_l(\alpha^f + \alpha)}{b_l\alpha^f + (2 - b_l)\alpha} \left(y_L^f(\mathbf{b}) + y_H^f(\mathbf{b}) \right) - \frac{(1 - b_l)2\alpha}{b_l\alpha^f + (2 - b_l)\alpha} \left(y_L^{nf}(\mathbf{b}) + y_H^{nf}(\mathbf{b}) \right) \right].
\end{aligned}$$

Now, equipped with the auxiliary results, we are ready to prove Theorem 8, Lemma 6 and Theorem 3.

Proof of Theorem 8 Recall that the KS algorithm is asymptotically optimal under Condition 1. Specifically, by Condition 1 we find

$$\begin{aligned}
\mu(b_l, b_r) &= \lim_{n \rightarrow \infty} \frac{\mathbb{E}[\mathcal{M}_n(b_l, b_r)]}{n} = \lim_{n \rightarrow \infty} \frac{\mathbb{E}[|M_1^l| + |M_2^l|]}{n} = \lim_{n \rightarrow \infty} \frac{\mathbb{E}[n - \psi_1 - \psi_2]}{n} \\
&= 1 - \lim_{n \rightarrow \infty} \frac{\mathbb{E}[\psi_1]}{n} - \lim_{n \rightarrow \infty} \frac{\mathbb{E}[\psi_2]}{n} = 1 - \lim_{n \rightarrow \infty} \frac{\mathbb{E}[\psi_1]}{n}
\end{aligned}$$

provided that these limits exist. From Proposition 4 (v), we know

$$\begin{aligned}
\mu(b_l, b_r) &= 1 - \lim_{n \rightarrow \infty} \frac{\mathbb{E}[\psi_1]}{n} = 1 - \lim_{n \rightarrow \infty} \max \left\{ \mathbb{P} [v \in \Psi_1^l \mid v \in V_l], \mathbb{P} [v \in \Psi_1^r \mid v \in V_r] \right\} \\
&= 1 - \max \left\{ \lim_{n \rightarrow \infty} \mathbb{P} [v \text{ is a loser} \mid v \in V_l] - \lim_{n \rightarrow \infty} \mathbb{P} [v \text{ is a target} \mid v \in V_r], \right. \\
& \quad \left. \lim_{n \rightarrow \infty} \mathbb{P} [v \text{ is a loser} \mid v \in V_r] - \lim_{n \rightarrow \infty} \mathbb{P} [v \text{ is a target} \mid v \in V_l] \right\}
\end{aligned}$$

provided that these limits exist. By the law of iterated expectations, we have

$$\begin{aligned}
& \lim_{n \rightarrow \infty} \mathbb{P} [v \text{ is a loser} \mid v \in V_l] - \lim_{n \rightarrow \infty} \mathbb{P} [v \text{ is a target} \mid v \in V_r] \\
&= \lim_{n \rightarrow \infty} \mathbb{P} [v \text{ is a loser} \mid v \text{ is a flexible node in } V_l] \cdot \mathbb{P} [v \in v_l \text{ is a flexible node}]
\end{aligned}$$

$$\begin{aligned}
& + \lim_{n \rightarrow \infty} \mathbb{P} [v \text{ is a loser} \mid v \text{ is a regular node in } V_l] \cdot \mathbb{P} [v \in v_l \text{ is a regular node}] \\
& - \lim_{n \rightarrow \infty} \mathbb{P} [v \text{ is a target} \mid v \text{ is a flexible node in } V_r] \cdot \mathbb{P} [v \in v_r \text{ is a flexible node}] \\
& - \lim_{n \rightarrow \infty} \mathbb{P} [v \text{ is a target} \mid v \text{ is a regular node in } V_r] \cdot \mathbb{P} [v \in v_r \text{ is a regular node}]
\end{aligned}$$

provided that these limits exist.

Now we can plug in probabilities derived in Lemma 9, which we have shown in Claim 6 to be equal to the corresponding probabilities in random graphs:

$$\begin{aligned}
& \lim_{n \rightarrow \infty} \mathbb{P} [v \text{ is a loser} \mid v \in V_l] - \lim_{n \rightarrow \infty} \mathbb{P} [v \text{ is a target} \mid v \in V_r] \\
& = b_l \left(y_L^f(\mathbf{b}) + y_L^f(\mathbf{b}) \left((1 + b_r)\alpha^f + (1 - b_r)\alpha - b_r 2\alpha^f \hat{y}_H^f(\mathbf{b}) - (1 - b_r) (\alpha^f + \alpha) \hat{y}_H^{nf}(\mathbf{b}) \right) \right) - b_r \hat{y}_H^f(\mathbf{b}) \\
& \quad + (1 - b_l) \left(y_L^{nf}(\mathbf{b}) + y_L^{nf}(\mathbf{b}) \left(b_r \alpha^f + (2 - b_r)\alpha - b_r (\alpha^f + \alpha) \hat{y}_H^f(\mathbf{b}) - (1 - b_r) 2\alpha \hat{y}_H^{nf}(\mathbf{b}) \right) \right) - (1 - b_r) \hat{y}_H^{nf}(\mathbf{b}) \\
& = b_l \left(y_L^f(\mathbf{b}) + y_L^f(\mathbf{b}) \left(b_r 2\alpha^f (1 - \hat{y}_H^f(\mathbf{b})) + (1 - b_r) (\alpha^f + \alpha) (1 - \hat{y}_H^{nf}(\mathbf{b})) \right) \right) - 1 + b_r (1 - \hat{y}_H^f(\mathbf{b})) \\
& \quad + (1 - b_l) \left(y_L^{nf}(\mathbf{b}) + y_L^{nf}(\mathbf{b}) \left(b_r (\alpha^f + \alpha) (1 - \hat{y}_H^f(\mathbf{b})) + (1 - b_r) 2\alpha (1 - \hat{y}_H^{nf}(\mathbf{b})) \right) \right) + (1 - b_r) (1 - \hat{y}_H^{nf}(\mathbf{b})) \\
& = b_l y_L^f(\mathbf{b}) + b_r (1 - \hat{y}_H^f(\mathbf{b})) \left(2b_l \alpha^f y_L^f(\mathbf{b}) + (1 - b_l) (\alpha^f + \alpha) y_L^{nf}(\mathbf{b}) \right) - 1 + b_r (1 - \hat{y}_H^f(\mathbf{b})) \\
& \quad + (1 - b_l) y_L^{nf}(\mathbf{b}) + (1 - b_r) (1 - \hat{y}_H^{nf}(\mathbf{b})) \left(b_l (\alpha^f + \alpha) y_L^f(\mathbf{b}) + 2(1 - b_l) \alpha y_L^{nf}(\mathbf{b}) \right) + (1 - b_r) (1 - \hat{y}_H^{nf}(\mathbf{b})) \\
& =: 1 - \xi(b_l, b_r).
\end{aligned}$$

Similarly, we find that

$$\begin{aligned}
& \lim_{n \rightarrow \infty} \mathbb{P} [v \text{ is a loser} \mid v \in V_r] - \lim_{n \rightarrow \infty} \mathbb{P} [v \text{ is a target} \mid v \in V_l] \\
& = b_r \hat{y}_L^f(\mathbf{b}) + b_l (1 - y_H^f(\mathbf{b})) \left(2b_r \alpha^f \hat{y}_L^f(\mathbf{b}) + (1 - b_r) (\alpha^f + \alpha) \hat{y}_L^{nf}(\mathbf{b}) \right) - 1 + b_l (1 - y_H^f(\mathbf{b})) \\
& \quad + (1 - b_r) \hat{y}_L^{nf}(\mathbf{b}) + (1 - b_l) (1 - y_H^{nf}(\mathbf{b})) \left(b_r (\alpha^f + \alpha) \hat{y}_L^f(\mathbf{b}) + 2(1 - b_r) \alpha \hat{y}_L^{nf}(\mathbf{b}) \right) + (1 - b_l) (1 - y_H^{nf}(\mathbf{b})) \\
& =: 1 - \hat{\xi}(b_l, b_r).
\end{aligned}$$

Thus, under Condition 1

$$\begin{aligned}
\mu(b_l, b_r) & = 1 - \max \left\{ \lim_{n \rightarrow \infty} \mathbb{P} [v \text{ is a loser} \mid v \in V_l] - \lim_{n \rightarrow \infty} \mathbb{P} [v \text{ is a target} \mid v \in V_r], \right. \\
& \quad \left. \lim_{n \rightarrow \infty} \mathbb{P} [v \text{ is a loser} \mid v \in V_r] - \lim_{n \rightarrow \infty} \mathbb{P} [v \text{ is a target} \mid v \in V_l] \right\} \\
& = 1 - \max \left(1 - \xi(b_l, b_r), 1 - \hat{\xi}(b_l, b_r) \right) = \min \left(\xi(b_l, b_r), \hat{\xi}(b_l, b_r) \right) := \mu^{\text{KS}}(b_l, b_r).
\end{aligned}$$

□

Proof of Lemma 6 From Proposition 4 (i), it is known that

$$\lim_{n \rightarrow \infty} \frac{\mathbb{E}[m_1 + \psi_1]}{n} = \max \left\{ \lim_{n \rightarrow \infty} \mathbb{P} [v \text{ in a derivation} \mid v \in V_l], \lim_{n \rightarrow \infty} \mathbb{P} [v \text{ in a derivation} \mid v \in V_r] \right\}.$$

We next demonstrate that if the solution to (11) is unique, then

$$\lim_{n \rightarrow \infty} \mathbb{P} [v \text{ in a derivation} \mid v \in V_l] = \lim_{n \rightarrow \infty} \mathbb{P} [v \text{ in a derivation} \mid v \in V_r] = 1. \quad (14)$$

To establish (14), we leverage Proposition 5 and consider a random node v in G , which can be either flexible or regular and either in V_l or in V_r . be a flexible node in V_l , a regular node in V_l , a flexible node in V_r , or a regular node in V_r . We shall demonstrate that $\lim_{n \rightarrow \infty} \mathbb{P}[v \text{ in a derivation}] = 1$ when the solution to (11) is unique.

Note that for any solution vector \mathbf{w} to (11), it is always feasible to construct

$$\begin{aligned} x_L^f(b_l, b_r) &= w_L^f(\mathbf{b}), x_H^f(b_l, b_r) = 1 - w_L^f(\mathbf{b}), \\ x_L^{nf}(b_l, b_r) &= w_L^{nf}(\mathbf{b}), x_H^{nf}(b_l, b_r) = 1 - w_L^{nf}(\mathbf{b}), \\ \hat{x}_L^f(b_l, b_r) &= \hat{w}_L^f(\mathbf{b}), \hat{x}_H^f(b_l, b_r) = 1 - \hat{w}_L^f(\mathbf{b}), \\ \hat{x}_L^{nf}(b_l, b_r) &= \hat{w}_L^{nf}(\mathbf{b}), \hat{x}_H^{nf}(b_l, b_r) = 1 - \hat{w}_L^{nf}(\mathbf{b}), \end{aligned} \tag{15}$$

so that \mathbf{x} is provably a solution to (11). Consequently, when (11) admits a unique solution, the smallest set of solutions \mathbf{y} must satisfy (15). We next substitute (15) into the expressions derived in Proposition 5 and simplify to find that

$$\begin{aligned} & \lim_{n \rightarrow \infty} \mathbb{P}[v \text{ in a derivation} \mid v \text{ is a flexible node in } V_l] \\ &= y_H^f(\mathbf{b}) + y_L^f(\mathbf{b}) + y_L^f(\mathbf{b}) \left[(1 + b_r)\alpha^f + (1 - b_r)\alpha \right] \cdot \\ & \quad \left[1 - \frac{b_r 2\alpha^f}{(1 + b_r)\alpha^f + (1 - b_r)\alpha} \left(\hat{y}_L^f(\mathbf{b}) + \hat{y}_H^f(\mathbf{b}) \right) - \frac{(1 - b_r)(\alpha^f + \alpha)}{(1 + b_r)\alpha^f + (1 - b_r)\alpha} \left(\hat{y}_L^{nf}(\mathbf{b}) + \hat{y}_H^{nf}(\mathbf{b}) \right) \right] \\ &= 1 + y_L^f(\mathbf{b}) \left[(1 + b_r)\alpha^f + (1 - b_r)\alpha \right] \cdot \left[1 - \frac{b_r 2\alpha^f}{(1 + b_r)\alpha^f + (1 - b_r)\alpha} - \frac{(1 - b_r)(\alpha^f + \alpha)}{(1 + b_r)\alpha^f + (1 - b_r)\alpha} \right] \\ &= 1 + y_L^f(\mathbf{b}) \left[(1 + b_r)\alpha^f + (1 - b_r)\alpha \right] \cdot 0 \\ &= 1. \end{aligned}$$

One can show analogously that nodes in V_r or regular nodes in V_l have a probability of 1, asymptotically, to be in a derivation.

Consequently, we have

$$\begin{aligned} \lim_{n \rightarrow \infty} \frac{\mathbb{E}[\psi_2]}{n} &\leq 1 - \lim_{n \rightarrow \infty} \frac{\mathbb{E}[m_1 + \psi_1]}{n} \\ &= 1 - \max \left\{ \lim_{n \rightarrow \infty} \mathbb{P}[v \text{ in a derivation} \mid v \in V_l], \lim_{n \rightarrow \infty} \mathbb{P}[v \text{ in a derivation} \mid v \in V_r] \right\} = 0, \end{aligned}$$

thereby verifying Condition 1. \square

Proof of Theorem 3 By Theorem 8 and Lemma 6, to establish Theorem 3 it is sufficient to demonstrate that when $10^{-4} < \alpha < \alpha^f$ and $\alpha^f + \alpha < e$ the solution to (11) is unique at the points $\mathbf{b} = (1, 0)$, $(0, 1)$ and $(1/2, 1/2)$.

When $\mathbf{b} = (1, 0)$, all nodes in V_l are flexible nodes, while those in V_r are regular nodes. Thus, it suffices to analyze $w_L^f(\mathbf{b})$, $w_H^f(\mathbf{b})$, $\hat{w}_L^{nf}(\mathbf{b})$ and $\hat{w}_H^{nf}(\mathbf{b})$. Then, (11) reduces to

$$w_L^f(\mathbf{b}) = e^{-(\alpha^f + \alpha)(1 - \hat{w}_H^{nf}(\mathbf{b}))}, \hat{w}_H^{nf}(\mathbf{b}) = 1 - e^{-(\alpha^f + \alpha)w_L^f(\mathbf{b})}, \tag{16}$$

$$\hat{w}_L^{nf}(\mathbf{b}) = e^{-(\alpha^f + \alpha)(1 - w_H^f(\mathbf{b}))}, w_H^f(\mathbf{b}) = 1 - e^{-(\alpha^f + \alpha)\hat{w}_L^{nf}(\mathbf{b})}. \tag{17}$$

Since (16) and (17) are equivalent, it suffices to show that solution to the pair $(w_L^f(\mathbf{b}), \hat{w}_H^{nf}(\mathbf{b}))$ in (16) is unique. This is a direct application of the following result from Karp and Sipser (1981), by taking $L = w_L^f(\mathbf{b})$, $W = \hat{w}_H^{nf}(\mathbf{b})$ and $\lambda = \alpha^f + \alpha$:

CLAIM 1 (**Lemma 1 in Karp and Sipser (1981)**). Define $L = e^{-\lambda(1-W)}$, $W = 1 - e^{-\lambda L}$. Then, $L + W \leq 1$, with equality if and only if $\lambda \leq e$.

The case for $\mathbf{b} = (0, 1)$ is symmetric.

For the case of $\mathbf{b} = (1/2, 1/2)$, symmetry implies that

$$w_L^f(\mathbf{b}) = \hat{w}_L^f(\mathbf{b}), w_L^{nf}(\mathbf{b}) = \hat{w}_L^{nf}(\mathbf{b}), w_H^f(\mathbf{b}) = \hat{w}_H^f(\mathbf{b}), w_H^{nf}(\mathbf{b}) = \hat{w}_H^{nf}(\mathbf{b}).$$

Substituting $\mathbf{b} = (1/2, 1/2)$ into (11), we obtain the following equations:

$$\begin{aligned} w_L^f(\mathbf{b}) &= e^{-\frac{1}{2}2\alpha^f(1-\hat{w}_H^f(\mathbf{b}))-\frac{1}{2}(\alpha^f+\alpha)(1-\hat{w}_H^{nf}(\mathbf{b}))}, \\ w_L^{nf}(\mathbf{b}) &= e^{-\frac{1}{2}(\alpha^f+\alpha)(1-\hat{w}_H^f(\mathbf{b}))-\frac{1}{2}2\alpha(1-\hat{w}_H^{nf}(\mathbf{b}))}, \\ \hat{w}_H^f(\mathbf{b}) &= 1 - e^{-\frac{1}{2}2\alpha^f w_L^f(\mathbf{b})-\frac{1}{2}(\alpha^f+\alpha)w_L^{nf}(\mathbf{b})}, \\ \hat{w}_H^{nf}(\mathbf{b}) &= 1 - e^{-\frac{1}{2}(\alpha^f+\alpha)w_L^f(\mathbf{b})-\frac{1}{2}2\alpha w_L^{nf}(\mathbf{b})}. \end{aligned} \tag{18}$$

We observe that values of $w_L^f(\mathbf{b}), w_L^{nf}(\mathbf{b}), \hat{w}_H^f(\mathbf{b})$ and $\hat{w}_H^{nf}(\mathbf{b})$ are trivially bounded between 0 and 1, and all of the variables are increasing in each other. Thus, we initialize the values of $(w_L^f(\mathbf{b}, 0), w_L^{nf}(\mathbf{b}, 0), \hat{w}_H^f(\mathbf{b}, 0), \hat{w}_H^{nf}(\mathbf{b}, 0)) = (0, 0, 0, 0)$ and define, for any $d \in \mathbb{Z}^+$,

$$\begin{aligned} w_L^f(\mathbf{b}, d) &= e^{-\frac{1}{2}2\alpha^f(1-\hat{w}_H^f(\mathbf{b}, d-1))-\frac{1}{2}(\alpha^f+\alpha)(1-\hat{w}_H^{nf}(\mathbf{b}, d-1))}, \\ w_L^{nf}(\mathbf{b}, d) &= e^{-\frac{1}{2}(\alpha^f+\alpha)(1-\hat{w}_H^f(\mathbf{b}, d-1))-\frac{1}{2}2\alpha(1-\hat{w}_H^{nf}(\mathbf{b}, d-1))}, \\ \hat{w}_H^f(\mathbf{b}, d) &= 1 - e^{-\frac{1}{2}2\alpha^f w_L^f(\mathbf{b}, d-1)-\frac{1}{2}(\alpha^f+\alpha)w_L^{nf}(\mathbf{b}, d-1)}, \\ \hat{w}_H^{nf}(\mathbf{b}, d) &= 1 - e^{-\frac{1}{2}(\alpha^f+\alpha)w_L^f(\mathbf{b}, d-1)-\frac{1}{2}2\alpha w_L^{nf}(\mathbf{b}, d-1)}. \end{aligned}$$

Then, the smallest set of solutions to (18) is given by $\lim_{d \rightarrow \infty} (w_L^f(\mathbf{b}, d), w_L^{nf}(\mathbf{b}, d), \hat{w}_H^f(\mathbf{b}, d), \hat{w}_H^{nf}(\mathbf{b}, d))$.

For any $\vec{\mathbf{x}} \in \mathbb{R}^2$, define

$$F(\vec{\mathbf{x}}) = \begin{pmatrix} e^{-\frac{1}{2}2\alpha^f x_1 - \frac{1}{2}(\alpha^f + \alpha)x_2} \\ e^{-\frac{1}{2}(\alpha^f + \alpha)x_1 - \frac{1}{2}2\alpha x_2} \end{pmatrix}$$

and define $F^t(\vec{\mathbf{x}})$ the t th application of the function F on $\vec{\mathbf{x}}$. That is, $F^0(\vec{\mathbf{x}}) = \vec{\mathbf{x}}$, $F^1(\vec{\mathbf{x}}) = F(\vec{\mathbf{x}})$ and $F^2(\vec{\mathbf{x}}) = F(F(\vec{\mathbf{x}}))$. Then, the smallest solutions to $\begin{pmatrix} w_L^f(\mathbf{b}) \\ w_L^{nf}(\mathbf{b}) \end{pmatrix}$ and $\vec{\mathbf{1}} - \begin{pmatrix} \hat{w}_H^f(\mathbf{b}) \\ \hat{w}_H^{nf}(\mathbf{b}) \end{pmatrix}$ are respectively given by $\lim_{t \rightarrow \infty} F^{2t}(\vec{\mathbf{1}})$ and $\lim_{t \rightarrow \infty} F^{2t+1}(\vec{\mathbf{1}})$. In particular, $\begin{pmatrix} w_L^f(\mathbf{b}) \\ w_L^{nf}(\mathbf{b}) \end{pmatrix} = \vec{\mathbf{1}} - \begin{pmatrix} \hat{w}_H^f(\mathbf{b}) \\ \hat{w}_H^{nf}(\mathbf{b}) \end{pmatrix}$ and the solution is unique if $F(\vec{\mathbf{x}})$ has a unique fixed point, i.e., there exists a unique $\vec{\mathbf{x}}^*$ such that $F(\vec{\mathbf{x}}^*) = \vec{\mathbf{x}}^*$. Notice that in $F(\vec{\mathbf{x}}) = \vec{\mathbf{x}}$ we have $x_1 = e^{-\alpha^f x_1 - \frac{1}{2}(\alpha^f + \alpha)x_2}$, so $x_2 = -2\frac{\log(x_1) + \alpha^f x_1}{\alpha^f + \alpha}$. Plugging this into $x_2 = e^{-\frac{1}{2}(\alpha^f + \alpha)x_1 - \frac{1}{2}2\alpha x_2}$, we find that

$$-2\frac{\log(x_1) + \alpha^f x_1}{\alpha^f + \alpha} = e^{-\frac{1}{2}(\alpha^f + \alpha)x_1 + 2\frac{\alpha}{\alpha^f + \alpha}(\log(x_1) + \alpha^f x_1)}, \tag{19}$$

so it suffices to show that (19) has a unique solution when $\alpha^f + \alpha < e$.

Let

$$f_1(x_1) := e^{-\frac{1}{2}(\alpha^f + \alpha)x_1 + 2\frac{\alpha}{\alpha^f + \alpha}(\log(x_1) + \alpha^f x_1)} + 2\frac{\log(x_1) + \alpha^f x_1}{\alpha^f + \alpha}. \tag{20}$$

The next result establishes a monotonicity property of this function:

CLAIM 2. When $10^{-4} < \alpha < \alpha^f$ and $\alpha^f + \alpha < e$, $f_1'(x_1) > 1$ for any $x_1 \in (0, 1]$.

Since $f_1(0) = -\infty$ and $f_1(1) \geq 0$, by continuity of $f_1(x_1)$ with respect to x_1 we know that $f_1(x_1) = 0$ has at least one solution in $(0, 1]$. Since we also know from Claim 2 that $f_1(x_1)$ is strictly monotonically increasing with respect to x_1 in $(0, 1]$ when $10^{-4} < \alpha < \alpha^f$ and $\alpha^f + \alpha < e$, such solution for x_1 is unique. This completes the proof of Theorem 3. \square

C.3.3. Proof of Theorem 4

Proof. Recall from Theorem 3 that, in the stated parameter regimes, $\mu(b_l, b_r) = \mu^{\text{KS}}(b_l, b_r)$ at $\mathbf{b} = (1, 0)$ and $(1/2, 1/2)$. Since the solution to (11) is unique at these points, (15) is satisfied by the smallest set of solutions \mathbf{y} . Plugging

$$y_L^f(\mathbf{b}) = 1 - y_H^f(\mathbf{b}), y_L^{nf}(\mathbf{b}) = y_H^{nf}(\mathbf{b})$$

into (12) and (13), we find that at these values of \mathbf{b}

$$\begin{aligned} \mu(b_l, b_r) &= \xi(b_l, b_r) = \hat{\xi}(b_l, b_r) \\ &= 2 - b_l y_L^f(\mathbf{b}) - b_r e^{-b_1(b_l, b_r)} (1 + b_1(b_l, b_r)) - (1 - b_l) y_L^{nf}(\mathbf{b}) - (1 - b_r) e^{-b_2(b_l, b_r)} (1 + b_2(b_l, b_r)), \end{aligned}$$

where

$$\begin{aligned} b_1(b_l, b_r) &= b_l 2\alpha^f y_L^f(\mathbf{b}) + (1 - b_l) (\alpha^f + \alpha) y_L^{nf}(\mathbf{b}), \\ b_2(b_l, b_r) &= b_l (\alpha^f + \alpha) y_L^f(\mathbf{b}) + (1 - b_l) 2\alpha y_L^{nf}(\mathbf{b}). \end{aligned}$$

When $\mathbf{b} = (1, 0)$, $\mu(b_l, b_r)$ depends only on $y_L^f(\mathbf{b})$, which can be solved as the unique solution x^* to

$$x = e^{-(\alpha^f + \alpha)} e^{-(\alpha^f + \alpha)x}. \quad (21)$$

When $\mathbf{b} = (1/2, 1/2)$, $\mu(b_l, b_r)$ depends only on $(y_L^f(\mathbf{b}), y_L^{nf}(\mathbf{b}))$, which can be solved as the unique set of solution (x_1^*, x_2^*) to

$$\begin{aligned} x_1 &= e^{-\frac{1}{2}2\alpha^f x_1 - \frac{1}{2}(\alpha^f + \alpha)x_2}, \\ x_2 &= e^{-\frac{1}{2}(\alpha^f + \alpha)x_1 - \frac{1}{2}2\alpha x_2}. \end{aligned} \quad (22)$$

Our objective is to show that $\mu(1, 0) > \mu(1/2, 1/2)$ for any α^f and α satisfying $10^{-4} < \alpha < \alpha^f$ and $\alpha^f + \alpha < e$. To do so, we divide the parameter regions into small cells and prove the inequality by deriving bounds within each cell. We fix a constant $\delta > 0$ and derive for any α, α^f , a lower bound for the expression $\mu(1, 0) - \mu(1/2, 1/2)$ for any $(\bar{\alpha}^f, \bar{\alpha}) \in \mathcal{I}(\alpha, \alpha^f, \delta) := \{(\bar{\alpha}, \bar{\alpha}^f) : \bar{\alpha} \in [\alpha, \alpha + \delta), \bar{\alpha}^f \in [\alpha^f, \alpha^f + \delta)\}$. We then employ a computer-aided proof to iterate over all cells in the claimed region and verify if this lower bound is positive for the respective cell. To do so, we need to bound $\bar{\alpha}^f, \bar{\alpha}$ and the resulting \bar{x}, \bar{x}_1 and \bar{x}_2 in each cell. In $\mathcal{I}(\alpha, \alpha^f, \delta)$, if we know the respective lower and upper bounds of \bar{x}, \bar{x}_1 and \bar{x}_2 , which we denote by $x^{lb}, x^{ub}, x_1^{lb}, x_1^{ub}, x_2^{lb}$ and x_2^{ub} , then we can lower bound

$$\begin{aligned} \mu(1, 0) &= 2 - \bar{x} - e^{-(\bar{\alpha}^f + \bar{\alpha})\bar{x}} \left[1 + (\bar{\alpha}^f + \bar{\alpha})\bar{x} \right] \\ &\geq 2 - x^{ub} - e^{-(\alpha^f + \alpha)x^{ub}} \left[1 + (\alpha^f + \alpha + 2\delta)x^{ub} \right], \forall (\bar{\alpha}^f, \bar{\alpha}) \in \mathcal{I}(\alpha, \alpha^f, \delta). \end{aligned} \quad (23)$$

Similarly, we can upper bound

$$\begin{aligned}
\mu(1/2, 1/2) &= 2 - \frac{1}{2}\bar{x}_1 - \frac{1}{2}\bar{x}_2 - \frac{1}{2}e^{-(\bar{\alpha}^f)\bar{x}_1 - \frac{1}{2}(\bar{\alpha}^f + \bar{\alpha})\bar{x}_2} \left[1 + \bar{\alpha}^f \bar{x}_1 + \frac{1}{2}(\bar{\alpha}^f + \bar{\alpha})\bar{x}_2 \right] \\
&\quad - \frac{1}{2}e^{-\frac{1}{2}(\bar{\alpha}^f + \bar{\alpha})\bar{x}_1 - (\bar{\alpha})\bar{x}_2} \left[1 + \frac{1}{2}(\bar{\alpha}^f + \bar{\alpha})\bar{x}_1 + \bar{\alpha}\bar{x}_2 \right] \\
&\leq 2 - \frac{1}{2}x_1^{lb} - \frac{1}{2}x_2^{lb} \\
&\quad - \frac{1}{2}e^{-(\alpha^f + \delta)x_1^{ub} - \frac{1}{2}(\alpha^f + \alpha + 2\delta)x_2^{ub}} \left[1 + \alpha^f x_1^{lb} + \frac{1}{2}(\alpha^f + \alpha)x_2^{lb} \right] \\
&\quad - \frac{1}{2}e^{-\frac{1}{2}(\alpha^f + \alpha + 2\delta)x_1^{ub} - (\alpha + \delta)x_2^{ub}} \left[1 + \frac{1}{2}(\alpha^f + \alpha)x_1^{lb} + \alpha x_2^{lb} \right], \forall (\bar{\alpha}^f, \bar{\alpha}) \in \mathcal{I}(\alpha, \alpha^f, \delta).
\end{aligned} \tag{24}$$

Thus, it suffices to find $x^{lb}, x^{ub}, x_1^{lb}, x_1^{ub}, x_2^{lb}$ and x_2^{ub} in the corresponding cell. To do this, we start by showing that, for given α^f and α , the solution returned by `nlsolve` package in Julia programming language is provably close to the true solution x^*, x_1^* and x_2^* , and then provide a continuity argument to bound the solution \bar{x}, \bar{x}_1 and \bar{x}_2 for any $(\bar{\alpha}^f, \bar{\alpha}) \in \mathcal{I}(\alpha, \alpha^f, \delta)$.

We start by bounding the value of x^*, x_1^* , and x_2^* based on the numerical solutions returned by Julia `nlsolve`. We parameterize the tolerance level `ftol` in `nlsolve` by ϵ , which guarantees that, when solving the equation $g(x) = 0$ for any function $g: \mathbb{R} \mapsto \mathbb{R}$, `nlsolve` returns a solution x such that $|g(x)| < \epsilon$. We let $f(x) := x - e^{-(\alpha^f + \alpha)x}$ and recall from (20) that $f_1(x_1) = e^{-\frac{1}{2}(\alpha^f + \alpha)x_1 + 2\frac{\alpha}{\alpha^f + \alpha}(\log(x_1) + \alpha^f x_1)} + 2\frac{\log(x_1) + \alpha^f x_1}{\alpha^f + \alpha}$. Then, we leverage monotonicity properties of $f(x)$ and $f_1(x_1)$ to derive the following bounds on x^*, x_1^* and x_2^* :

CLAIM 3. *Let x^{sol} and x_1^{sol} respectively denote the solutions returned by `nlsolve` for solving $f(x) = 0$ and $f_1(x_1) = 0$ with `ftol` = ϵ . When $10^{-4} < \alpha < \alpha^f$ and $\alpha^f + \alpha < e$, we have:*

$$\begin{aligned}
x^* &\in [x^{sol} - \epsilon, x^{sol} + \epsilon], x_1^* \in [x_1^{sol} - \epsilon, x_1^{sol} + \epsilon], \text{ and} \\
x_2^* &\in \left[-2\frac{\log(x_1^{sol} - \epsilon) + \alpha^f(x_1^{sol} - \epsilon)}{\alpha^f + \alpha}, -2\frac{\log(x_1^{sol} + \epsilon) + \alpha^f(x_1^{sol} + \epsilon)}{\alpha^f + \alpha} \right].
\end{aligned}$$

Having established bounds on x^*, x_1^* and x_2^* for fixed α and α^f , we continue to bound \bar{x}, \bar{x}_1 and \bar{x}_2 for $(\bar{\alpha}^f, \bar{\alpha}) \in \mathcal{I}(\alpha, \alpha^f, \delta)$. Specifically, we leverage the following result on the continuity of x^*, x_1^* and x_2^* with respect to α^f and α .

CLAIM 4. *Let x^*, x_1^* and x_2^* be the solution to (21) and (22) given α^f and α . Moreover, let \bar{x}, \bar{x}_1 and \bar{x}_2 be the solution to (21) and (22) given $\bar{\alpha}^f$ and $\bar{\alpha}$. Then, given any $\delta \in (0, 1/2)$, we know that for any $(\bar{\alpha}^f, \bar{\alpha}) \in \mathcal{I}(\alpha, \alpha^f, \delta)$ such that $10^{-4} < \bar{\alpha} < \bar{\alpha}^f$ and $\bar{\alpha}^f + \bar{\alpha} < e$:*

(i) $\bar{x} \in [x^*(1 - \delta), x^*];$

(ii) $\bar{x}_1 \in [x_1^*(1 - 2\delta), x_1^*]$ and $\bar{x}_2 \in [x_2^*(1 - 2\delta), x_2^*].$

Combining Claim 3 and Claim 4, we can lower and upper bound the solution of \bar{x}, \bar{x}_1 and \bar{x}_2 for $(\bar{\alpha}^f, \bar{\alpha}) \in \mathcal{I}(\alpha, \alpha^f, \delta)$ where $\bar{\alpha}^f + \bar{\alpha} < e$. In particular, for given $\delta > 0$, we take

$$\begin{aligned} x^{lb} &= (x^{sol} - \epsilon)(1 - \delta), x^{ub} = (x^{sol} + \epsilon), \\ x_1^{lb} &= (x_1^{sol} - \epsilon)(1 - 2\delta), x_1^{ub} = (x_1^{sol} + \epsilon), \\ x_2^{lb} &= -2 \frac{\log(x_1^{sol} - \epsilon) + \alpha^f (x_1^{sol} - \epsilon)}{\alpha^f + \alpha} (1 - 2\delta), \\ x_2^{ub} &= -2 \frac{\log(x_1^{sol} + \epsilon) + \alpha^f (x_1^{sol} + \epsilon)}{\alpha^f + \alpha}. \end{aligned} \quad (25)$$

Plugging these values into (23) - (24), we obtain a lower bound of $\mu(1, 0) - \mu(1/2, 1/2)$ in each cell $\mathcal{I}(\alpha, \alpha^f, \delta)$. Whenever this lower bound exceeds 0, our reasoning implies that $\mu(1, 0) > \mu(1/2, 1/2)$ for any $(\bar{\alpha}^f, \bar{\alpha})$ within this cell. In `Theorem3.ipynb`,²⁵ we fix $\epsilon = 10^{-8}$ and compute the value of this lower bound for $\alpha^f, \alpha = \delta, 2\delta, \dots, e$ where $\alpha^f + \alpha < e$. We find that by taking $\delta = 0.01, 0.005, 0.0025$ and 0.001 we are able to verify $\mu(1, 0) > \mu(1/2, 1/2)$ in the respective red regions in Fig. 25.

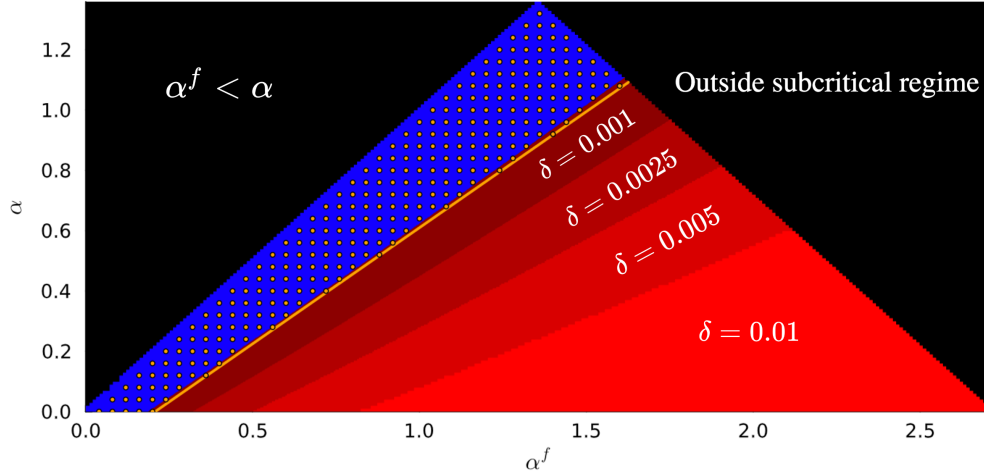


Figure 25 In the figure we denote the boundary where $\alpha = 0.77\alpha^f - 0.16$ by the orange line, and the area of subcritical regime where one-sided allocation dominates the balanced allocation is displayed in varying shades of red to the right of this boundary. This growth in the validation area with respect to δ is depicted through different red gradients. The black zone denotes parameters outside the feasible or subcritical regime. Although the inequality cannot be confirmed in the blue region when $\delta = 0.001$, by taking $\delta = 0$ we verify the inequality for a wide range of (α^f, α) values highlighted as orange dots.

□

Proof of Claim 3 For $f(x) = x - e^{-(\alpha^f + \alpha)x}$, we find that $f'(x) > 1 \forall x$. When solving $f(x) = 0$, `nlsolve` is guaranteed to return a solution x^{sol} with $|f(x^{sol})| < \epsilon$. Since $f'(x) > 1 \forall x$, if $x^* > x^{sol} + \epsilon$ then

$$f(x^*) > f(x^{sol} + \epsilon) > f(x^{sol}) + \epsilon > 0,$$

²⁵The computer-aided proof can be found at <https://bit.ly/3UUVFRX>.

which contradicts the fact that $f(x^*) = 0$. Similarly, we must have $x^* > x^{sol} - \epsilon$ and thus $x^* \in [x^{sol} - \epsilon, x^{sol} + \epsilon]$.

Since we know from Claim 2 that $f'_1(x_1) > 1$ in the specified parameter regime of α and α^f , through the same argument on $f_1(x_1)$ we find that $x_1^* \in [x_1^{sol} - \epsilon, x_1^{sol} + \epsilon]$. From (22) we know that $x_2^* = -2 \frac{\log(x_1^*) + \alpha^f x_1^*}{\alpha^f + \alpha}$, which allows us to lower bound x_2^* by $-2 \frac{\log(x_1^{sol} - \epsilon) + \alpha^f (x_1^{sol} - \epsilon)}{\alpha^f + \alpha}$ and upper bound x_2 by $-2 \frac{\log(x_1^{sol} + \epsilon) + \alpha^f (x_1^{sol} + \epsilon)}{\alpha^f + \alpha}$. \square

Proof of Claim 4 We start by proving Claim 4 (i). We have shown in the proof of Theorem 3 that the solution to (21) is unique in the stated parameter regimes. Thus, we know that $x^* = e^{-(\alpha^f + \alpha)x^*}$ because this construction trivially satisfies (21). Similarly, $\bar{x} = e^{-(\bar{\alpha}^f + \bar{\alpha})\bar{x}}$. Now, given that $e^{-(\bar{\alpha}^f + \bar{\alpha})x^*} \leq e^{-(\alpha^f + \alpha)x^*} = x^*$ for any $(\bar{\alpha}^f, \bar{\alpha}) \in \mathcal{I}(\alpha, \alpha^f, \delta)$, we know that $\bar{x} \leq x^*$. Moreover, from the uniqueness of solution we know that it suffices to show that

$$x^*(1 - \delta) \leq e^{-(\alpha^f + \alpha + 2\delta)x^*(1 - \delta)} \leq e^{-(\bar{\alpha}^f + \bar{\alpha})x^*(1 - \delta)}$$

so then the unique solution $\bar{x} \geq x^*(1 - \delta)$. To do so, we observe that

$$e^{-(\alpha^f + \alpha)x^* - \delta x^*(1 - \delta)} \leq e^{-(\alpha^f + \alpha + 2\delta)x^*(1 - \delta)},$$

so it suffices to show that

$$x^*(1 - \delta) \leq e^{-(\alpha^f + \alpha)x^* - \delta x^*(1 - \delta)} = x^* e^{-\delta x^*(1 - \delta)}. \quad (26)$$

Since we trivially have $x^* \in (0, 1]$, we can cancel out x^* and take logarithm on both sides. We find that (26) is equivalent to $-\log(1 - \delta) \geq x^* \delta(1 - \delta)$. Since $x^* \in (0, 1]$, it is then sufficient to show that $\frac{-\log(1 - \delta)}{\delta(1 - \delta)} \geq 1$, which holds for all $\delta \in (0, 1)$.

We next prove Claim 4 (ii). Given that in the claimed region

$$\begin{aligned} x_1^* &= e^{-\frac{1}{2}2\alpha^f x_1^* - \frac{1}{2}(\alpha^f + \alpha)x_2^*} \geq e^{-\frac{1}{2}2\bar{\alpha}^f x_1^* - \frac{1}{2}(\bar{\alpha}^f + \bar{\alpha})x_2^*}, \\ x_2^* &= e^{-\frac{1}{2}(\alpha^f + \alpha)x_1^* - \frac{1}{2}2\alpha x_2^*} \geq e^{-\frac{1}{2}(\bar{\alpha}^f + \bar{\alpha})x_1^* - \frac{1}{2}2\bar{\alpha}x_2^*} \end{aligned}$$

for any $(\bar{\alpha}^f, \bar{\alpha}) \in \mathcal{I}(\alpha, \alpha^f, \delta)$, we know that $\bar{x}_1 \leq x_1^*$ and $\bar{x}_2 \leq x_2^*$.

To prove the claimed lower bound on \bar{x}_1 and \bar{x}_2 , we show that

$$\begin{aligned} x_1^*(1 - 2\delta) &\leq e^{-\frac{1}{2}2\bar{\alpha}^f x_1^*(1 - 2\delta) - \frac{1}{2}(\bar{\alpha}^f + \bar{\alpha})x_2^*(1 - 2\delta)}, \\ x_2^*(1 - 2\delta) &\leq e^{-\frac{1}{2}(\bar{\alpha}^f + \bar{\alpha})x_1^*(1 - 2\delta) - \frac{1}{2}2\bar{\alpha}x_2^*(1 - 2\delta)}. \end{aligned} \quad (27)$$

In particular, (27) is implied by

$$x_1^*(1 - 2\delta) \leq e^{-\frac{1}{2}2\alpha^f x_1^* - \delta x_1^*(1 - 2\delta) - \frac{1}{2}(\alpha^f + \alpha)x_2^* - \delta x_2^*(1 - 2\delta)} = x_1^* \cdot e^{-\delta x_1^*(1 - 2\delta) - \delta x_2^*(1 - 2\delta)}.$$

Since we trivially have $x_1^* \in (0, 1]$, we can cancel out x_1^* and take logarithm on both sides. We find that (27) is equivalent to $-\log(1 - 2\delta) \geq (x_1^* + x_2^*)\delta(1 - 2\delta)$. Since $x_1^* + x_2^* \in [0, 2]$, it is then sufficient to show that $\frac{-\log(1 - 2\delta)}{2\delta(1 - 2\delta)} \geq 1$, which holds for all $\delta \in (0, 1/2)$. The proof of $\bar{x}_2 \geq x_2^*(1 - 2\delta)$ is symmetric. \square

C.3.4. Proof of Theorem 6

Proof. We start by proving the convexity result in Theorem 6 (ii). Recall from (12) that

$$\begin{aligned}\xi(b_l, b_r) &= 2 - b_l y_L^f(\mathbf{b}) - b_r \left(1 - \hat{y}_H^f(\mathbf{b})\right) \\ &\quad - b_r \left(1 - \hat{y}_H^f(\mathbf{b})\right) \left(2b_l \alpha^f y_L^f(\mathbf{b}) + (1 - b_l)(\alpha^f + \alpha) y_L^{nf}(\mathbf{b})\right) \\ &\quad - (1 - b_l) y_L^{nf}(\mathbf{b}) - (1 - b_r) \left(1 - \hat{y}_H^{nf}(\mathbf{b})\right) \\ &\quad - (1 - b_r) \left(1 - \hat{y}_H^{nf}(\mathbf{b})\right) \left(b_l(\alpha^f + \alpha) y_L^f(\mathbf{b}) + 2(1 - b_l) \alpha y_L^{nf}(\mathbf{b})\right),\end{aligned}$$

Since we are interested in the direction $(1, -1)$, for ease of notation we denote the sum of flexibility by B and replace b_r with $B - b_l$. Then, we can re-write $\xi(b_l, b_r) = \xi(b_l, B - b_l)$ as

$$\begin{aligned}2 - b_l y_L^f(\mathbf{b}) - (B - b_l) \left(1 - \hat{y}_H^f(\mathbf{b})\right) \\ - (B - b_l) \left(1 - \hat{y}_H^f(\mathbf{b})\right) \left(2b_l \alpha^f y_L^f(\mathbf{b}) + (1 - b_l)(\alpha^f + \alpha) y_L^{nf}(\mathbf{b})\right) \\ - (1 - b_l) y_L^{nf}(\mathbf{b}) - (1 - B + b_l) \left(1 - \hat{y}_H^{nf}(\mathbf{b})\right) \\ - (1 - B + b_l) \left(1 - \hat{y}_H^{nf}(\mathbf{b})\right) \left(b_l(\alpha^f + \alpha) y_L^f(\mathbf{b}) + 2(1 - b_l) \alpha y_L^{nf}(\mathbf{b})\right).\end{aligned}\tag{28}$$

Then, the second-order derivative of $\xi(b_l, b_r)$ in the direction $(1, -1)$ is equal to $\frac{\partial^2 \xi(b_l, B - b_l)}{\partial b_l^2}$. We observe that

$$\xi(b_l, B - b_l) = 2 - b_l y_L^f(\mathbf{b}) - (B - b_l) e^{-b_l(b_l)} (1 + b_1(b_l)) - (1 - b_l) y_L^{nf}(\mathbf{b}) - (1 - B + b_l) e^{-b_2(b_l)} (1 + b_2(b_l)),$$

where

$$\begin{aligned}b_1(b_l) &= b_l \cdot 2\alpha^f \cdot y_L^f(\mathbf{b}) + (1 - b_l)(\alpha^f + \alpha) y_L^{nf}(\mathbf{b}), \\ b_2(b_l) &= b_l(\alpha^f + \alpha) y_L^f(\mathbf{b}) + (1 - b_l) \cdot 2\alpha \cdot y_L^{nf}(\mathbf{b}).\end{aligned}$$

Let

$$x_1(b_l, b_r) = e^{-b_l 2\alpha^f y_L^f(\mathbf{b}) - (1 - b_l)(\alpha^f + \alpha) y_L^{nf}(\mathbf{b})} \text{ and } x_2(b_l, b_r) = e^{-b_l(\alpha^f + \alpha) y_L^f(\mathbf{b}) - (1 - b_l) 2\alpha y_L^{nf}(\mathbf{b})}\tag{29}$$

For ease of notation we drop the dependency of x_1 and x_2 on \mathbf{b} . Then we simplify $\xi(b_l, B - b_l)$ into

$$\begin{aligned}\xi(b_l, B - b_l) &= 2 - b_l e^{-(B - b_l) 2\alpha^f x_1 - (1 - B + b_l)(\alpha^f + \alpha) x_2} - (B - b_l) x_1 (1 - \log(x_1)) \\ &\quad - (1 - b_l) e^{-(B - b_l)(\alpha^f + \alpha) x_1 - (1 - B + b_l) 2\alpha x_2} - (1 - B + b_l) x_2 (1 - \log(x_2)).\end{aligned}$$

By construction of x_1, x_2 and the definition of $y_L^f(q), y_L^{nf}(q)$, we have

$$\begin{aligned}x_1 &= e^{-b_l 2\alpha^f e^{-(B - b_l) 2\alpha^f x_1 - (1 - B + b_l)(\alpha^f + \alpha) x_2} - (1 - b_l)(\alpha^f + \alpha) e^{-(B - b_l)(\alpha^f + \alpha) x_1 - (1 - B + b_l) 2\alpha x_2}} \\ x_2 &= e^{-b_l(\alpha^f + \alpha) e^{-(B - b_l) 2\alpha^f x_1 - (1 - B + b_l)(\alpha^f + \alpha) x_2} - (1 - b_l) 2\alpha e^{-(B - b_l)(\alpha^f + \alpha) x_1 - (1 - B + b_l) 2\alpha x_2}}.\end{aligned}$$

For convenience we write

$$y_1 := e^{-(B - b_l) 2\alpha^f x_1 - (1 - B + b_l)(\alpha^f + \alpha) x_2} \text{ and } y_2 := e^{-(B - b_l)(\alpha^f + \alpha) x_1 - (1 - B + b_l) 2\alpha x_2},\tag{30}$$

so that

$$x_1 = e^{-b_l 2\alpha^f y_1 - (1 - b_l)(\alpha^f + \alpha) y_2}, x_2 = e^{-b_l(\alpha^f + \alpha) y_1 - (1 - b_l) 2\alpha y_2}.$$

Now, taking second order derivative of $\xi(b_l, B - b_l)$ with respect to b_l , we obtain

$$\begin{aligned}
\frac{\partial^2 \xi(b_l, B - b_l)}{\partial b_l^2} &= -b_l \left(-2\alpha^f x_1 + (\alpha^f + \alpha) x_2 + (B - b_l) 2\alpha^f \frac{\partial x_1}{\partial b_l} + (1 - B + b_l) (\alpha^f + \alpha) \frac{\partial x_2}{\partial b_l} \right)^2 y_1 \\
&\quad - (1 - b_l) \left(-(\alpha^f + \alpha) x_1 + 2\alpha x_2 + (B - b_l) (\alpha^f + \alpha) \frac{\partial x_1}{\partial b_l} + (1 - B + b_l) 2\alpha \frac{\partial x_2}{\partial b_l} \right)^2 y_2 \\
&\quad + 2 \left(-2\alpha^f y_1 + (\alpha^f + \alpha) y_2 \right) x_1 + 2 \left((\alpha^f + \alpha) y_1 - 2\alpha y_2 \right) x_2 \\
&\quad + (B - b_l) 2 \left(2\alpha^f y_1 - (\alpha^f + \alpha) y_2 \right) \left(\frac{\partial x_1}{\partial b_l} \right) + (1 - B + b_l) 2 \left((\alpha^f + \alpha) y_1 - 2\alpha y_2 \right) \left(\frac{\partial x_2}{\partial b_l} \right) \\
&\quad + (B - b_l) \left(\frac{\partial x_1}{\partial b_l} \right)^2 / x_1 + (1 - B + b_l) \left(\frac{\partial x_2}{\partial b_l} \right)^2 / x_2.
\end{aligned} \tag{31}$$

Moreover, by taking derivative of x_1 and x_2 with respect to b_l , we find that

$$\begin{aligned}
\frac{\partial x_1}{\partial b_l} &= y_1 2\alpha^f b_l 2\alpha^f (B - b_l) \frac{\partial x_1}{\partial b_l} + y_2 (1 - b_l) (\alpha^f + \alpha) (B - b_l) (\alpha^f + \alpha) \frac{\partial x_1}{\partial b_l} + \\
&\quad y_1 2\alpha^f b_l (\alpha^f + \alpha) (1 - B + b_l) \frac{\partial x_2}{\partial b_l} + y_2 (1 - b_l) (\alpha^f + \alpha) (1 - B + b_l) 2\alpha \frac{\partial x_2}{\partial b_l} + \\
&\quad y_1 2\alpha^f b_l \left[(\alpha^f + \alpha) x_2 - 2\alpha^f x_1 \right] + y_2 (\alpha^f + \alpha) (1 - b_l) \left[2\alpha x_2 - (\alpha^f + \alpha) x_1 \right] - \\
&\quad y_1 2\alpha^f + y_2 (\alpha^f + \alpha),
\end{aligned} \tag{32}$$

and

$$\begin{aligned}
\frac{\partial x_2}{\partial b_l} &= y_1 (\alpha^f + \alpha) b_l 2\alpha^f (B - b_l) \frac{\partial x_1}{\partial b_l} + y_2 (1 - b_l) 2\alpha (B - b_l) (\alpha^f + \alpha) \frac{\partial x_1}{\partial b_l} + \\
&\quad y_1 (\alpha^f + \alpha) b_l (\alpha^f + \alpha) (1 - B + b_l) \frac{\partial x_2}{\partial b_l} + y_2 (1 - b_l) 2\alpha (1 - B + b_l) 2\alpha \frac{\partial x_2}{\partial b_l} + \\
&\quad y_1 (\alpha^f + \alpha) b_l \left[(\alpha^f + \alpha) x_2 - 2\alpha^f x_1 \right] + y_2 2\alpha (1 - b_l) \left[2\alpha x_2 - (\alpha^f + \alpha) x_1 \right] - \\
&\quad y_1 (\alpha^f + \alpha) + y_2 2\alpha.
\end{aligned} \tag{33}$$

When $\mathbf{b} = (1/2, 1/2)$, $B = 1$ and $b_l = 1/2$. We find that $x_1 = y_1, x_2 = y_2$, which allows us to simplify (32) and (33) as:

$$\frac{\partial x_1}{\partial b_l} = \frac{2x_1 \left(\alpha^2 x_1 x_2 - 2\alpha^f \alpha x_1 x_2 - 2\alpha x_2 + (\alpha^f)^2 x_1 x_2 + 4\alpha^f x_1 - 2\alpha^f x_2 \right)}{\alpha^2 x_1 x_2 - 2\alpha \alpha^f x_1 x_2 + 4\alpha x_2 + (\alpha^f)^2 x_1 x_2 + 4\alpha^f x_1 - 4}, \tag{34}$$

$$\frac{\partial x_2}{\partial b_l} = - \frac{2x_2 \left(\alpha^2 x_1 x_2 - 2\alpha^f \alpha x_1 x_2 - 2\alpha x_1 + (\alpha^f)^2 x_1 x_2 + 4\alpha x_2 - 2\alpha^f x_1 \right)}{\alpha^2 x_1 x_2 - 2\alpha \alpha^f x_1 x_2 + 4\alpha x_2 + (\alpha^f)^2 x_1 x_2 + 4\alpha^f x_1 - 4}. \tag{35}$$

Then, plugging $x_1 = y_1, x_2 = y_2, B = 1$ and $b_l = 1/2$ into (31), we obtain

$$\begin{aligned}
\left. \frac{\partial^2 \xi(b_l, B - b_l)}{\partial b_l^2} \right|_{B=1, b_l=\frac{1}{2}} &= -\frac{1}{2} \left(-2\alpha^f x_1 + (\alpha^f + \alpha) x_2 + \frac{1}{2} 2\alpha^f \frac{\partial x_1}{\partial b_l} + \frac{1}{2} (\alpha^f + \alpha) \frac{\partial x_2}{\partial b_l} \right)^2 x_1 \\
&\quad - \frac{1}{2} \left(-(\alpha^f + \alpha) x_1 + 2\alpha x_2 + \frac{1}{2} (\alpha^f + \alpha) \frac{\partial x_1}{\partial b_l} + \frac{1}{2} 2\alpha \frac{\partial x_2}{\partial b_l} \right)^2 x_2 \\
&\quad + 2 \left(-2\alpha^f x_1 + (\alpha^f + \alpha) x_2 \right) x_1 + 2 \left((\alpha^f + \alpha) x_1 - 2\alpha x_2 \right) x_2
\end{aligned}$$

$$\begin{aligned}
& + \left(2\alpha^f x_1 - (\alpha^f + \alpha) x_2 \right) \left(\frac{\partial x_1}{\partial b_l} \right) + \left((\alpha^f + \alpha) x_1 - 2\alpha x_2 \right) \left(\frac{\partial x_2}{\partial b_l} \right) \\
& + \frac{1}{2} \left(\frac{\partial x_1}{\partial b_l} \right)^2 / x_1 + \frac{1}{2} \left(\frac{\partial x_2}{\partial b_l} \right)^2 / x_2.
\end{aligned}$$

By plugging the values of $\frac{\partial x_1}{\partial b_l}$ and $\frac{\partial x_2}{\partial b_l}$ from (34) and (35) into the above, we find that

$$\begin{aligned}
\left. \frac{\partial^2 \xi(b_l, B - b_l)}{\partial b_l^2} \right|_{B=1, b_l=\frac{1}{2}} &= \frac{1}{\alpha^2 x_1 x_2 - 2\alpha \alpha^f x_1 x_2 + 4\alpha x_2 + (\alpha^f)^2 x_1 x_2 + 4\alpha^f x_1 - 4} \\
& \quad (4\alpha^2 x_1^2 x_2 + 4\alpha^2 x_1 x_2^2 - 8\alpha \alpha^f x_1^2 x_2 - 8\alpha \alpha^f x_1 x_2^2 - 16\alpha x_1 x_2 \\
& \quad + 16\alpha x_2^2 + 4(\alpha^f)^2 x_1^2 x_2 + 4(\alpha^f)^2 x_1 x_2^2 + 16\alpha^f x_1^2 - 16\alpha^f x_1 x_2) \\
&= \frac{(\alpha^f - \alpha)^2 4x_1 x_2 (x_1 + x_2) - 16(x_2 - x_1)(\alpha^f x_1 - \alpha x_2)}{(\alpha^f - \alpha)^2 x_1 x_2 + 4(\alpha x_2 + \alpha^f x_1 - 1)}.
\end{aligned} \tag{36}$$

Recall that we have

$$x_1 = e^{-\alpha^f x_1 - 1/2(\alpha^f + \alpha)x_2}, x_2 = e^{-1/2(\alpha^f + \alpha)x_1 - \alpha x_2} \tag{37}$$

when $B = 1, b_l = 1/2$. This allows us to solve x_1 and x_2 and determine the size of convexity numerically. In particular, we know from (25) that we can provide bounds $x_1^{lb}, x_1^{ub}, x_2^{lb}, x_2^{ub}$ for any $(\bar{\alpha}^f, \bar{\alpha}) \in \mathcal{I}(\alpha, \alpha^f, \delta)$ where $10^{-4} < \bar{\alpha} < \bar{\alpha}^f$ and $\bar{\alpha}^f + \bar{\alpha} < e$. Thus, we can lower bound (36) for any $(\bar{\alpha}^f, \bar{\alpha}) \in \mathcal{I}(\alpha, \alpha^f, \delta)$ as:

$$\begin{aligned}
& \frac{(\bar{\alpha}^f - \bar{\alpha})^2 4\bar{x}_1 \bar{x}_2 (\bar{x}_1 + \bar{x}_2) - 16(\bar{x}_2 - \bar{x}_1)(\bar{\alpha}^f \bar{x}_1 - \bar{\alpha} \bar{x}_2)}{(\bar{\alpha}^f - \bar{\alpha})^2 \bar{x}_1 \bar{x}_2 + 4(\bar{\alpha} \bar{x}_2 + \bar{\alpha}^f \bar{x}_1 - 1)} \\
& \geq \frac{-(\alpha^f - \alpha + \delta)^2 4x_1^{ub} x_2^{ub} (x_1^{ub} + x_2^{ub}) + 16 \max(0, x_2^{lb} - x_1^{ub}) \alpha^f x_1^{lb} - 16(x_2^{ub} - x_1^{lb})(\alpha + \delta)x_2^{ub}}{-\left(\max(\alpha^f - \alpha - \delta, 0)\right)^2 x_1^{lb} x_2^{lb} + 4[1 - \alpha x_2^{lb} - \alpha^f x_1^{lb}]}.
\end{aligned} \tag{38}$$

If this lower bound exceeds 0, we know that $\xi(b_l, b_r)$ is strictly convex in the direction $(1, -1)$ at $\mathbf{b} = (1/2, 1/2)$ for any $(\bar{\alpha}^f, \bar{\alpha}) \in \mathcal{I}(\alpha, \alpha^f, \delta)$. At $\mathbf{b} = (1/2, 1/2)$, we find by symmetry that $\xi(b_l, b_r) = \hat{\xi}(b_l, b_r)$,

$$\left. \frac{\partial \xi(b_l, B - b_l)}{\partial b_l} \right|_{B=1, b_l=\frac{1}{2}} = \left. \frac{\partial \hat{\xi}(b_l, B - b_l)}{\partial b_l} \right|_{B=1, b_l=\frac{1}{2}} = 0 \text{ and } \left. \frac{\partial^2 \xi(b_l, B - b_l)}{\partial b_l^2} \right|_{B=1, b_l=\frac{1}{2}} = \left. \frac{\partial^2 \hat{\xi}(b_l, B - b_l)}{\partial b_l^2} \right|_{B=1, b_l=\frac{1}{2}}.$$

Thus, at $\mathbf{b} = (1/2, 1/2)$, by Claim 5 below we know that to show $\nabla_{(1,-1)}^2 \mu^{KS}(b_l, b_r) > 0$ it suffices to verify strict local convexity for $\xi(b_l, b_r)$ in the direction $(1, -1)$. That is, we verify $\left. \frac{\partial^2 \xi(b_l, B - b_l)}{\partial b_l^2} \right|_{B=1, b_l=\frac{1}{2}} > 0$.

CLAIM 5. *If for some $\mathbf{b}' \in (0, 1)^2$ and direction $v \in \mathbb{R}^2$, $\hat{\xi}(\mathbf{b}') = \hat{\xi}(\mathbf{b}')$, $\nabla_v \hat{\xi}(\mathbf{b}') = \nabla_v \hat{\xi}(\mathbf{b}')$ and $\nabla_v^2 \hat{\xi}(\mathbf{b}') = \nabla_v^2 \hat{\xi}(\mathbf{b}')$, then $\nabla_v^2 \mu^{KS}(\mathbf{b}') = \nabla_v^2 \hat{\xi}(\mathbf{b}') = \nabla_v^2 \hat{\xi}(\mathbf{b}')$.*

In Theorem7.ipynb,²⁶ we compute the lower bound of $\left. \frac{\partial^2 \xi(b_l, B - b_l)}{\partial b_l^2} \right|_{B=1, b_l=\frac{1}{2}}$ in (38) for $\alpha^f, \alpha = \delta, 2\delta, \dots, e$ where $\alpha^f + \alpha < e$. We find that by taking $\delta = 0.01, 0.005, 0.0025$ and 0.001 we are able to verify strict local convexity of $\mu^{KS}(1/2, 1/2)$ in the direction $(1, -1)$ in the respective red regions in Fig. 26.

²⁶The computer-aided proof can be found at <https://bit.ly/3P1f6oi>.

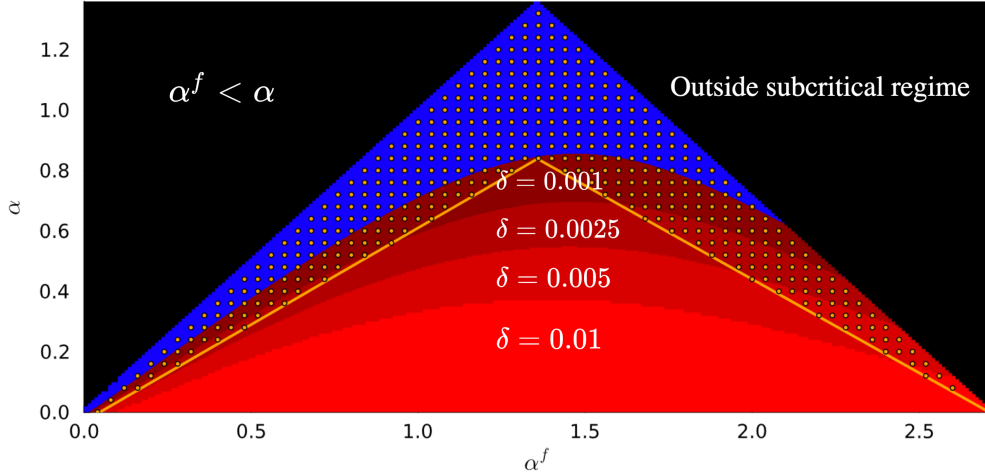


Figure 26 In the figure we denote the boundary where $10^{-4} < \alpha < 0.64\alpha^f - 0.03$ and $0.62\alpha^f + \alpha < 1.68$ by the orange lines, and the area of subcritical regime where convexity and concavity properties are verified is displayed in varying shades of red below this boundary. The growth in the validation area with respect to δ is depicted through different red gradients. The black zone denotes parameters outside the feasible or subcritical regime. Although the convexity and concavity properties cannot be confirmed in the blue region when $\delta = 0.001$, by taking $\delta = 0$ we verify the properties for a wide range of (α^f, α) values highlighted as orange dots.

We next prove the concavity result in Theorem 6 (i). We again focus on $\xi(b_l, b_r)$, and the second-order derivative of $\xi(b_l, b_r)$ in the direction $(0, 1)$ is equal to $\frac{\partial^2 \xi(b_l, B - b_l)}{\partial B^2}$.

Based on x_1, x_2, y_1, y_2 constructed in (29) and (30), we obtain

$$\begin{aligned} \frac{\partial^2 \xi(b_l, B - b_l)}{\partial B^2} &= -b_l \left(2\alpha^f x_1 - (\alpha^f + \alpha) x_2 + (B - b_l) 2\alpha^f \frac{\partial x_1}{\partial B} + (1 - B + b_l) (\alpha^f + \alpha) \frac{\partial x_2}{\partial B} \right)^2 y_1 \\ &\quad - (1 - b_l) \left((\alpha^f + \alpha) x_1 - 2\alpha x_2 + (B - b_l) (\alpha^f + \alpha) \frac{\partial x_1}{\partial B} + (1 - B + b_l) 2\alpha \frac{\partial x_2}{\partial B} \right)^2 y_2 \quad (39) \\ &\quad + (B - b_l) \left(\frac{\partial x_1}{\partial B} \right)^2 / x_1 + (1 - B + b_l) \left(\frac{\partial x_2}{\partial B} \right)^2 / x_2. \end{aligned}$$

Moreover, by taking derivative of x_1 and x_2 with respect to B , we find that

$$\begin{aligned} \frac{\partial x_1}{\partial B} &= y_1 2\alpha^f b_l 2\alpha^f (B - b_l) \frac{\partial x_1}{\partial B} + y_2 (1 - b_l) (\alpha^f + \alpha) (B - b_l) (\alpha^f + \alpha) \frac{\partial x_1}{\partial B} + \\ &\quad y_1 2\alpha^f b_l (\alpha^f + \alpha) (1 - B + b_l) \frac{\partial x_2}{\partial B} + y_2 (1 - b_l) (\alpha^f + \alpha) (1 - B + b_l) 2\alpha \frac{\partial x_2}{\partial B} - \\ &\quad y_1 2\alpha^f b_l \left[(\alpha^f + \alpha) x_2 - 2\alpha^f x_1 \right] - y_2 (\alpha^f + \alpha) (1 - b_l) \left[2\alpha x_2 - (\alpha^f + \alpha) x_1 \right], \end{aligned}$$

and

$$\begin{aligned} \frac{\partial x_2}{\partial B} &= y_1 (\alpha^f + \alpha) b_l 2\alpha^f (B - b_l) \frac{\partial x_1}{\partial B} + y_2 (1 - b_l) 2\alpha (B - b_l) (\alpha^f + \alpha) \frac{\partial x_1}{\partial B} + \\ &\quad y_1 (\alpha^f + \alpha) b_l (\alpha^f + \alpha) (1 - B + b_l) \frac{\partial x_2}{\partial B} + y_2 (1 - b_l) 2\alpha (1 - B + b_l) 2\alpha \frac{\partial x_2}{\partial B} - \\ &\quad y_1 (\alpha^f + \alpha) b_l \left[(\alpha^f + \alpha) x_2 - 2\alpha^f x_1 \right] - y_2 2\alpha (1 - b_l) \left[2\alpha x_2 - (\alpha^f + \alpha) x_1 \right]. \end{aligned}$$

When $B = 1$ and $b_l = 1/2$, we have $x_1 = y_1, x_2 = y_2$. Applying these observations to simplify (39), we obtain

$$\left. \frac{\partial^2 \xi(b_l, B - b_l)}{\partial B^2} \right|_{a=1, q=\frac{1}{2}} = \frac{1}{- \left(x_1 x_2 (\alpha^f - \alpha)^2 \right)^2 + 8x_1 x_2 (\alpha^f + \alpha)^2 + 16 \left(\alpha^2 x_2^2 + (\alpha^f)^2 x_1^2 - 1 \right)} \cdot \left(-2(x_1 + x_2) \left(x_1 x_2 (\alpha^f - \alpha)^2 \right)^2 - 16(x_1 + x_2) x_1 x_2 \alpha^f \alpha + 8(\alpha^f)^2 x_1 (x_2^2 - 3x_1 x_2 + 4x_1^2) + 8\alpha^2 x_2 (x_1^2 - 3x_1 x_2 + 4x_2^2) \right). \quad (40)$$

Again, we know from (25) that we can provide bounds $x_1^{lb}, x_1^{ub}, x_2^{lb}, x_2^{ub}$ for any $(\bar{\alpha}^f, \bar{\alpha}) \in \mathcal{I}(\alpha, \alpha^f, \delta)$ where $\bar{\alpha}^f + \bar{\alpha} < e$. Thus, we can upper bound (40) for any $(\bar{\alpha}^f, \bar{\alpha}) \in \mathcal{I}(\alpha, \alpha^f, \delta)$ as:

$$\begin{aligned} & \frac{1}{- \left[x_1^{ub} x_2^{ub} (\alpha^f - \alpha + \delta)^2 \right]^2 + 8(\alpha^f + \alpha)^2 x_1^{lb} x_2^{lb} + 16\alpha^2 (x_2^{lb})^2 + 16(\alpha^f)^2 (x_1^{lb})^2 - 16} \\ & \cdot \left(-2 \left(x_1^{lb} + x_2^{lb} \right) \left[x_1^{lb} x_2^{lb} \left(\max(0, \alpha^f - \alpha - \delta) \right)^2 \right]^2 - 16(x_1^{lb} + x_2^{lb}) x_1^{lb} x_2^{lb} \alpha^f \alpha \right. \\ & \left. + 8(\alpha^f + \delta)^2 \left(x_1^{ub} (x_2^{ub})^2 + 4(x_1^{ub})^3 \right) + 8(\alpha + \delta)^2 \left(x_2^{ub} (x_1^{ub})^2 + 4(x_2^{ub})^3 \right) \right. \\ & \left. - 24(\alpha^f)^2 (x_1^{lb})^2 x_2^{lb} - 24\alpha^2 (x_2^{lb})^2 x_1^{lb} \right). \end{aligned} \quad (41)$$

If this upper bound is strictly below 0, we know that $\xi(b_l, b_r)$ is strictly concave in the direction $(0, 1)$ at $\mathbf{b} = (1/2, 1/2)$ for any $(\bar{\alpha}^f, \bar{\alpha}) \in \mathcal{I}(\alpha, \alpha^f, \delta)$. By symmetry at $\mathbf{b} = (1/2, 1/2)$ we find that $\xi(b_l, b_r) = \hat{\xi}(b_l, b_r)$,

$$\left. \frac{\partial \xi(b_l, B - b_l)}{\partial B} \right|_{B=1, b_l=\frac{1}{2}} = \left. \frac{\partial \hat{\xi}(b_l, B - b_l)}{\partial B} \right|_{B=1, b_l=\frac{1}{2}} \quad \text{and} \quad \left. \frac{\partial^2 \xi(b_l, B - b_l)}{\partial B^2} \right|_{B=1, b_l=\frac{1}{2}} = \left. \frac{\partial^2 \hat{\xi}(b_l, B - b_l)}{\partial B^2} \right|_{B=1, b_l=\frac{1}{2}}.$$

Thus, at $\mathbf{b} = (1/2, 1/2)$, by Claim 5 we know it suffices to verify strict local concavity for $\xi(b_l, b_r)$ in the direction $(0, 1)$. That is, we verify $\left. \frac{\partial^2 \xi(b_l, B - b_l)}{\partial B^2} \right|_{B=1, b_l=\frac{1}{2}} < 0$.

In `Theorem7.ipynb`,²⁷ we compute the upper bound of $\left. \frac{\partial^2 \xi(b_l, B - b_l)}{\partial B^2} \right|_{a=1, q=\frac{1}{2}}$ in (41) for $\alpha^f, \alpha = 10^{-4}, \delta, 2\delta, \dots, e$ where $\alpha^f + \alpha < e$. We find that taking $\delta = 0.01$ is sufficient for verifying (41) < 0 for all α^f and α such that $10^{-4} < \alpha < \alpha^f$ and $\alpha^f + \alpha < e$. The concavity in the direction $(1, 0)$ is exactly symmetric. □

Proof of Claim 5 By definition, we need to show that

$$\nabla_{\mathbf{v}}^2 \mu^{\text{KS}}(\mathbf{b}') = \lim_{h \rightarrow 0} \frac{\mu^{\text{KS}}(\mathbf{b}' + \mathbf{v}h) - 2\mu^{\text{KS}}(\mathbf{b}') + \mu^{\text{KS}}(\mathbf{b}' - \mathbf{v}h)}{h^2}$$

exists and is equal to the claimed value. By Taylor series expansion, we know that for $h \in \mathbb{R}$,

$$\begin{aligned} \xi(\mathbf{b}' + \mathbf{v}h) &= \xi(\mathbf{b}') + h \cdot \nabla_{\mathbf{v}} \xi(\mathbf{b}') + h^2 \cdot \nabla_{\mathbf{v}}^2 \xi(\mathbf{b}') + o(h^2), \\ \hat{\xi}(\mathbf{b}' + \mathbf{v}h) &= \hat{\xi}(\mathbf{b}') + h \cdot \nabla_{\mathbf{v}} \hat{\xi}(\mathbf{b}') + h^2 \cdot \nabla_{\mathbf{v}}^2 \hat{\xi}(\mathbf{b}') + o(h^2), \\ \xi(\mathbf{b}' - \mathbf{v}h) &= \xi(\mathbf{b}') - h \cdot \nabla_{\mathbf{v}} \xi(\mathbf{b}') - h^2 \cdot \nabla_{\mathbf{v}}^2 \xi(\mathbf{b}') - o(h^2), \\ \hat{\xi}(\mathbf{b}' - \mathbf{v}h) &= \hat{\xi}(\mathbf{b}') - h \cdot \nabla_{\mathbf{v}} \hat{\xi}(\mathbf{b}') - h^2 \cdot \nabla_{\mathbf{v}}^2 \hat{\xi}(\mathbf{b}') - o(h^2). \end{aligned}$$

²⁷The computer-aided proof can be found at <https://bit.ly/3P1f6oi>.

In particular, since $\hat{\xi}(\mathbf{b}') = \hat{\xi}(\mathbf{b}')$, $\nabla_v \hat{\xi}(\mathbf{b}') = \nabla_v \hat{\xi}(\mathbf{b}')$ and $\nabla_v^2 \hat{\xi}(\mathbf{b}') = \nabla_v^2 \hat{\xi}(\mathbf{b}')$, from the above we know that

$$\xi(\mathbf{b}' + \mathbf{v}h) - \hat{\xi}(\mathbf{b}' + \mathbf{v}h) = o(h^2) \text{ and } \xi(\mathbf{b}' - \mathbf{v}h) - \hat{\xi}(\mathbf{b}' - \mathbf{v}h) = o(h^2).$$

Thus,

$$\begin{aligned} \nabla_v^2 \mu^{\text{KS}}(\mathbf{b}') &= \lim_{h \rightarrow 0} \frac{\mu^{\text{KS}}(\mathbf{b}' + \mathbf{v}h) - 2\mu^{\text{KS}}(\mathbf{b}') + \mu^{\text{KS}}(\mathbf{b}' - \mathbf{v}h)}{h^2} \\ &= \lim_{h \rightarrow 0} \frac{\min(\xi(\mathbf{b}' + \mathbf{v}h), \hat{\xi}(\mathbf{b}' + \mathbf{v}h)) - 2\min(\xi(\mathbf{b}'), \hat{\xi}(\mathbf{b}')) + \min(\xi(\mathbf{b}' - \mathbf{v}h), \hat{\xi}(\mathbf{b}' - \mathbf{v}h))}{h^2} \\ &= \lim_{h \rightarrow 0} \frac{\xi(\mathbf{b}' + \mathbf{v}h) - 2\xi(\mathbf{b}') + \xi(\mathbf{b}' - \mathbf{v}h) + o(h^2)}{h^2} \\ &= \nabla_v^2 \xi(\mathbf{b}') = \nabla_v^2 \hat{\xi}(\mathbf{b}'). \end{aligned}$$

□

C.3.5. Proofs of the Auxiliary Results in Appendix C.3.2

Proof of Proposition 4 Theorem 8 in Karp and Sipser (1981) (1) - (4) establishes the validity of the statements in Proposition 4 (i) - (iv) for a general graph $G = (V, E)$. Since bipartite graphs are a subset of such general graphs, these results immediately extend.

For Proposition 4 (v), to determine $|\Psi_1^l|$ and $|\Psi_1^r|$, we start by finding m_1 . By (iii), every edge in M_1 is connected to at least one target. By (ii), if an edge in M_1 is connected to two targets u and v , then $v \otimes u$ and $u \otimes v$. Hence,

$$m_1 = |M_1| = \left| \{v \in V_l \mid v \text{ is a target}\} \right| + \left| \{v \in V_r \mid v \text{ is a target}\} \right| - \left| \{(v, u) \mid v \otimes u \text{ and } u \otimes v\} \right|.$$

The equality follows from (ii) because every target is connected to an edge in M_1 .

By Theorem 9 (4) in Karp and Sipser (1981), a node v appears in a derivation if and only if it is a target or a loser or both. Furthermore, v is both a target and a loser if and only if there exists a unique u such that $v \otimes u$ and $u \otimes v$. Hence, the number of nodes in V_l that appear in a derivation is given by

$$\left| \{v \in V_l \mid v \text{ is a target}\} \right| + \left| \{v \in V_l \mid v \text{ is a loser}\} \right| - \left| \{(v, u) \mid v \otimes u \text{ and } u \otimes v\} \right|.$$

Then, we can find Ψ_1^l as the set of nodes in V_l that appear in a derivation but do not belong to M_1^l . Specifically,

$$\begin{aligned} |\Psi_1^l| &= \left| \{v \in V_l \mid v \text{ is a target}\} \right| + \left| \{v \in V_l \mid v \text{ is a loser}\} \right| - \left| \{(v, u) \mid v \otimes u \text{ and } u \otimes v\} \right| \\ &\quad - \left(\left| \{v \in V_l \mid v \text{ is a target}\} \right| + \left| \{v \in V_r \mid v \text{ is a target}\} \right| - \left| \{(v, u) \mid v \otimes u \text{ and } u \otimes v\} \right| \right) \\ &= \left| \{v \in V_l \mid v \text{ is a loser}\} \right| - \left| \{v \in V_r \mid v \text{ is a target}\} \right|. \end{aligned}$$

The computation of $|\Psi_1^r|$ is symmetric. Since $\psi_1 = \max\{|\Psi_1^l|, |\Psi_1^r|\}$ by definition, we obtain Proposition 4 (v). □

Proof of Lemma 8 We start from the leaf of a random tree, i.e., $d = 1$, and iteratively trace back to the root of the tree as d scales large. For a flexible node $u \in S_L$, the number of its children follows a Binomial distribution $\text{Binom}(n, (1 + b_r)p_n^f + (1 - b_r)p_n)$. Thus, the probability for it to have k children is given by

$$z_k^f(\mathbf{b}) := \binom{n}{k} \left((1 + b_r)p_n^f + (1 - b_r)p_n \right)^k \left(1 - (1 + b_r)p_n^f - (1 - b_r)p_n \right)^{n-k} \quad \forall k.$$

Moreover, since the probability that u connects with a flexible node is $2p^f$ and the probability that it connects with a regular node is $p^f + p$, by Bayes' Theorem we have

$$\begin{aligned} \mathbb{P}[u' \text{ is flexible} | u \text{ is flexible, } u' \text{ is a child of } u] &= \frac{b_r \cdot 2p_n^f}{b_r \cdot 2p_n^f + (1 - b_r) \cdot (p_n^f + p_n)} \\ &= \frac{b_r \cdot 2p_n^f}{(1 + b_r)p_n^f + (1 - b_r)p_n} \end{aligned}$$

and similarly

$$\mathbb{P}[u' \text{ is regular} | u \text{ is flexible, } u' \text{ is a child of } u] = \frac{(1 - b_r) \cdot (p_n^f + p_n)}{(1 + b_r)p_n^f + (1 - b_r)p_n}.$$

By definition, u is in L if all of its children are in H , including when it has no children. Thus,

$$\begin{aligned} y_L^f(\mathbf{b}, d) &= \sum_{k=0}^n z_k^f(\mathbf{b}) \cdot \left(\frac{2b_r p_n^f}{(1 + b_r)p_n^f + (1 - b_r)p_n} \hat{y}_H^f(\mathbf{b}, d-1) + \frac{(1 - b_r) \cdot (p_n^f + p_n)}{(1 + b_r)p_n^f + (1 - b_r)p_n} \hat{y}_H^{nf}(\mathbf{b}, d-1) \right)^k \\ &= \sum_{k=0}^n \binom{n}{k} \left((1 + b_r)p_n^f + (1 - b_r)p_n \right)^k \left(1 - (1 + b_r)p_n^f - (1 - b_r)p_n \right)^{n-k} \\ &\quad \cdot \left(\frac{2b_r p_n^f}{(1 + b_r)p_n^f + (1 - b_r)p_n} \hat{y}_H^f(\mathbf{b}, d-1) + \frac{(1 - b_r) \cdot (p_n^f + p_n)}{(1 + b_r)p_n^f + (1 - b_r)p_n} \hat{y}_H^{nf}(\mathbf{b}, d-1) \right)^k \\ &= \sum_{k=1}^n \binom{n}{k} \left(1 - (1 + b_r)p_n^f - (1 - b_r)p_n \right)^{n-k} \cdot \left(2b_r p_n^f \hat{y}_H^f(\mathbf{b}, d-1) + (1 - b_r) \cdot (p_n^f + p_n) \hat{y}_H^{nf}(\mathbf{b}, d-1) \right)^k \\ &= \left[2b_r p_n^f \hat{y}_H^f(\mathbf{b}, d-1) + (1 - b_r) \cdot (p_n^f + p_n) \hat{y}_H^{nf}(\mathbf{b}, d-1) + 1 - (1 + b_r)p_n^f - (1 - b_r)p_n \right]^n \\ &= \left[1 - 2b_r p_n^f \left(1 - \hat{y}_H^f(\mathbf{b}, d-1) \right) - (1 - b_r) \cdot (p_n^f + p_n) \left(1 - \hat{y}_H^{nf}(\mathbf{b}, d-1) \right) \right]^n \\ &= \left[1 - \frac{2b_r \alpha^f \left(1 - \hat{y}_H^f(\mathbf{b}, d-1) \right) - (1 - b_r) \cdot (\alpha^f + \alpha) \left(1 - \hat{y}_H^{nf}(\mathbf{b}, d-1) \right)}{n} \right]^n \\ &= e^{-2b_r \alpha^f (1 - \hat{y}_H^f(\mathbf{b}, d-1)) - (1 - b_r) \cdot (\alpha^f + \alpha) (1 - \hat{y}_H^{nf}(\mathbf{b}, d-1))} \quad \text{as } n \rightarrow \infty. \end{aligned}$$

Notice that the fourth equality is an application of the Binomial Theorem, and the last equality follows from

$$\lim_{n \rightarrow \infty} \left(1 - \frac{x}{n} \right)^n = e^{-x}, \quad \forall x.$$

The expressions for $y_L^{nf}(\mathbf{b}, d)$, $\hat{y}_L^f(\mathbf{b}, d)$ and $\hat{y}_L^{nf}(\mathbf{b}, d)$ can be derived in a similar fashion.

Next, by definition, u is in H if it has at least one child in L . Thus,

$$y_H^f(\mathbf{b}, d) = 1 - \sum_{k=0}^n z_k^f(\mathbf{b}) \cdot \left(\frac{2b_r p_n^f}{(1 + b_r)p_n^f + (1 - b_r)p_n} \left(1 - \hat{y}_L^f(\mathbf{b}, d-1) \right) + \frac{(1 - b_r) \cdot (p_n^f + p_n)}{(1 + b_r)p_n^f + (1 - b_r)p_n} \left(1 - \hat{y}_L^{nf}(\mathbf{b}, d-1) \right) \right)^k$$

$$\begin{aligned}
&= 1 - \sum_{k=0}^n \binom{n}{k} \left((1+b_r)p_n^f + (1-b_r)p_n \right)^k \left(1 - (1+b_r)p_n^f - (1-b_r)p_n \right)^{n-k} \\
&\quad \cdot \left(\frac{2b_r p_n^f}{(1+b_r)p_n^f + (1-b_r)p_n} \left(1 - \hat{y}_L^f(\mathbf{b}, d-1) \right) + \frac{(1-b_r) \cdot (p_n^f + p_n)}{(1+b_r)p_n^f + (1-b_r)p_n} \left(1 - \hat{y}_L^{nf}(\mathbf{b}, d-1) \right) \right)^k \\
&= 1 - \sum_{k=1}^n \binom{n}{k} \left(1 - (1+b_r)p_n^f - (1-b_r)p_n \right)^{n-k} \\
&\quad \cdot \left(2b_r p_n^f \left(1 - \hat{y}_L^f(\mathbf{b}, d-1) \right) + (1-b_r) \cdot (p_n^f + p_n) \left(1 - \hat{y}_L^{nf}(\mathbf{b}, d-1) \right) \right)^k \\
&= 1 - \left[2b_r p_n^f \left(1 - \hat{y}_L^f(\mathbf{b}, d-1) \right) + (1-b_r) \cdot (p_n^f + p_n) \left(1 - \hat{y}_L^{nf}(\mathbf{b}, d-1) \right) + 1 - (1+b_r)p_n^f - (1-b_r)p_n \right]^n \\
&= 1 - \left[1 - 2b_r p_n^f \hat{y}_L^f(\mathbf{b}, d-1) - (1-b_r) \cdot (p_n^f + p_n) \hat{y}_L^{nf}(\mathbf{b}, d-1) \right]^n \\
&= 1 - \left[1 - \frac{2b_r \alpha^f \hat{y}_L^f(\mathbf{b}, d-1) - (1-b_r) \cdot (\alpha^f + \alpha) \hat{y}_L^{nf}(\mathbf{b}, d-1)}{n} \right]^n \\
&= 1 - e^{-2b_r \alpha^f \hat{y}_L^f(\mathbf{b}, d-1) - (1-b_r) \cdot (\alpha^f + \alpha) \hat{y}_L^{nf}(\mathbf{b}, d-1)} \text{ as } n \rightarrow \infty.
\end{aligned}$$

The expressions for $y_H^{nf}(\mathbf{b}, d)$, $\hat{y}_H^f(\mathbf{b}, d)$ and $\hat{y}_H^{nf}(\mathbf{b}, d)$ can be derived in a similar fashion. Since all leaf nodes are in L , we have

$$y_H^f(\mathbf{b}, 1) = y_H^{nf}(\mathbf{b}, 1) = \hat{y}_H^f(\mathbf{b}, 1) = \hat{y}_H^{nf}(\mathbf{b}, 1) = 0.$$

Moreover, since $y_L^f(\mathbf{b}, d)$, $y_L^{nf}(\mathbf{b}, d)$, $y_H^f(\mathbf{b}, d)$, $y_H^{nf}(\mathbf{b}, d)$, $\hat{y}_L^f(\mathbf{b}, d)$, $\hat{y}_L^{nf}(\mathbf{b}, d)$, $\hat{y}_H^f(\mathbf{b}, d)$, $\hat{y}_H^{nf}(\mathbf{b}, d)$ are all bounded increasing sequences with respect to d , these sequences converge as $d \rightarrow \infty$ and \mathbf{y} is given by the smallest solution to (11). \square

Proof of Lemma 7 Lemma 3.1 and 3.2 in Karp and Sipser (1981) respectively establish the statements in Lemma 7(i) and (ii) for a general tree rooted at vertex v . As \bar{G} under consideration is also rooted at vertex v , these results immediately extend. \square

Proof of Lemma 9 By Lemma 7 (i), we have

$$\mathbb{P}[v \text{ is a target} | v \text{ is a flexible node in } S_l] = \mathbb{P}[v \in H | v \text{ is a flexible node in } S_l] = y_H^f(\mathbf{b}).$$

To find the probability for a flexible node v in S_l to be a loser, we need to sum the probability that v is in L and that v has exactly 1 child which is not in H . The former is simply given by $y_L^f(\mathbf{b})$, while the latter can be computed as

$$\begin{aligned}
&\mathbb{P}[v \text{ has exactly 1 child that is in } H | v \text{ is a flexible node in } S_l] \\
&= \sum_{k=0}^n z_k^f(\mathbf{b}) \cdot k \cdot \left(\frac{2b_r p_n^f}{(1+b_r)p_n^f + (1-b_r)p_n} \hat{y}_H^f(\mathbf{b}) + \frac{(1-b_r) \cdot (p_n^f + p_n)}{(1+b_r)p_n^f + (1-b_r)p_n} \hat{y}_H^{nf}(\mathbf{b}) \right)^{k-1} \\
&\quad \cdot \left(1 - \frac{2b_r p_n^f}{(1+b_r)p_n^f + (1-b_r)p_n} \hat{y}_H^f(\mathbf{b}) - \frac{(1-b_r) \cdot (p_n^f + p_n)}{(1+b_r)p_n^f + (1-b_r)p_n} \hat{y}_H^{nf}(\mathbf{b}) \right) \\
&= \sum_{k=0}^n \binom{n}{k} \left((1+b_r)p_n^f + (1-b_r)p_n \right)^k \left(1 - (1+b_r)p_n^f - (1-b_r)p_n \right)^{n-k} \\
&\quad \cdot k \cdot \left(\frac{2b_r p_n^f}{(1+b_r)p_n^f + (1-b_r)p_n} \hat{y}_H^f(\mathbf{b}) + \frac{(1-b_r) \cdot (p_n^f + p_n)}{(1+b_r)p_n^f + (1-b_r)p_n} \hat{y}_H^{nf}(\mathbf{b}) \right)^{k-1}
\end{aligned}$$

$$\begin{aligned}
& \cdot \left(1 - \frac{2b_r p_n^f}{(1+b_r)p_n^f + (1-b_r)p_n} \hat{y}_H^f(\mathbf{b}) - \frac{(1-b_r) \cdot (p_n^f + p_n)}{(1+b_r)p_n^f + (1-b_r)p_n} \hat{y}_H^{nf}(\mathbf{b}) \right) \\
& = \sum_{k=1}^n n \binom{n-1}{k-1} \left((1+b_r)p_n^f + (1-b_r)p_n \right)^{k-1} \left(1 - (1+b_r)p_n^f - (1-b_r)p_n \right)^{n-k} \\
& \cdot \left(\frac{2b_r p_n^f}{(1+b_r)p_n^f + (1-b_r)p_n} \hat{y}_H^f(\mathbf{b}) + \frac{(1-b_r) \cdot (p_n^f + p_n)}{(1+b_r)p_n^f + (1-b_r)p_n} \cdot \hat{y}_H^{nf}(\mathbf{b}) \right)^{k-1} \\
& \cdot \left((1+b_r)p_n^f + (1-b_r)p_n - 2b_r p_n^f \hat{y}_H^f(\mathbf{b}) - (1-b_r) \cdot (p_n^f + p_n) \hat{y}_H^{nf}(\mathbf{b}) \right) \\
& = \sum_{k=0}^n \binom{n-1}{k} \left((1+b_r)p_n^f + (1-b_r)p_n \right)^k \left(1 - (1+b_r)p_n^f - (1-b_r)p_n \right)^{n-1-k} \\
& \cdot \left(\frac{2b_r p_n^f}{(1+b_r)p_n^f + (1-b_r)p_n} \hat{y}_H^f(\mathbf{b}) + \frac{(1-b_r) \cdot (p_n^f + p_n)}{(1+b_r)p_n^f + (1-b_r)p_n} \cdot \hat{y}_H^{nf}(\mathbf{b}) \right)^k \\
& \cdot n \cdot \left((1+b_r)p_n^f + (1-b_r)p_n - 2b_r p_n^f \hat{y}_H^f(\mathbf{b}) - (1-b_r) \cdot (p_n^f + p_n) \hat{y}_H^{nf}(\mathbf{b}) \right) \\
& = \sum_{k=0}^n \binom{n-1}{k} \left(1 - (1+b_r)p_n^f - (1-b_r)p_n \right)^{n-1-k} \cdot \left(2b_r p_n^f \hat{y}_H^f(\mathbf{b}) + (1-b_r) \cdot (p_n^f + p_n) \hat{y}_H^{nf}(\mathbf{b}) \right)^k \\
& \cdot \left((1+b_r)\alpha^f + (1-b_r)\alpha - 2b_r \alpha^f \hat{y}_H^f(\mathbf{b}) - (1-b_r) \cdot (\alpha^f + \alpha) \hat{y}_H^{nf}(\mathbf{b}) \right) \\
& = \left(1 - (1+b_r)p_n^f - (1-b_r)p_n + 2b_r p_n^f \hat{y}_H^f(\mathbf{b}) + (1-b_r) \cdot (p_n^f + p_n) \hat{y}_H^{nf}(\mathbf{b}) \right)^{n-1} \\
& \cdot \left((1+b_r)\alpha^f + (1-b_r)\alpha - 2b_r \alpha^f \hat{y}_H^f(\mathbf{b}) - (1-b_r) \cdot (\alpha^f + \alpha) \hat{y}_H^{nf}(\mathbf{b}) \right) \\
& = \left[1 - \frac{2b_r \alpha^f \left(1 - \hat{y}_H^f(\mathbf{b}) \right) - (1-b_r) \cdot (\alpha^f + \alpha) \left(1 - \hat{y}_H^{nf}(\mathbf{b}) \right)}{n} \right]^{n-1} \\
& \cdot \left((1+b_r)\alpha^f + (1-b_r)\alpha - 2b_r \alpha^f \hat{y}_H^f(\mathbf{b}) - (1-b_r) \cdot (\alpha^f + \alpha) \hat{y}_H^{nf}(\mathbf{b}) \right) \\
& = e^{-2b_r \alpha^f (1 - \hat{y}_H^f(\mathbf{b})) - (1-b_r) \cdot (\alpha^f + \alpha) (1 - \hat{y}_H^{nf}(\mathbf{b}))} \\
& \cdot \left((1+b_r)\alpha^f + (1-b_r)\alpha - 2b_r \alpha^f \hat{y}_H^f(\mathbf{b}) - (1-b_r) \cdot (\alpha^f + \alpha) \hat{y}_H^{nf}(\mathbf{b}) \right) \text{ as } n \rightarrow \infty \\
& = y_L^f(\mathbf{b}) \left((1+b_r)\alpha^f + (1-b_r)\alpha - b_r 2\alpha^f \hat{y}_H^f(\mathbf{b}) - (1-b_r) (\alpha^f + \alpha) \hat{y}_H^{nf}(\mathbf{b}) \right) \text{ as } n \rightarrow \infty.
\end{aligned}$$

Notice that the third equality above follows from $k \binom{n}{k} = n \binom{n-1}{k-1}$, the fourth equality substitutes k with $k-1$ everywhere and starts summation from $k=0$, and the sixth equality is an application of the Binomial Theorem.

Thus, $\mathbb{P}[v \text{ is a target} | v \text{ is a flexible node in } S_l]$ is given by

$$y_L^f(\mathbf{b}) + y_L^f(\mathbf{b}) \left((1+b_r)\alpha^f + (1-b_r)\alpha - b_r 2\alpha^f \hat{y}_H^f(\mathbf{b}) - (1-b_r) (\alpha^f + \alpha) \hat{y}_H^{nf}(\mathbf{b}) \right).$$

The probabilities conditional on v being a regular node or being from S_r can be derived analogously. \square

Proof of Proposition 5 Following closely the proof of Theorem 9 in Karp and Sipser (1981), we start by showing that a random tree is a good approximation to the structure obtained by conducting a breadth-first search from v . Denote the subgraph of G induced by vertices at most distance d from v as the d -neighborhood of v . A vertex v is referred to as a d -target if there exists a derivation proving v to be a target within the

d -neighborhood of v . Note that if d -neighborhood proves that v is a target then v is a target in any other graph that yields the same d -neighborhood.

Let

$$\begin{aligned} Y_n &:= \mathbb{P} [v \text{ is a target in } G_n \mid v \text{ is a flexible node in } V_l], \\ Y_n^d &:= \mathbb{P} [v \text{ is a } d\text{-target in } G_n \mid v \text{ is a flexible node in } V_l], \\ Y^d &:= \mathbb{P} [v \text{ is a } d\text{-target root in } \bar{G} \mid v \text{ is a flexible node in } S_l]. \end{aligned}$$

Claim 6 shows that, for large n , the probability that a d -neighborhood occurs in a random graph approaches the probability of that d -neighborhood occurring in a random tree.

CLAIM 6.

$$\lim_{n \rightarrow \infty} Y_n = \lim_{n \rightarrow \infty} \lim_{d \rightarrow \infty} Y_n^d = \lim_{d \rightarrow \infty} \lim_{n \rightarrow \infty} Y_n^d = \lim_{d \rightarrow \infty} Y^d = y_H^f(\mathbf{b}).$$

That is, $\mathbb{P} [v \text{ is a target} \mid v \text{ is a flexible node in } V_l] = y_H^f(\mathbf{b})$ as $n \rightarrow \infty$. Similarly, the probabilities for v to be a target or a loser, when $v \in V_l$ or V_r , and when v is a flexible or regular node, follow those derived for random trees in Lemma 9.

Since all members of derivations are targets or losers or both, we next find the probability for a random edge (v, u) in G to satisfy both $v \otimes u$ and $u \otimes v$ i.e., v is both a target and a loser. By Theorem 9 (3) in Karp and Sipser (1981), in \bar{G} this occurs if and only if both u and v are in L . We compute this probability conditional on the types of root nodes v , and the extension from \bar{G} to G follows from Claim 6.

$$\begin{aligned} & \lim_{n \rightarrow \infty} \mathbb{P} [v \otimes u \text{ and } u \otimes v \mid v \text{ is a flexible node in } V_l] \\ &= \mathbb{P} [v, u \text{ are both in } L \mid v \text{ is a flexible node in } V_l] \\ &= y_L^f(\mathbf{b}) \mathbb{P} [u \text{ is a flexible node} \mid (v, u) \in E] \hat{y}_L^f(\mathbf{b}) + y_L^f(\mathbf{b}) \mathbb{P} [u \text{ is a regular node} \mid (v, u) \in E] \hat{y}_L^{nf}(\mathbf{b}) \\ &= y_L^f(\mathbf{b}) \frac{b_r 2\alpha^f}{(1+b_r)\alpha^f + (1-b_r)\alpha} \hat{y}_L^f(\mathbf{b}) + y_L^f(\mathbf{b}) \frac{(1-b_r)(\alpha^f + \alpha)}{(1+b_r)\alpha^f + (1-b_r)\alpha} \hat{y}_L^{nf}(\mathbf{b}). \end{aligned}$$

Similarly, we find

$$\begin{aligned} & \lim_{n \rightarrow \infty} \mathbb{P} [v \otimes u \text{ and } u \otimes v \mid v \text{ is a regular node in } V_l] \\ &= y_L^{nf}(\mathbf{b}) \frac{b_r(\alpha^f + \alpha)}{b_r\alpha^f + (2-b_r)\alpha} \hat{y}_L^f(\mathbf{b}) + y_L^{nf}(\mathbf{b}) \frac{(1-b_r)2\alpha}{b_r\alpha^f + (2-b_r)\alpha} \hat{y}_L^{nf}(\mathbf{b}), \\ & \lim_{n \rightarrow \infty} \mathbb{P} [v \otimes u \text{ and } u \otimes v \mid v \text{ is a flexible node in } V_r] \\ &= \hat{y}_L^f(\mathbf{b}) \frac{b_l 2\alpha^f}{(1+b_l)\alpha^f + (1-b_l)\alpha} y_L^f(\mathbf{b}) + \hat{y}_L^f(\mathbf{b}) \frac{(1-b_l)(\alpha^f + \alpha)}{(1+b_l)\alpha^f + (1-b_l)\alpha} y_L^{nf}(\mathbf{b}), \\ & \lim_{n \rightarrow \infty} \mathbb{P} [v \otimes u \text{ and } u \otimes v \mid v \text{ is a regular node in } V_r] \\ &= \hat{y}_L^{nf}(\mathbf{b}) \frac{b_l(\alpha^f + \alpha)}{b_l\alpha^f + (2-b_l)\alpha} y_L^f(\mathbf{b}) + \hat{y}_L^{nf}(\mathbf{b}) \frac{(1-b_l)2\alpha}{b_l\alpha^f + (2-b_l)\alpha} y_L^{nf}(\mathbf{b}). \end{aligned}$$

Thus,

$$\begin{aligned}
& \lim_{n \rightarrow \infty} \mathbb{P} [v \text{ in a derivation} \mid v \text{ is a flexible node in } V_l] \\
&= \lim_{n \rightarrow \infty} \mathbb{P} [v \text{ is a target} \mid v \text{ is a flexible node in } V_l] + \lim_{n \rightarrow \infty} \mathbb{P} [v \text{ is a loser} \mid v \text{ is a flexible node in } V_l] \\
&\quad - \lim_{n \rightarrow \infty} \mathbb{P} [v \otimes u \text{ and } u \otimes v \mid v \text{ is a regular node in } V_l] \cdot \mathbb{E} \left[\left| u \text{ s.t. } (v, u) \in E \mid v \text{ is a regular node in } V_l \right| \right] \\
&= y_H^f(\mathbf{b}) + y_L^f(\mathbf{b}) + y_L^f(\mathbf{b}) \left((1+b_r)\alpha^f + (1-b_r)\alpha - b_r 2\alpha^f \hat{y}_H^f(\mathbf{b}) - (1-b_r)(\alpha^f + \alpha) \hat{y}_H^{nf}(\mathbf{b}) \right) \\
&\quad - \left[y_L^f(\mathbf{b}) \frac{b_r 2\alpha^f}{(1+b_r)\alpha^f + (1-b_r)\alpha} \hat{y}_L^f(\mathbf{b}) + y_L^f(\mathbf{b}) \frac{(1-b_r)(\alpha^f + \alpha)}{(1+b_r)\alpha^f + (1-b_r)\alpha} \hat{y}_L^{nf}(\mathbf{b}) \right] \cdot \left((1+b_r)\alpha^f + (1-b_r)\alpha \right) \\
&= y_H^f(\mathbf{b}) + y_L^f(\mathbf{b}) + y_L^f(\mathbf{b}) \left[(1+b_r)\alpha^f + (1-b_r)\alpha \right] \cdot \\
&\quad \left[1 - \frac{b_r 2\alpha^f}{(1+b_r)\alpha^f + (1-b_r)\alpha} \left(\hat{y}_L^f(\mathbf{b}) + \hat{y}_H^f(\mathbf{b}) \right) - \frac{(1-b_r)(\alpha^f + \alpha)}{(1+b_r)\alpha^f + (1-b_r)\alpha} \left(\hat{y}_L^{nf}(\mathbf{b}) + \hat{y}_H^{nf}(\mathbf{b}) \right) \right].
\end{aligned}$$

The probabilities conditional on other types of nodes are computed similarly. \square

Proof of Claim 6 The first and last equalities in the claim arise directly from our definitions and Lemma 9. We now prove the third and the second equality. By the Poisson Limit Theorem, for any flexible node $v \in V_l$, the distribution of its degrees follows Poisson $(b_r 2\alpha^f + (1-b_r)(\alpha^f + \alpha))$ as $n \rightarrow \infty$. Thus, for any $\epsilon > 0$ there is a constant k such that $\lim_{n \rightarrow \infty} \mathbb{P}[\text{there is a node of degree } > k \text{ in the } d\text{-neighborhood of } v] < \epsilon$. The rest of the analyses exactly follow the proof of Theorem 9 (1) in Karp and Sipser (1981), which shows $\lim_{n \rightarrow \infty} Y_n^d = Y^d$ because (i) there are finitely many d -neighborhoods that lack a vertex of degree $> k$, and (ii) the probability of encountering each such d -neighborhood around a node v in G_n is close to that around a root v in \bar{G} as $n \rightarrow \infty$. This proves the third equality.

Finally, we justify the limit exchange in the second equality. We leverage the result from Theorem 9 (1) in Karp and Sipser (1981) that, for every positive ϵ , there exists a d such that for all sufficiently large n , $\mathbb{P}[v \text{ is a target but not a } d\text{-target}] < \epsilon$.²⁸ This implies that for all sufficiently large $n, n'd, d', Y_n^d$ is close to $Y_n^{d'}$ and thus we may exchange limit. \square

Proof of Claim 2 Firstly, we calculate the derivative of $f_1(x_1)$:

$$\begin{aligned}
f_1'(x_1) &= \frac{\partial e^{-\frac{1}{2}(\alpha^f + \alpha)x_1 + 2\frac{\alpha}{\alpha^f + \alpha}(\log(x_1) + \alpha^f x_1)} + 2\frac{\log(x_1) + \alpha^f x_1}{\alpha^f + \alpha}}{\partial x_1} \\
&= e^{-\frac{1}{2}(\alpha^f + \alpha)x_1 + 2\frac{\alpha}{\alpha^f + \alpha}(\log(x_1) + \alpha^f x_1)} \left(-\frac{1}{2}(\alpha^f + \alpha) + 2\frac{\alpha}{\alpha^f + \alpha}(\alpha^f + 1/x_1) \right) + \frac{2}{\alpha^f + \alpha}(\alpha^f + 1/x_1).
\end{aligned}$$

²⁸This result relies on probabilistic bounds on the length of a shortest derivation that proves v to be a target.

We next employ a computer-aided proof to verify that $f'_1(x_1) > 1$ for any $x_1 \in (0, 1]$ when $10^{-4} < \alpha < \alpha^f$ and $\alpha^f + \alpha < e$. Fixing $\delta_1, \delta_2 > 0$, we establish a lower bound on the value of $f'_1(x_1)$ for any $(\bar{\alpha}^f, \bar{\alpha}, \bar{x}_1)$ in the set $[\alpha^f, \alpha^f + \delta_1) \times [\alpha, \alpha + \delta_1) \times [x_1, x_1 + \delta_2)$, where $10^{-4} < \alpha < \alpha^f$ and $\alpha^f + \alpha < e$. We find that:

$$\begin{aligned}
f'_1(x_1) &\geq e^{-\frac{1}{2}(\alpha^f + \alpha)x_1 + 2\frac{2(\alpha^f + \delta_1)(\alpha + \delta_1)(x_1 + \delta_2)}{\alpha^f + \alpha} + \frac{2\alpha \log(x_1 + \delta_2)}{\alpha^f + \alpha + 2\delta_1}} \left(-\frac{1}{2}(\alpha^f + \alpha + 2\delta_1) \right) \\
&\quad + e^{-\frac{1}{2}(\alpha^f + \alpha + 2\delta_1)(x_1 + \delta_2) + 2\frac{2\alpha^f \alpha x_1}{\alpha^f + \alpha + 2\delta_1} + \frac{2(\alpha + \delta_1) \log(x_1)}{\alpha^f + \alpha}} \left(\frac{2\alpha \left(\alpha^f + \frac{1}{x_1 + \delta_2} \right)}{\alpha^f + \alpha + 2\delta_1} \right) \\
&\quad + \frac{2 \left(\alpha^f + \frac{1}{x_1 + \delta_2} \right)}{\alpha^f + \alpha + 2\delta_1} \text{ when } x_1 > 0, \\
f'_1(x_1) &\geq e^{-\frac{1}{2}(\alpha^f + \alpha)x_1 + 2\frac{2(\alpha^f + \delta_1)(\alpha + \delta_1)(x_1 + \delta_2)}{\alpha^f + \alpha} + \frac{2\alpha \log(x_1 + \delta_2)}{\alpha^f + \alpha + 2\delta_1}} \left(-\frac{1}{2}(\alpha^f + \alpha + 2\delta_1) \right) \\
&\quad + \frac{2 \left(\alpha^f + \frac{1}{x_1 + \delta_2} \right)}{\alpha^f + \alpha + 2\delta_1} \text{ when } x_1 = 0.
\end{aligned} \tag{42}$$

For given $\delta_1, \delta_2 > 0$, if the lower bound in (42) is greater than 1, then $f'_1(x_1) > 1$ for any $(\bar{\alpha}^f, \bar{\alpha}, \bar{x}_1)$ in the corresponding set $[\alpha^f, \alpha^f + \delta_1) \times [\alpha, \alpha + \delta_1) \times [x_1, x_1 + \delta_2)$. In the computational notebook titled `Claim3.ipynb`,²⁹ we compute the value of (42) for $x_1 = 0, \delta_2, 2\delta_2, \dots, 1$ and $\alpha^f, \alpha = 10^{-4}, \delta_1, 2\delta_1, \dots, e$, under the constraint $\alpha^f + \alpha < e$. Through this computation, we find that taking $\delta_1 = \delta_2 = 0.01$ is sufficient for verifying (42) > 1 for all $x_1 \in (0, 1]$, $10^{-4} < \alpha < \alpha^f$ and $\alpha^f + \alpha < e$. □

C.3.6. Computational results based on $\mu^{\text{KS}}(b_l, b_r)$. To compute $\mu^{\text{KS}}(b_l, b_r)$, we resort to the `NLsolve` package available in the Julia Programming Language to solve (11) at a tolerance level $ftol = 10^{-8}$. Specifically, `NLsolve` iteratively refines candidate solutions using the Trust Region Method until the infinite norm of the residuals of the current solution falls below the threshold $ftol = 10^{-8}$ (NLsolve 2017). When $10^{-4} < \alpha < \alpha^f$ and $\alpha^f + \alpha < e$, at $\mathbf{b} = (1/2, 1/2), (1, 0)$ and $(0, 1)$ we find that (11) reduces to a single non-linear equation that exhibits strict monotonicity on both sides and can be solved to provable precision using this method (see the proof of Theorem 4 for details). In other cases where there are no theoretical guarantees for the closeness of $\mu^{\text{KS}}(b_l, b_r)$ to $\mu(b_l, b_r)$, numerical studies indicate that $\mu_n^{\text{EMP}}(b_l, b_r)$ still tends to converge to $\mu^{\text{KS}}(b_l, b_r)$ as n scales large. We thus employ $\mu^{\text{KS}}(b_l, b_r)$ to compare the one-sided and the balanced allocations for a wide range of parameters. Specifically, the findings presented in Section 5 are based on values of $(B, b_l, \alpha^f, \alpha)$ in a set S that contains all $B \in \{0.1, 0.2, \dots, 1\}, b_l \in \{0, 0.01, \dots, 1\}, \alpha^f \in \{0.05, 0.10, \dots, 7.45, 7.50\}$ and $\alpha \in \{0, 0.05, 0.10, \dots, 2.95, 3.00\}$ such that $B \geq b_l$ and $\alpha^f > \alpha$.

Appendix D: Proofs of the Local Model

In this section, we prove the results for the local model. We derive a closed-form expression for $\mu(b_l, b_r)$ as a rational function, in which both the denominator and numerator are eighth-order polynomials in terms of b_l, b_r, p^f , and p . This expression facilitates the comparison between one-sided and balanced allocation, as well as the analysis of the convexity and concavity properties of $\mu(b_l, b_r)$ along specific diagonals where analyses of directional second-order derivatives are tractable.

²⁹The computer-aided proof can be found at <https://bit.ly/3VhfumL>.

D.1. Proof of Theorem 5

Proof. We begin by characterizing the asymptotic fraction of nodes matched in the local model. Let E denote the set of all edges. We propose Algorithm 3 to construct a matching M , and argue that it is at most 1 below the size of a maximum matching (thus, the matching probability under Algorithm 3 is the same, asymptotically, as that under a maximum matching).

Algorithm 3 Maximum Matching Construction in Local Model

- 1: Initialize the matching set $M \leftarrow \emptyset$
 - 2: **if** $(v_1^l, v_1^r) \in E$ **then**
 - 3: Add (v_1^l, v_1^r) to M
 - 4: **for** each subsequent node v_i^r with $i > 1$ **do**
 - 5: **if** $(v_{i-1}^l, v_i^r) \in E$ and v_{i-1}^l is not already matched in M **then**
 - 6: Add (v_{i-1}^l, v_i^r) to M
 - 7: **else if** $(v_i^l, v_i^r) \in E$ **then**
 - 8: Add (v_i^l, v_i^r) to M
 - 9: **return** M
-

Our analysis focuses on the nodes in V_r that are being matched through Algorithm 3, as opposed to the ones that could be matched in a maximum matching. Recall that each node v_i^l in V_l can only connect to its two neighbors in V_r . If $(v_i^l, v_i^r) \notin E$ and $(v_i^l, v_{i+1}^r) \in E$, then there exists a maximum matching that contains (v_i^l, v_{i+1}^r) . This is because node v_i^l cannot be matched otherwise, and not using (v_i^l, v_{i+1}^r) in the matching would at most save v_{i+1}^r for one additional match. Hence, this algorithm is provably optimal for all nodes in V_r except v_1^r , which is myopically matched to v_1^l if an edge exists. As we are interested in computing $\mu(b_l, b_r) = \lim_{n \rightarrow \infty} \mathbb{E} \left[\frac{\mathcal{M}_n(b_l, b_r)}{n} \right]$, the resulting error in $\mu(b_l, b_r)$ approaches 0 in the asymptotic setting where $n \rightarrow \infty$.

Therefore, to compute $\mu(b_l, b_r)$ it is sufficient to calculate the asymptotic fraction of nodes matched through this algorithm. Observe that whether a node $v_i^r \in V_r$ is matched to $v_{i-1}^l \in V_l$ depends only on edges incident to v_{i-1}^l and is independent of v_i^l . For each v_i^r with $i \in \{2, \dots, n\}$, we define

$$x_i^f := \mathbb{P} \left[(v_{i-1}^l, v_i^r) \in M \mid v_i^r \text{ is flexible} \right] \text{ and } x_i^n := \mathbb{P} \left[(v_{i-1}^l, v_i^r) \in M \mid v_i^r \text{ is regular} \right].$$

We now establish a system of equations to compute (x_{i+1}^f, x_{i+1}^n) based on (x_i^f, x_i^n) , which hold for any $i \in \{2, \dots, n\}$. To compute x_{i+1}^f , we consider all possible scenarios in which v_{i+1}^r gets matched to v_i^l : (1) $(v_{i-1}^l, v_i^r) \in M$ and $(v_i^l, v_{i+1}^r) \in E$, or (2) $(v_{i-1}^l, v_i^r) \notin M$, $(v_i^l, v_i^r) \notin E$ and $(v_i^l, v_{i+1}^r) \in E$. Suppose v_i^l and v_i^r are both flexible nodes; if v_{i+1}^r is also flexible then (1) occurs *w.p.* $x_i^f 2p^f$ and (2) occurs *w.p.* $(1 - x_i^f)(1 - 2p^f)2p^f$. Thus, conditioned on v_i^l , v_i^r , and v_{i+1}^r all being flexible nodes, $(v_i^l, v_{i+1}^r) \in M$ with probability $x_i^f 2p^f + (1 - x_i^f)(1 - 2p^f)2p^f$.

For the cases where v_i^l or v_i^r are of other node types, we compute (conditioned on node types) the respective probabilities of the events

$$\left\{ \left\{ (v_{i-1}^l, v_i^r) \in M \right\} \cap \left\{ (v_i^l, v_{i+1}^r) \in E \right\} \right\} \text{ and } \left\{ \left\{ (v_{i-1}^l, v_i^r) \notin M \right\} \cap \left\{ (v_i^l, v_i^r) \notin E \right\} \cap \left\{ (v_i^l, v_{i+1}^r) \in E \right\} \right\}$$

accordingly and find that:

$$\begin{aligned} x_{i+1}^f = f_1(x_i^f, x_i^n) := & b_l b_r \left[x_i^f 2p^f + (1 - x_i^f)(1 - 2p^f)2p^f \right] + (1 - b_l) b_r \left[x_i^f (p^f + p) + (1 - x_i^f)(1 - p^f - p)(p^f + p) \right] \\ & + b_l(1 - b_r) \left[x_i^n 2p^f + (1 - x_i^n)(1 - p^f - p)2p^f \right] + (1 - b_l)(1 - b_r) \left[x_i^n (p^f + p) + (1 - x_i^n)(1 - 2p)(p^f + p) \right]. \end{aligned} \quad (43)$$

Similarly, for x_{i+1}^n we find that:

$$\begin{aligned} x_{i+1}^n = f_2(x_i^f, x_i^n) := & b_l b_r \left[x_i^f (p^f + p) + (1 - x_i^f)(1 - 2p^f)(p^f + p) \right] + (1 - b_l) b_r \left[x_i^f 2p + (1 - x_i^f)(1 - p^f - p)2p \right] \\ & + b_l(1 - b_r) \left[x_i^n (p^f + p) + (1 - x_i^n)(1 - p^f - p)(p^f + p) \right] + (1 - b_l)(1 - b_r) \left[x_i^n 2p + (1 - x_i^n)(1 - 2p)2p \right]. \end{aligned} \quad (44)$$

Since $f_1(x_i^f, x_i^n)$ and $f_2(x_i^f, x_i^n)$ are linear with respect to x_i^f and x_i^n , they are trivially continuous. Since $b_l, b_r \in [0, 1]$ and $0 \leq 2p < p + p^f < 2p^f \leq 1$, we also find that $\frac{\partial f_1(x_i^f, x_i^n)}{\partial x_i^f}, \frac{\partial f_1(x_i^f, x_i^n)}{\partial x_i^n}, \frac{\partial f_2(x_i^f, x_i^n)}{\partial x_i^f}, \frac{\partial f_2(x_i^f, x_i^n)}{\partial x_i^n} \in [0, 1)$. Thus, by applying the Banach fixed-point theorem, we know that as $i \rightarrow \infty$ the fixed-point iteration $(x_{i+1}^f, x_{i+1}^n) = (f_1(x_i^f, x_i^n), f_2(x_i^f, x_i^n))$ converges to the unique fixed point (x^f, x^n) such that $(x^f, x^n) = (f_1(x^f, x^n), f_2(x^f, x^n))$. This is a linear system of equations, the solutions of which provide the limiting values for x^f and x^n (see below in (46)).

We next compute $\mu(b_l, b_r)$ using x^f and x^n . The asymptotic fraction of matched nodes is equal to the asymptotic probability that a random node $v_i^r \in V_r$ is matched. If v_i^r is a flexible node, it is matched with v_{i-1}^l with probability x_i^f and matched with v_i^l with probability $(1 - x_i^f) [(1 + b_l)p^f + (1 - b_l)p]$. If it is a regular node, it is matched with v_{i-1}^l with probability x_i^n and matched with v_i^l with probability $(1 - x_i^n) [b_l p^f + (2 - b_l)p]$. Thus,

$$\begin{aligned} \mu(b_l, b_r) = \lim_{i \rightarrow \infty} & b_r x_i^f + b_r(1 - x_i^f) \left[(1 + b_l)p^f + (1 - b_l)p \right] + (1 - b_r)x_i^n + (1 - b_r)(1 - x_i^n) \left[b_l p^f + (2 - b_l)p \right] \\ = & b_r x^f + b_r(1 - x^f) \left[(1 + b_l)p^f + (1 - b_l)p \right] + (1 - b_r)x^n + (1 - b_r)(1 - x^n) \left[b_l p^f + (2 - b_l)p \right]. \end{aligned} \quad (45)$$

Solving x^f and x^n from (43)-(44) and plugging into (45), we obtain

$$\begin{aligned} \mu(b_l, b_r) = & \left(2(b_l + b_r)^2 p^4 b_l^2 - 2(b_l + b_r)^2 p^4 b_l - 8(b_l + b_r)^2 p^3 p^f b_l^2 + 8(b_l + b_r)^2 p^3 p^f b_l + 12(b_l + b_r)^2 p^2 (p^f)^2 b_l^2 \right. \\ & - 12(b_l + b_r)^2 p^2 (p^f)^2 b_l - (b_l + b_r)^2 p^2 - 8(b_l + b_r)^2 p (p^f)^3 b_l^2 + 8(b_l + b_r)^2 p (p^f)^3 b_l + 2(b_l + b_r)^2 p p^f \\ & + 2(b_l + b_r)^2 (p^f)^4 b_l^2 - 2(b_l + b_r)^2 (p^f)^4 b_l - (b_l + b_r)^2 (p^f)^2 - 4(b_l + b_r) p^4 b_l^3 + 2(b_l + b_r) p^4 b_l^2 \\ & + 2(b_l + b_r) p^4 b_l + 16(b_l + b_r) p^3 p^f b_l^3 - 8(b_l + b_r) p^3 p^f b_l^2 - 8(b_l + b_r) p^3 p^f b_l - 24(b_l + b_r) p^2 (p^f)^2 b_l^3 \\ & + 12(b_l + b_r) p^2 (p^f)^2 b_l^2 + 12(b_l + b_r) p^2 (p^f)^2 b_l - 2(b_l + b_r) p^2 b_l + 7(b_l + b_r) p^2 + 16(b_l + b_r) p (p^f)^3 b_l^3 \\ & \left. - 8(b_l + b_r) p (p^f)^3 b_l^2 - 8(b_l + b_r) p (p^f)^3 b_l + 4(b_l + b_r) p p^f b_l - 6(b_l + b_r) p p^f - 2(b_l + b_r) p \right) \end{aligned}$$

$$\begin{aligned}
& -4(b_l + b_r) \left(p^f\right)^4 b_l^3 + 2(b_l + b_r) \left(p^f\right)^4 b_l^2 + 2(b_l + b_r) \left(p^f\right)^4 b_l - 2(b_l + b_r) \left(p^f\right)^2 b_l - (b_l + b_r) \left(p^f\right)^2 \\
& + 2(b_l + b_r)p^f + 2p^4 b_l^4 - 2p^4 b_l^2 - 8p^3 p^f b_l^4 + 8p^3 p^f b_l^2 + 12p^2 \left(p^f\right)^2 b_l^4 - 12p^2 \left(p^f\right)^2 b_l^2 \\
& + 2p^2 b_l^2 - 8p^2 - 8p \left(p^f\right)^3 b_l^4 + 8p \left(p^f\right)^3 b_l^2 - 4pp^f b_l^2 + 4p + 2 \left(p^f\right)^4 b_l^4 - 2 \left(p^f\right)^4 b_l^2 + 2 \left(p^f\right)^2 b_l^2) / \\
& \left((b_l + b_r)^2 p^4 b_l^2 - (b_l + b_r)^2 p^4 b_l - 4(b_l + b_r)^2 p^3 p^f b_l^2 + 4(b_l + b_r)^2 p^3 p^f b_l + 6(b_l + b_r)^2 p^2 \left(p^f\right)^2 b_l^2 \right. \\
& - 6(b_l + b_r)^2 p^2 \left(p^f\right)^2 b_l - 4(b_l + b_r)^2 p \left(p^f\right)^3 b_l^2 + 4(b_l + b_r)^2 p \left(p^f\right)^3 b_l + (b_l + b_r)^2 \left(p^f\right)^4 b_l^2 \\
& - (b_l + b_r)^2 \left(p^f\right)^4 b_l - 2(b_l + b_r)p^4 b_l^3 + (b_l + b_r)p^4 b_l^2 + (b_l + b_r)p^4 b_l + 8(b_l + b_r)p^3 p^f b_l^3 - 4(b_l + b_r)p^3 p^f b_l^2 \\
& - 4(b_l + b_r)p^3 p^f b_l - 12(b_l + b_r)p^2 \left(p^f\right)^2 b_l^3 + 6(b_l + b_r)p^2 \left(p^f\right)^2 b_l^2 + 6(b_l + b_r)p^2 \left(p^f\right)^2 b_l - 2(b_l + b_r)p^2 b_l \\
& + 3(b_l + b_r)p^2 + 8(b_l + b_r)p \left(p^f\right)^3 b_l^3 - 4(b_l + b_r)p \left(p^f\right)^3 b_l^2 - 4(b_l + b_r)p \left(p^f\right)^3 b_l + 4(b_l + b_r)pp^f b_l \\
& - 2(b_l + b_r)pp^f - 2(b_l + b_r) \left(p^f\right)^4 b_l^3 + (b_l + b_r) \left(p^f\right)^4 b_l^2 + (b_l + b_r) \left(p^f\right)^4 b_l - 2(b_l + b_r) \left(p^f\right)^2 b_l \\
& - (b_l + b_r) \left(p^f\right)^2 + p^4 b_l^4 - p^4 b_l^2 - 4p^3 p^f b_l^4 + 4p^3 p^f b_l^2 + 6p^2 \left(p^f\right)^2 b_l^4 - 6p^2 \left(p^f\right)^2 b_l^2 + 2p^2 b_l^2 - 4p^2 \\
& \left. - 4p \left(p^f\right)^3 b_l^4 + 4p \left(p^f\right)^3 b_l^2 - 4pp^f b_l^2 + \left(p^f\right)^4 b_l^4 - \left(p^f\right)^4 b_l^2 + 2 \left(p^f\right)^2 b_l^2 + 1 \right). \tag{46}
\end{aligned}$$

Given the closed-form expression for $\mu(b_l, b_r)$ in (46), to prove Theorem 5 it suffices to compute $\mu(B, 0) - \mu(B/2, B/2)$ and verify that the difference is strictly positive. Using Wolfram Mathematica in `Theorem2.nb`,³⁰ we verify that $\mu(B, 0) - \mu(B/2, B/2) > 0$ for all $B \in (0, 1]$ and $0 \leq p < p^f \leq 1/2$. \square

D.2. Proof of Theorem 7

Proof. For the concavity result, we evaluate $\nabla_{(0,1)}^2 \mu(b_l, b_r)$ with $b_l = 1/2$, which is equivalent to $\frac{\partial^2 \mu(1/2, b_r)}{\partial b_r^2}$. In `Theorem6.nb`,³¹ we again use Wolfram Mathematica to verify that $\frac{\partial^2 \mu(1/2, b_r)}{\partial b_r^2} < 0$ for all $b_r \in (0, 1)$ and $0 \leq p < p^f \leq 1/2$. The case for the direction $(1, 0)$ is symmetric. The proof for $\frac{\partial^2 \mu(0, b_r)}{\partial b_r^2} < 0$ for all $b_r \in (0, 1)$ and $0 \leq p < p^f \leq 1/2$ follows from the same analyses by taking $b_l = 0$.

The convexity result is easier to analyze by hands. We set $b_r = 1 - b_l$ to simplify (46) to

$$\mu(b_l, 1 - b_l) = 2 \frac{(p^f)^2 b_l^2 - (p^f)^2 b_l - 2p^f p b_l^2 + 2p^f p b_l + p^f + p^2 b_l^2 - p^2 b_l + p}{(p^f)^2 b_l^2 - (p^f)^2 b_l - 2p^f p b_l^2 + 2p^f p b_l + p^f + p^2 b_l^2 - p^2 b_l + p + 1}.$$

Taking the second-order derivative with respect to b_l , we obtain

$$\frac{\partial^2 \mu(b_l, 1 - b_l)}{\partial b_l^2} = \frac{4(p^f - p)^2 \underbrace{\left[-\left(p^f\right)^2 - 3b_l^2 \left(p^f - p\right)^2 + 3b_l \left(p^f - p\right)^2 + 2p^f p + p^f - p^2 + p + 1 \right]}_{(I)}}{\left(\underbrace{b_l^2 \left(p^f - p\right)^2 - b_l \left(p^f - p\right)^2 + p^f + p + 1}_{II} \right)^3}.$$

³⁰The codes can be found at <https://bit.ly/3uS7wW6>.

³¹The codes can be found at <https://bit.ly/3uRh6bQ>.

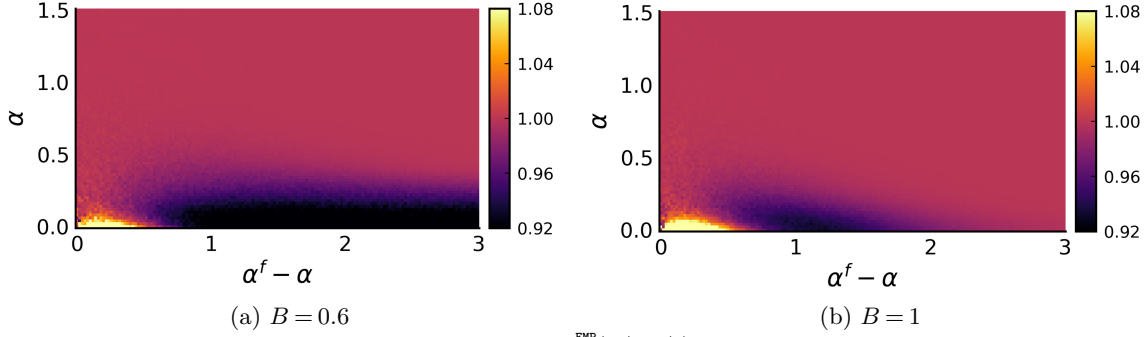


Figure 27 The plots present heat-map values of $\frac{\mu^{\text{EMP}}(B/2, B/2)}{\mu^{\text{EMP}}(B, 0)}$ across varying α and $\alpha^f - \alpha$ when $\lambda = 0.8$.

We demonstrate that both (I) and (II) are strictly positive for all $b_l \in (0, 1)$ and $0 \leq p < p^f \leq 1/2$, ensuring $\frac{\partial^2 \mu(b_l, 1-b_l)}{\partial b_l^2} > 0$.

For (I) we have

$$\begin{aligned}
 (I) &= 3b_l(1-b_l) \left(p^f - p\right)^2 - \left(p^f - p\right)^2 + p^f + p + 1 \\
 &= (3b_l - 3b_l^2 - 1) \left(p^f - p\right)^2 + p^f + p + 1 \\
 &\geq - \left(p^f - p\right)^2 + p^f + p + 1 \geq -0.25 + p^f + p + 1 > 0,
 \end{aligned}$$

where the first inequality comes from $b_l - b_l^2 \geq 0$ and the second from $(p^f - p)^2 \leq 0.25$.

For (II) we have

$$(II) = (b_l^2 - b_l) \left(p^f - p\right)^2 + p^f + p + 1 \geq -0.25 + p^f + p + 1 > 0,$$

where the first inequality comes from $b_l^2 - b_l \geq -1$ and $(p^f - p)^2 \leq 0.25$. (since $p^f \leq 1/2$). Since $\nabla_{(1,-1)}^2 \mu(b_l, b_r)$ with $b_l + b_r = 1$ is equivalent to $\frac{\partial^2 \mu(b_l, 1-b_l)}{\partial b_l^2} > 0$, we conclude the proof. \square

Appendix E: Additional Simulation Results

In this section we consider an alternative model of an imbalanced market in which a flexibility allocation (b_l, b_r) means that drivers and riders are flexible with probability b_l and b_r , respectively. This modeling approach guarantees that the expected number of edges for flexibility allocations $(B, 0)$ and $(0, B)$ are the same, though they result in a different expected number of flexible nodes. Indeed, with this modeling approach the one-sided allocation $(B, 0)$ produces more flexible nodes in expectation than any other flexibility design with the same flexibility budget B , and this leads to a significant advantage for the one-sided allocation. Fig. 27 (a) and (b) show that the additional flexible nodes ensure that the one-sided allocation $(B, 0)$ outperforms the balanced allocation for any sufficiently large α and α^f , regardless of whether $B < 1$, overshadowing the flexibility asymmetry effect. Thus, the asymmetry effect disappears, while the cannibalization effect remains. At the same time, we still observe the balanced allocation outperforming the one-sided allocation in the regime with very small α, α^f , where the number of edges is much larger for the balanced allocation (see Section 7.2).